INTERDISCIPLINARY STUDIES TOWARDS NEUTRON SYNOVECTOMY

INTERDISCIPLINARY STUDIES TOWARDS BORON NEUTRON CAPTURE SYNOVECTOMY AT MCMASTER UNIVERSITY

By

VICTOR KREFT, M.Sc. B.Sc. (Hons.)

A Thesis

Submitted to the School of Graduate Studies

in Partial Fulfillment of the Requirements

for the Degree

Doctor of Philosophy

McMaster University

DOCTOR OF PHILOSOPHY (2014) McMaster University
(Medical Physics) Hamilton, Ontario

TITLE: **Interdisciplinary Studies Towards Boron Neutron Capture Synovectomy at McMaster University**

AUTHOR: Victor A. Kreft, M. Sc. B.Sc. (Hons.)
(McMaster University)

SUPERVISOR: Dr. Fiona E. McNeill

NUMBER OF PAGES: xii, 140, A8

Abstract

Rheumatoid arthritis is a chronic autoimmune disease of the joints that affects 1% of the world's population. One proposed treatment, Boron Neutron Capture Synovectomy (BNCS), seeks to exploit the $^{10}B(n,\alpha)^{7}Li$ nuclear reaction by injecting boronated chemical compounds into the joint and subsequently irradiating with neutrons. Numerous boron compounds have been generated at McMaster University and require evaluation in order to determine potential candidates for BNCS applications. A non-chemical process exploiting technology available at McMaster University is proposed for evaluating boron compounds for BNCS. Studies to determine the feasibility of the process have been undertaken. A standard protocol for lymphocyte isolation has been successfully modified to incorporate incubation periods with candidate boron compounds. Results have demonstrated no significant deleterious impact to the cell population versus the standard protocol. The McMaster Nuclear Reactor (MNR) Prompt Gamma Neutron Activation Analysis (PGNAA) site was modified to accommodate liquid biological samples to determine boron content. The minimum detectable limit (MDL) of boron for the liquid sample set up was determined to be on the order of 1-3 ppm. Preliminary boron compound testing on isolated lymphocytes was undertaken and flowcytometry studies were successfully utilized to indicate minimal toxicity. However, uptake was shown to be less than the MDL for the liquid samples. Suggested methods of improving the testing process, including lowering the MDL of boron by preparing lyophilized samples and increasing the sample counting time, were investigated. The automation of the PGNAA Rabbit System at MNR to support the improved boron content measurements was implemented. Several improvements in the PGNAA testing process were unsuccessful in improving the MDL of boron. A number of improvements are proposed for future investigation and consideration for testing and evaluating boron compounds at McMaster University.

Acknowledgements

I wish to express my sincere thanks to my supervisor Dr. Fiona E. McNeill for her advice and guidance throughout not only this thesis but all of my undergraduate and graduate studies at McMaster University. Her ability to listen, encourage, and envision are among but a few of her qualities to which I aspire. Thank you for your trust and faith in me as a student, and to the opportunities you have opened up for me.

I am grateful to the current and former members of my supervisory committee, Dr. Doug Boreham, Dr. David Chettle, Dr. John Valliant, and Dr. Joanne O'Meara, whose insight into the multifaceted world of physics, chemistry, and biology that BNCS is, has been invaluable. I would also like to thank Dr. Soo Hyun Byun, whose review and input to this thesis has been an asset.

Many thanks are owed to the unsung heroes of the laboratory facilities without whose help this thesis would never have come to fruition: Alice Pidruczny, John Avelar, Nicole McFarlane, Mary Ellen Cybulski, and Lisa Laframboise.

I owe a debt of gratitude to my loving wife Lina. Without her support I could not have stayed on the path and crossed the finish line. I sincerely thank you for your endless love, patience and encouragement. Ana bhebik kteer ya albi.

Finally I wish to thank my parents for the years of love and trust invested in me. They have been there since the beginning, encouraging me to strive forward in my life. Words cannot express my gratitude for everything they have given me. This work is dedicated to them. Kocham was.

Table of Contents

List of Figures and Tables

1 Introduction

1.1 Background

Rheumatoid arthritis is an autoimmune disease that causes chronic joint inflammation.[1,2] It is estimated to affect 1% of the world's population with women roughly twice as likely as men to develop the disease.[1,2] Although several theories exist as to the causes, no specific culprit has been identified.[1,3,4] It is known, however, that both genetic and environmental factors contribute to the infliction, based on epidemiological evidence from monozygotic twins and various ethnic subpopulations.[1,2]

Rheumatoid arthritis is characterized by the proliferation of the joint lining, known as the synovium, of diarthrodial (moveable) joints. Synovium consists of three layers: synovial lining, subintimal stroma and vasculature. Two cell types make up the synovial lining layer: macrophage-like type-A synoviocytes and fibroblast-like type-B synoviocytes. In rheumatic patients, these cells proliferate to roughly 5 times normal levels. The synovium of rheumatoid arthritis patients is also known to contain increased levels of cytokines, signaling proteins which act as pro-inflammatory chemical messengers. The resulting inflammatory response yields an accumulation of a host of defense cells, including lymphocytes, monocytes and macrophages. The consequence of a

perpetuating inflammatory response is the replacement of the synovial fluid, normally a nutrient rich viscous emollient, with a lytic fluid known as pannus. The formation of pannus leads to cartilage destruction and bone degradation.[1-5]

Treatment of the disease has long been addressed by a myriad of pharmaceuticals including non-steroidal anti-inflammatory drugs (e.g. acetylsalycilic acid ["Aspirin"]), disease-modifying anti-rheumatic drugs (e.g. methotrexate) and immunosuppressive agents (e.g. hydrocortisone). In the past decade the approval of biological response modifiers (BRMs) has improved patient palliation. BRMs act by interfering with the specific messenger proteins known to be involved in the inflammatory response.[1,2,4] However, as with immunosuppressive agents, this effect leads to patient susceptibility to serious infections.[1-6]

Advanced chronic inflammation ultimately leads to deterioration of affected joints and resultant loss of motion.[1-4] Surgical removal of the inflamed tissues is widely considered to be the most effective method of preventing such a negative outcome in joints unresponsive to standard treatment.[1-4] Approximately 10% of rheumatoid arthritis patients have at least one joint which remains unresponsive to pharmaceutical treatments and requires surgical intervention.[5]

Surgical synovial ablation is performed both via open synovectomy and arthroscopy. While therapeutically effective, inflammatory symptoms generally reappear in 2-5 years.[5] The cause of this reemergence of disease is hypothesized to be the result of incomplete ablation during surgical procedures.[5,19] Synovial tissue is convoluted, entering crevices which are impossible to completely ablate and rheumatic synovium is thought to re-grow from the remains (synovial tissues have been shown to be highly regenerative in animal models).[5,19]

Another mode of synovectomy that has been used in Canada, Europe and Australia is the intra-articular injection of radiocolloids. Trials have shown success rates of up to 80%, on par with those of the standard surgical procedures listed above.[6-8] However, concerns over radiation dose to the patient via leakage of the radioactive compounds from the intra-articular cavity have impeded the general acceptance of such techniques.[5]

1.2 Boron Neutron Capture Synovectomy

One approach called boron neutron capture synovectomy (BNCS) has been proposed as a treatment for rheumatoid arthritis.[5] BNCS is based on the same principles as boron neutron capture therapy (BNCT) for cancer, in which a non-radioactive compound containing ^{10}B is administered into the joint cavity. Subsequent neutron irradiation yields two highly ionizing particles per ^{10}B atom

as a result of the nuclear reaction between ^{10}B and the incident neutrons. This method attempts to draw on the positive aspects of radiocolloid synovectomy, namely requirement of only local anesthesia, without the concern for radiocolloid leakage and long term patient irradiation.

Both BNCT and BNCS take advantage of the high thermal neutron capture cross section of ^{10}B (3837 barns). Thermal neutrons are those in which the kinetic energy of the neutron is comparable to the kinetic energy of molecular motion of the medium, nominally defined as having an average velocity of 2200 m/s (0.0253 eV). Thermal neutron capture in ^{10}B results in atomic fission yielding emission of a ^{7}Li atom and an alpha particle as fission products, as well as a 478 keV gamma ray 94% of the time:

$$^{10}B + n_{th} \longrightarrow {}^{7}Li_{1.16MeV} + \alpha_{1.78MeV} \quad \textit{(Q value = 2.792 MeV, ground state)}$$

$$^{10}B + n_{th} \longrightarrow {}^{7}Li_{0.84MeV} + \alpha_{1.47MeV} + \gamma_{0.48MeV} \quad \textit{(Q value = 2.310 MeV, excited state)}$$

The two fission products have a high linear energy transfer (LET) with a range of 12-13 microns. Since the range of the ^{7}Li atom and alpha particle is roughly 1-2 cells in diameter the radiation damage is localized within the cell(s).

The goal of BNCT and BNCS is to load ^{10}B preferentially into the diseased target cells via a carrier molecule and irradiate the tissue with neutrons,

thereby causing intracellular damage resulting from the high LET fission products arising from thermal neutron interactions with the ^{10}B. The relative success of BNCT and BNCS over other radiation treatment modalities relies on achieving a higher concentration of ^{10}B into the diseased cells versus surrounding healthy cells. The result is a selective targeting of diseased cells upon neutron irradiation due to the boron neutron capture reaction above. In theory, the range of the two fission products limits the radiation effect to the diseased cells with high levels of boron, sparing healthy cells.

However, in practice the relative success of BNCT and BNCS is complicated by a number of factors. Although the thermal neutron cross section of ^{10}B is orders of magnitude greater than that of isotopes of elements comprising tissue, the concentrations of those elements, particularly hydrogen and nitrogen, is so high that a significant undesirable background dose may be delivered to healthy tissues due to neutron capture reactions in those tissues:

$$^{14}N + n_{th} \longrightarrow {}^{14}C + p \quad (Q\ value = 0.626\ MeV)$$

$$^{1}H + n_{th} \longrightarrow {}^{2}H + \gamma \quad (Q\ value = 2.225\ MeV)$$

Additionally, the boron neutron capture reaction dose is dependent on an adequately moderated flux of thermal neutrons to the diseased tissue. The challenge of BNCT and BNCS dose planning, therefore, is to load a high enough

boron concentration to the diseased tissue and accurately deliver a sufficiently moderated and localized thermal neutron flux such that the boron neutron capture dose is much higher relative to the background dose in order to achieve an acceptable trade off. This is particularly difficult given the multitude of biological mechanisms for compound dissipation in tissue, geometries and composition of various tissues in the treatment area, and types and energies of available neutron sources.

Boron neutron capture therapy for glioblastoma multiforme, a particularly aggressive form of brain cancer, was first proposed in 1936 by Gordon Locher. BNCT has been widely studied since, and is now undergoing clinical trials at select sites internationally.[9] BNCS, however, has had limited attention since first being proposed in the 1990's. In the past several years rather few laboratory studies have been initiated to begin quantification of the physical and biological characteristics of BNCS treatments. Although BNCS is, in theory, based on the same principles as BNCT, target compound, target organ and ultimately radiation field differences exist between the two treatment modalities. Certainly, however, studies of BNCS can take advantage of the groundwork laid out by the numerous studies performed for BNCT, due to the similarities between the two treatment modalities.

Although first proposed in documented format by Zamenhof et al. (1992), and further established in thesis material by Emanuela Binello (1995), it was not until Yanch et al. (1999) from The Department of Nuclear Engineering and Whitaker College of Health Sciences and Technology at Massachusetts Institute of Technology (MIT) that the general concept and feasibility study data were first published in detail to the general scientific community regarding the novel application of BNCT as a treatment for rheumatoid arthritis.[10,11,5] In that publication, drug uptake of the lead drug of many tested, potassium dodecahydrododecaborate (KBH) was presented. *In vivo* studies showed that efflux of the compound was rapid, with less that 20% remaining in the synovium after only 15 minutes.[5] While physical irradiation parameters showed the technique to be largely feasible, the necessity to determine tissue/compound specific Relative Biological Effectiveness (RBE) values and utility of a compound which would have longer synovial uptake properties was expressed.

Since the initial publication, two follow-up journal publications have been produced by the MIT group. The first one showed that the accelerator-based $^{7}Li(p,n)^{7}Be$ reaction produced a neutron spectrum with the most amenable therapeutic characteristics.[12] It was noted, however, that due to thermomechanical properties of lithium targets it was not favorable to utilize this reaction in the consideration that currents of up to 1 mA were required for realistic treatment times.

The second paper demonstrated the proof of principle of BNCS. New Zealand rabbits were induced with arthritis, injected intra-articularly with KBH, and irradiated with neutrons tailored to ideal treatment energy.[13] Synovial ablation was accomplished at doses of 6000 to 7000 RBE-cGy, lower than the dose of 10000 RBE-cGy anticipated by Yanch et al. (1999).[5,13] At this dose level, cartilage necrosis was minimal in arthritic animals. However, in the treated control group that was non-arthritic, considerable cartilage necrosis was evident. The necrosis was attributed to the observation that normal synovium has a smaller occupancy volume in the joint cavity, leading to less compound absorption. With the compound used having a relatively low molecular weight and specificity for synoviocytes, greater effusion into the cartilaginous matrix was possible. This result again highlighted the need for improved boron compounds.

1.3 Motivation

The desire to initiate studies into BNCS at McMaster University is multifaceted. Valliant et al. (2000) of McMaster University showed that a corticosteroid-carborane ester could be synthesized.[14] Such a compound could exhibit the specificity of cortisone proven in rheumatic synovium, while delivering boron to the treatment site. Recently several other high molecular weight organically-based boron compounds have been developed.[50]

McMaster University has a research reactor with functional beam ports and two accelerators capable of producing neutrons via the $^{7}Li(p,n)^{7}Be$ reaction. Of the two accelerators, the new Tandetron has recently been shown to achieve currents of up to 0.5 mA on a lithium target, and is designed for a maximum output of 1 mA.[15] The McMaster Nuclear Reactor (MNR) is equipped with a prompt gamma neutron activation analysis (PGNAA) laboratory. Additionally, McMaster University is equipped with a fully functional high level radiation biology laboratory including state-of-the-art flow cytometry and spectroscopic karyotyping (SKY) capabilities. The implementation of Monte Carlo N-Particle (MCNP) radiation transport code on the parallel clusters of the Shared Hierarchical Academic Research Computing Network (SHARCNET), allows for efficient, high throughput dosimetric computing capabilities ideal for dose optimization (see Chapter 3).

Clearly the technical expertise and experimental requirements for investigating boron neutron capture synovectomy are available at McMaster University. Given that roughly 1% of the world's population suffers from rheumatoid arthritis, and of those 10% require synovectomy, the result is a possible patient population of 6 million worldwide. For a treatment alternative with such promise as BNCS, studies remain in their infancy and are due further investigation at McMaster University.

1.4 Biological Studies

Generally speaking, the goal of BNCS studies at McMaster University is two-fold: (1) To develop a screening process for new BNCS agents which can be used as (2) a basis to apply to Health Canada for permission and funding to undergo pharmacokinetic and eventually human clinical *in vivo* studies. To this end, biological testing of the proposed compounds must be performed. As with any compound intended for human administration, initial testing must be composed of *in vitro* cellular and *in vivo* animal studies.

Boron neutron capture synovectomy research should utilize the resources and technology available at McMaster University while at the same time not disregarding the successful methodology of testing utilized by other groups worldwide. Keeping to a similar strategy of testing will allow for near direct comparison of results and aid in the conclusion of success or failure of a developmental compound. In addition to biological safety, the performance of the compound with respect to the dosimetric impact need be addressed. Of critical importance is the evaluation of the RBE values for the tissues and compounds.

The MIT group performed *in vitro* compound uptake analysis using minced excised human synovium and cartilage obtained during surgical synovectomy of rheumatic patients.[5,11,16] Tissue samples were incubated for one

hour in medium containing 1000 ppm ^{10}B in unenriched KBH followed by washout time course studies in which the samples were reincubated in fresh medium for 0, 30, 60, and 120 minutes.[5] Bulk ^{10}B uptake was evaluated using PGNAA, where the ratio of ^{10}B to ^{1}H signal was used to correct for spatial inconsistencies in the sample positioning at the irradiation location. Boric acid standards were used to create $^{10}B/^{1}H$ ratio versus ^{10}B ppm concentration calibration curves. While promising uptake levels were determined, successive animal studies showed the effusion of the compound to be roughly 10 times higher, indicating that blood flow/active removal at the site could greatly affect the uptake concentration *in vivo*.[5]

Stritt (2001) and Crompton et al. (2001) described compound uptake and apoptosis studies performed using peripheral blood lymphocytes, HCT human breast carcinoma cells and TK6 lymblastoid cells at the Paul Scherrer Institut (PSI) in Switzerland.[17,18] Uptake of KBH was studied using PGNAA and apoptosis levels of treated cells following neutron irradiation were determined via flow cytometry. While uptake of the compound by the cells could not be measured, apoptosis studies did show increased cell killing when treating cells with KBH under neutron irradiation.

In order to determine RBE values for the radiation components of treatment, a method of evaluating cellular endpoints is necessary. Using

methodology similar to that of the PSI group, flow cytometry with staining markers can be utilized to determine several cellular endpoints: near apoptosis, apoptosis, and clonogenic death. Using SKY it is possible to measure the level of mutagenesis resulting from treatment. The endpoint for defining the RBE value should be apoptosis and/or necrosis, but RBE values for the endpoint of clonogenic death and mutagenesis could also be investigated as these pathways could also affect therapeutic action.

In order to use these biological techniques cells must be obtained from a reasonable source. One source of such cells could be via harvesting from synovial tissue samples, as per the BNCS studies at MIT. However, the impediment with this source is the lack of readily available patients, the necessity to co-ordinate with rheumatology/orthopedics, and the complex ethical approval process for such studies. A more practical source of cells is to use cells obtained from blood donors, as was performed by the PSI group.

Although there is great debate in the field of rheumatology as to the most critical target for arthritis therapies, there exists a large body of evidence that shows that monocytes, macrophages and lymphocytes play an especially critical role in the onset and continuation of rheumatic inflammatory episodes.[1-4,20-22] Glucocorticoids (steroids) have long been the most effective pharmaceutical treatment for rheumatoid arthritis.[23] The effect of these compounds is ubiquitous

in the cell types present in arthritic joints but is particularly directed towards monocytes and synovial macrophages. In these cell types glucocorticoids interfere with the DNA transcription of cytokine genes, leading to a reduction in the production of pro-inflammatory cell signals and ultimately suppression of the inflammatory response.[23-25] Glucocorticoids have been shown to induce apoptosis in monocytes and alter the differentiation of monocytes to macrophages.[25,26]

Recently it has been shown that encapsulating glucocorticoids in liposomes, microscopic phospholipid bilayers, strongly increases their therapeutic benefit in arthritic animal models.[27,28] Encapsulating clodronate, a widely prescribed pharmaceutical in bone diseases which prevents bone resorption, within liposomes has been shown to cause significant macrophage depletion when injected intra-articularly in rheumatic patients.[29,30] The common mechanism of therapeutic action in targeting these cell types has been identified to have initiated from the phagocytotic behavior of these cell types. Liposomal encapsulation has already been exploited for BNCS studies with both complex organic boronates and salt forms of the polyhedral closo-boronate ion.[31,32] Specifically, van Lent et al. (2006) showed selective elimination of synovial macrophages by neutron treatment of liposome-encapsulated sodium dodecahydrododecaborane.[32]

Apoptosis studies using flow cytometry have been widely performed at McMaster University using leukocytes from the extracted blood of volunteer

donors obtained via histopaque gradient isolation.[33] Although the studies to date have focused on the lymphocyte subpopulation, included in the isolated leukocytes are also monocyte and macrophage subpopulations, which as discussed above have a related treatment response to type-A synoviocytes. Given that monocytes and macrophages also play a significant role in the arthritic inflammatory response, these cell types should be studied in addition to lymphocytes to infer boron compound performance in rheumatic joints of animal models. Using the histopaque gradient isolation method on peripheral blood of volunteer donors provides a reliable means of obtaining monocytes and macrophages. Since the lymphocyte subpopulation is included in the isolated leukocytes, studies can easily incorporate the additional information gained from this cell type and allow for direct comparison with studies published using lymphocytes as the cell-type of choice.

Cartilage tissue is composed mainly of chondrocytes, which would also need to be harvested to compare acquired data for cartilage tissue. Alternatively, type-B synoviocytes and chondrocytes are available in both arthritic and healthy human form from cell culture banks such as Asterand Plc. (Detroit, MI, USA). Thus, in place of tissue samples acquired during surgical synovectomy, composite joint tissue cell lines could be used for compound testing if desired.

In vitro toxicity, uptake, washout, and RBE studies can be performed using these cell lines. If the therapeutic performance of the compound so merits, studies in animal models can proceed. Once the testing process has been proven to work, it can be repeated for other boron compounds.

2 Preliminary Boron Measurement Studies

2.1 Preliminary Boron Measurements - Introduction and Background

The primary techniques used throughout chemistry for boron quantification are neutron activation analysis (NAA) and inductively coupled plasma mass spectrometry (ICP-MS). While ICP-MS offers extreme sensitivity, in the range of parts per billion (ppb) to parts per trillion (ppt), this form of measurement is not available to exploit at McMaster University and requires outsourcing at a cost on the order of $200 per sample.[42] ICP-MS requires that samples with particulate, such as those with cells and biological contaminants, go through moderate preparation via chemical digestion prior to analysis. Additionally, ICP-MS requires analysis via technically skilled personnel to ensure accurate calibration and quantification of the elemental composition of the sample.

The widely known advantage of NAA is that samples require no *a priori* chemical preparation since the detection technique exploits radiative emissions that follow nuclear interactions of the samples' elements with incident neutrons. Generally, however, sensitivities are on the order of parts per million (ppm), significantly worse than ICP-MS. Neutron activation analysis of boron is based on the same nuclear capture reaction as that utilized for BNCS. The reaction,

$^{10}B(n,\alpha)^{7}Li$, produces energetically excited ^{7}Li 94% of the time.[43] The de-excitation is accompanied by the emission of a 478 keV gamma ray with a half-life on the order of femtoseconds. Thus, the emission of the gamma ray is virtually instantaneous after interaction with a neutron, from which the term prompt gamma neutron activation analysis (PGNAA) was coined.

The source of neutrons at the PGNAA facility at McMaster University is generated within the reactor core of the McMaster Nuclear Reactor. McMaster Nuclear Reactor (MNR) is a water-cooled open swimming pool-type reactor that utilizes low enriched uranium (19.75% ^{235}U) fuel assemblies in U_3Si_2-Al form. The reactor core consists of a 9 x 6 matrix of 8 cm x 8 cm x 60 cm fuel, reflector and irradiation assemblies. Of the 54 assemblies, 35 are fuel assemblies consisting of 225 or 284 g of ^{235}U per assembly. The PGNAA irradiation site is located at beam port (BP) #4 of MNR. Beam port #4 is built as an extension to beam tube #4 which allows neutrons to be transported from the reactor core region through the reactor pool wall.

Beam collimation and shielding at BP#4 is achieved through the combination of concrete, aluminum, lead, steel, polyethylene and wood utilized in the walls and beam components. High energy neutron filtration is achieved via dual silicon (Si) and sapphire (Al_2O_3) beam filters. These compounds possess the useful property that their macroscopic cross section is dependent on the

de Broglie wavelength of neutrons; the cross section for low energy neutrons (thermal) is low and increases exponentially for higher energy neutrons. This allows for high energy neutrons to be effectively filtered out from a beam of neutrons with a wide energy distribution that exists within the reactor core. At the beam exit the resonance to thermal neutron fluence rate ratio is on the order of 6 x 10^{-4}. Along with both the distance from the reactor core and the collimating components, the result is a highly collimated and very pure thermal neutron beam (99.94% thermal neutrons with cadmium ratio of 148). The average thermal neutron fluence rate is 3.98 x 10^{7} neutrons/cm^{2}s at a nominal reactor power of 3 MW. Figure 1 (over) is a schematic of the PGNAA facility showing major components of the BP#4 prompt gamma irradiation facility.

The facilities for PGNAA at McMaster Nuclear Reactor are well established and utilized routinely to analyze geological samples for various commercial compositional quantification companies, including Activation Laboratories Limited in Ancaster, ON, Canada. The pneumatic system employed, known as the "Rabbit System", utilizes durable plastic tubing with half inch inner diameter to transport sealed cylindrical polyethylene vials containing the material to be quantified. Samples are transported to and from the sample irradiation and counting position via pneumatic pressure bursts. Typical samples measured at MNR include soil, dried plant material and mined rock.

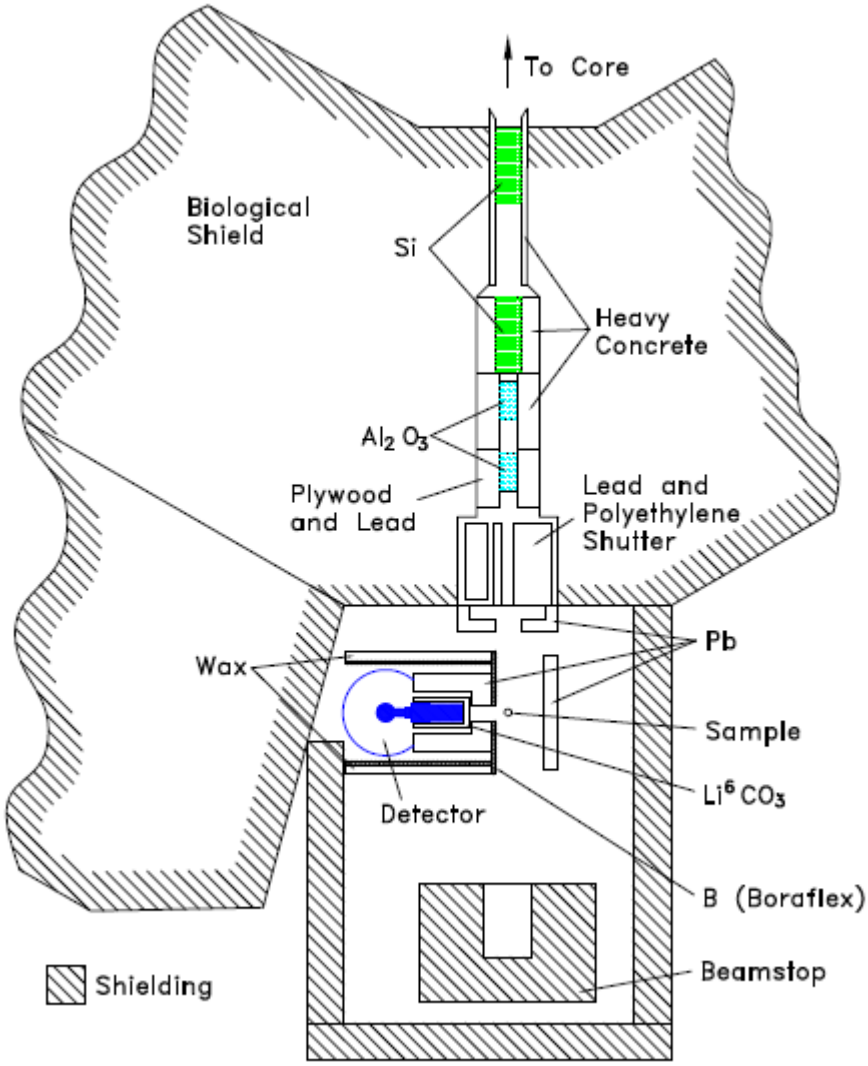

Fig. 1 Plan view schematic of the MNR PGNAA facility showing major components of BP#4. (Schematic courtesy of John Avelar, McMaster University).

The samples to be analyzed for the study of the biological uptake of boron compounds differ in that the samples are composed of cells suspended in solutions in liquid form, rather than dry samples. This posed a technical challenge in that there were no assurances that the vials could be properly sealed to a liquid tight state. Should any sample solution elute from the vials, the tubing and sample site could become contaminated with boron, requiring costly replacement of the

tubing and cleaning of the sample loader and diverter. In order to analyze the samples a new manually inserted apparatus was developed in this thesis work specifically for low volume liquid samples. In order to evaluate the performance of the new experimental setup, as well as to establish a baseline for future biological measurements, subsequent calibration curves for the liquid boron samples were generated to determine the minimum detection limit (MDL) of boron at the PGNAA site.

2.2 Preliminary Boron Measurements - Materials and Methods

Sample containers were prepared from 9" long-stem 2.3 ml capacity LDPE disposable transfer pipettes (EW-06226-10, Cole Parmer, Montreal, QC, Canada). Pipette tips were removed with scissors roughly 1 inch from the end. Sample solutions were transferred to the bulbs of the remaining pipettes via disposable syringes using 22 gauge needles attached to thin, fitted polyethylene tubing. Upon filling the chamber of the syringes, additional air was sucked into the chamber to remove solution from the distal end of the fitted polyethylene tubing. The tubing was then inserted into the inverted, modified pipettes until the end of the tubing was inside the bulbs of the pipettes, into which the sample solutions were dispensed. Having previously weighed and tarred the empty pipettes, the pipettes containing the sample solution were weighed prior to being sealed using a heat gun and pliers, and labeled.

A manual sample holder was modified to accompany the inverted sample filled pipettes. The manual positioning apparatus at the PGNAA of MNR utilizes a keyed base to ensure the proper positioning of the apparatus within the neutron field at the beam port (BP) window of MNR BP#4. The holder for the modified pipettes was a simple rod with welded machine screw of the same outer diameter as the inner diameter of the pipette stem. Upon manual attachment of the sample pipettes to the screwed end of the holder, the rod could be inserted into the manual apparatus via a hollow channel so that the sample pipettes were positioned within the neutron field. Positioning of the height level of the sample pipettes to be in the neutron field was accomplished using a drawn template of the manual apparatus and sample holder rod. A sketch of the experimental setup is provided in Figure 2 below.

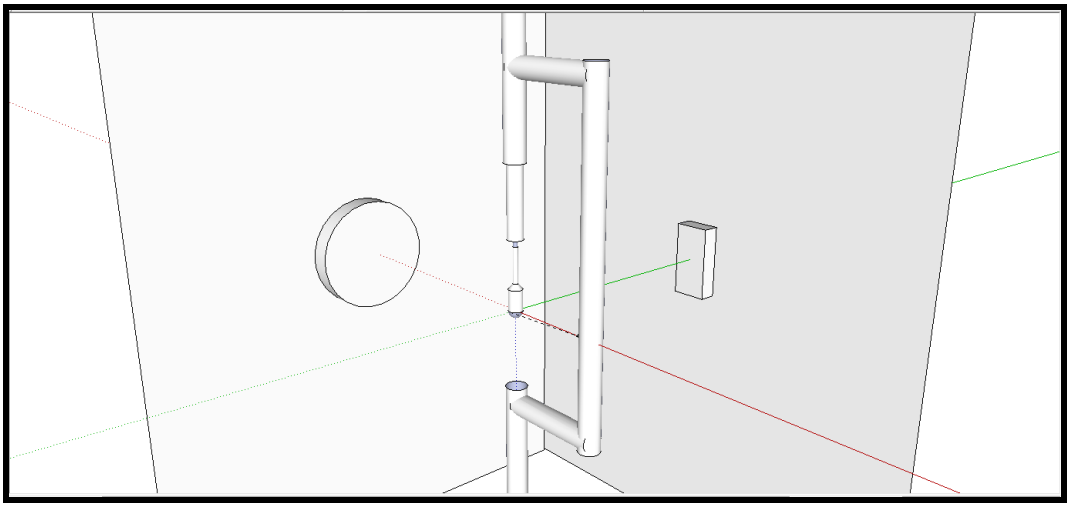

Fig. 2 Three-dimensional sketch of the experimental sample setup within the irradiation cavity of BP#4 of MNR. In the centre (origin) the modified sample pipette is shown supported by the manual loading apparatus. To the left, the cylindrical gamma detector face shielding is shown at the shield wall. To the right, the beam port exit is shown at the reactor pool wall.
(N.B. Diagram not to scale.)

The detection system included an Ortec GMX-13180 Hyper-Germanium Photon Detector System (Ortec Inc., Oak Ridge, Tennessee), Canberra Model 2020 Spectroscopy Amplifier (Canberra Co., Meriden, CT), ND581 Analogue-to-Digital Convertor and ND599 Loss-Free Counting System (Nuclear Data Inc., Schaumburg, IL), and Aptec MCArd AHV Version 7.04.00.03 (Canberra Co., Meriden, CT). Spectrum collection software employed was Aptec 5.11 Release 9 (Aptec Engineering Limited, Canberra Co., Meriden, CT). A schematic of the detection system setup is provided in Figure 3 below.

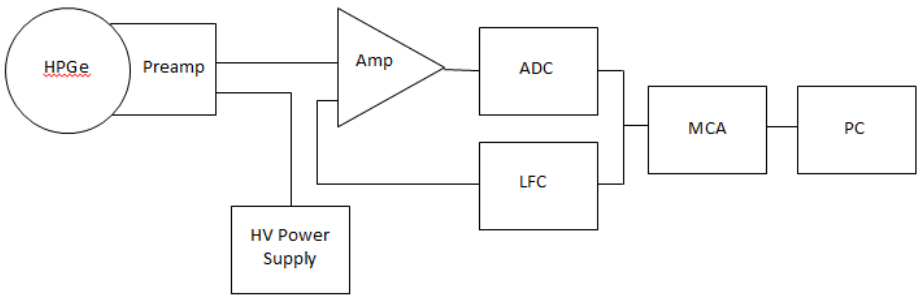

Fig. 3 Schematic diagram of electronic setup used for PGNAA detection.

Sample irradiation and concurrent spectrum collection was performed for 30 minute time intervals for low quantity boron samples and background counts. The counting time interval was shortened to as low as 60 seconds for larger quantities of boron that yielded count rates that provided sufficient peak statistics (~5000-10000 counts). Since radiation detection uncertainties are governed by Poisson statistics this equates to relative uncertainties of ~1-1.5%. Prior to irradiation and collection of the first sample on any given day, a 1000 ppm ^{10}B

standard and sample blank were irradiated and counted to ensure neutron flux stability and preclude boron contamination from previous days' measurements.

Calibration standards with water as the substrate solution were prepared with two boron sources. Nominal elemental boron solutions with concentrations of 1000, 100, 10, and 1 ppm were prepared using the stock solution and serial dilutions of 1000 ppm "Boron atomic absorption standard solution" (Sigma-Aldrich Canada Ltd., Oakville, ON, Canada) with high-performace liquid chromatography (HPLC) water (Caledon Laboratories Ltd., Georgetown, ON, Canada). Additionally, an 8575 ppm elemental boron stock solution was prepared by dissolving 0.49035 g of boric acid in 10 ml HPLC water. Serial dilutions resulted in additional standards of 857.5, 85.75, 8.575, and 0.8575 ppm elemental boron. Calibration standards for both complete RPMI and Hank's Balanced Salt Solution (HBSS) were prepared by generating 5000 ppm stock solutions wherein 0.28585 g of boric acid was diluted in the respective solutions. Serial dilutions resulted in standards of the following concentrations (all quoted in ppm elemental boron): 5000, 1000, 500, 100, 50, 10, 5, 1. All dilutions were prepared using analytical balance and volumetric flask and resulted in errors of less than 1%. Additionally, 0 ppm blanks were included for calibration purposes by using the respective solutions alone.

2.3 Preliminary Boron Measurements - Analysis

In order to correct for geometric and volumetric inconsistencies between samples a relative method of measurement was employed to analyze the specific quantities of boron as was performed by Yanch et al. (1999), Baechler et al. (2002) and Byun et al. (2004).[5,44,45] Whereas the absolute method requires experimentally determining the neutron flux and performing timely calculations to arrive at the boron concentration, the relative method requires selecting a spectral line from an elemental component in the spectrum that is also proportional to the neutron flux, whose peak area acts as a normalizing factor.[44] The normalized signal for various standard boron concentrations is then plotted against the known boron concentration, from which the MDL and unknown sample concentrations can be determined.

The spectral line chosen was that of hydrogen, which is highly prevalent in neutron activation spectra due to the large quantities of wax shielding implemented in the surrounding areas. The hydrogen capture reaction, $^{1}H(n,\gamma)^{2}H$, yields a 2.2 MeV gamma ray which is well above the spectral line of ^{10}B. Hydrogen is also present in the aqueous samples which could possibly enhance the hydrogen peak signal. However, in these studies it was determined that the hydrogen signal was weakly correlated to the mass of the samples ($R<0.6$), leading to the realization that the hydrogen background from the shielding and the

sample holder had a more profound effect on the hydrogen signal than aqueous hydrogen in the sample.

The relative method of measurement in this work comprises calculating the "specific signal" by normalizing the boron signal with the hydrogen signal arising from the hydrogen capture reaction, $^{1}H(n,\gamma)^{2}H$, and the mass of the sample as follows:

$$A = \frac{B}{H \cdot m_{sample}} \tag{1}$$

where A is the specific signal, B is the area of the ^{10}B 478 keV gamma peak in units of counts, H is the ^{2}H 2.2 MeV gamma peak in units of counts, and m_{sample} is the net sample mass in units of grams. Calibration curves for boron are then generated by plotting the specific signal as a function of the boron concentration of the boron standards at varying dilutions of boron, and performing a linear regression of the data. The resulting calibration curve takes the following form:

$$A = S \cdot C_B + I \tag{2}$$

where S is the slope of the calibration curve, C_B is the concentration of boron and I is the intercept of the calibration curve. Rearranging this equation and

solving for C_B yields the equation for calculation of unknown sample boron content based on the specific signal of the unknown sample:

$$C_B = \frac{A - I}{S} \tag{3}$$

As stated above, the hydrogen signal was poorly correlated to the sample mass (<0.6) indicating that the hydrogen signal was not being strongly contributed to by the sample contents itself but rather by the surrounding materials including the sample vial and beamline shielding. Since the hydrogen signal did not account for mass inconsistencies, the boron signal was exposed to inconsistencies in aliquoted volumes unless mass normalization was used to correct for such inconsistencies.

The variance in C_B is derived from the expansion of the partial derivatives of the component terms of Equation 3:

$$\sigma_{C_B}{}^2 = \left(\frac{\partial C_B}{\partial A}\delta A\right)^2 + \left(\frac{\partial C_B}{\partial I}\delta I\right)^2 + \left(\frac{\partial C_B}{\partial S}\delta S\right)^2 + 2Cov\frac{\partial C_B}{\partial I}\frac{\partial C_B}{\partial S} \tag{4}$$

where Cov is the covariance between the slope and the intercept. Taking the partial derivatives of Equation 3 and substituting into Equation 4 yields the

equation of the variance in C_B:

$$\sigma_{C_B}{}^2 = \left(\frac{1}{S}\right)^2 \delta A^2 + \left(\frac{-1}{S}\right)^2 \delta I^2 + \left(\frac{I-A}{S^2}\right)^2 \delta S^2 - 2\overline{C}_{B,cal}\,\delta S^2 \left(\frac{A-I}{S^3}\right) \qquad (5)$$

where δA is the uncertainty in specific signal, δI is the uncertainty in the intercept, δS is the uncertainty in the slope and $\overline{C}_{B,cal}$ is the average boron concentration in the calibration line. The minimum detectable limit (MDL) representing the nominal 95% confidence interval (i.e. $\sigma = 95.45\%$) is then defined as:

$$MDL = 2\sigma_{C_B} \qquad (6)$$

Analysis of the boron peak was performed using Origin 6.0 (Microcal Software, Northampton, MA, USA). The function fitted over the range of the boron peak was the following:

$$F(E) = F_{Bckg}(E) + F(E)_B \qquad (7)$$

where $F_{Bckg}(E)$ is the function of the background signal and $F_B(E)$ is the function of the boron peak. The background signal was modeled as a simple linear

function, namely:

$$F_{Bckg}(E) = aE + b \tag{8}$$

The boron peak does not display the typical Gaussian shape of spectral lines due to the Doppler-broadening of the gamma peak signal. This effect arises since the ^{7}Li fission product following the boron neutron capture reaction has finite energy and the emission of the gamma ray occurs while in motion relative to the lab frame of reference. Employed by both Baechler et al. (2002) and Byun et al. (2004), the method of Magara and Yonezawa (1998) was used to model the boron peak function.[44-46] This method models the boron peak as the difference of two error functions:

$$F_B(E) = \frac{A_B}{4}\{erf\,\frac{(E - E_{0,B} + k_B)}{\sigma_B\sqrt{2}} - erf\,\frac{(E - E_{0,B} - k_B)}{\sigma_B\sqrt{2}}\} \tag{9}$$

where A_B is the area of the boron peak solved for via non-linear curve fitting routines with Origin 6.0, $E_{B,0}$ is the central energy of the boron peak, and k_B and σ_B are additional fitting parameters.

In addition to the summation of the two functions in Equation (7), for boron samples with either complete RPMI or saline solution as the substrate, the following Gaussian function for ^{23}Na was modeled:

$$F_{Na}(E) = \frac{A_{Na}}{w_{Na}\sqrt{\frac{\pi}{2}}} e^{-2\frac{(E-E_{0,Na})^2}{w_{Na}^2}} \tag{10}$$

where A_{Na} is the area of the sodium peak, $E_{0,Na}$ is the central energy of the sodium peak, and w_{Na} is the width of the Gaussian-shaped peak. This peak was included due to the detectable quantities of sodium present in the biological solutions. Since the gamma ray of ^{23}Na at 472 keV overlaps the Doppler-broadened ^{10}B peak it is necessary to analyze the ^{23}Na peak function together with the background and ^{10}B peak.

Peak fitting and parameter analysis was accomplished using Origin 6.0's built-in non-linear curve fitting routine. The curve fitting routine offers parameter optimization via both Levenberg-Marquardt and Simplex methods. During fitting it was observed that for some spectra one method or the other yielded more stable parameter fitting and/or improved Chi-squared statistic reduction. Thus, by manner of observation the method which yielded improved results was used on any given spectrum.

The 2.2 MeV hydrogen gamma ray from the neutron capture reaction was found to show poor overall fitting statistics to a Gaussian function which resulted in overestimation of the error in the peak and ultimately the overall error via propagation through the B/H signal ratio calculation. The fitting of the hydrogen peak was also inconvenient due to frequent peak centre channel shifts that necessitated constant parameter verification and manual finessing of the variables in the fitting routine. A simple channel by channel Riemman summation over the range was applied as an alternate method to determine the integral hydrogen peak area. The application of this method was valid since there were no other peaks interfering over the integrated range.

The peak area was corrected for background signal by subtracting the estimated background, which was arrived at by simple linear regression over the range of the hydrogen peak integration. Channel by channel variation from the regression line was used to determine the error in the hydrogen peak area. The calculations were performed by a simple software program developed in Java 1.6.0 (Sun Microsystems, Santa Clara, CA, United States of America) executed on multiple raw-channel-input data files via MS-DOS batch executable commands, allowing for rapid automated data analysis. The linear regression routine incorporated into the program was obtained from open source scientific computing libraries and benchmarked against results from Microsoft Excel regression analysis and peak data obtained from fitting in Origin 6.0.[47]

2.4 Preliminary Boron Measurements - Results and Discussion

A sample boron spectrum for the 10 ppm boron calibration standard in HBSS showing sample fitted parameters is shown in Figure 4 below.

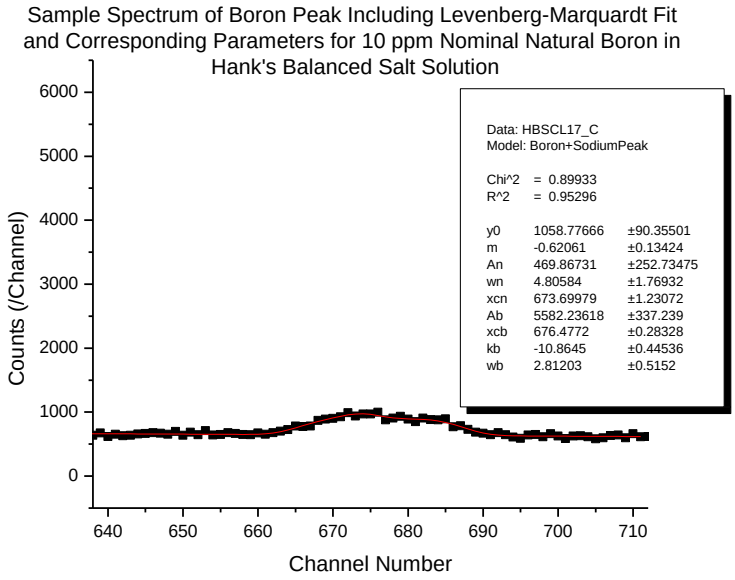

Fig. 4 A sample spectrum over the range of the boron peak for 10 ppm nominal elemental boron in Hank's Balanced Salt Solution (HBSS). The function fitted for Equations 8, 9 and 10 via Levenberg-Marquardt optimization, and the corresponding parameter values are also shown.

Calibration graphs for elemental boron in HPLC water, HBSS, and complete RPMI are shown over in Figures 5, 6 and 7, respectively. Regression analysis was performed using the built-in linear fitting routine of Origin 6.0 with error weighting.

The correlation coefficients of the results for boron in HPLC water, HBSS, and complete RPMI were 0.98556, 0.99878 and 0.99507, respectively,

showing that the response is strongly linear over the range of boron concentrations tested. The linearity of the results also indicates that there are no

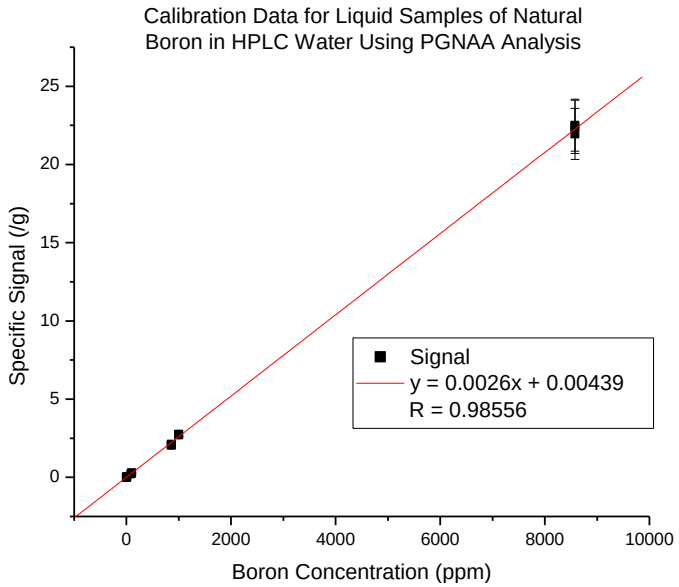

Fig. 5 Calibration curve for elemental boron in HPLC water. Linear regression, regression equation and correlation coefficient are also shown. (N.B. Error bars for 1000 ppm boron and less are indiscernible from the data points.)

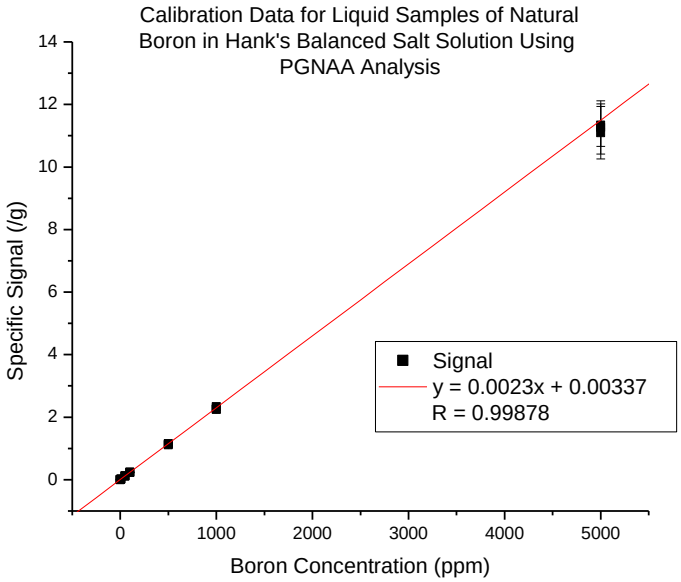

Fig. 6 Calibration curve for elemental boron in HBSS. Linear regression, regression equation and correlation coefficient are also shown. (N.B. Error bars for 1000 ppm boron and less are indiscernible from the data points.)

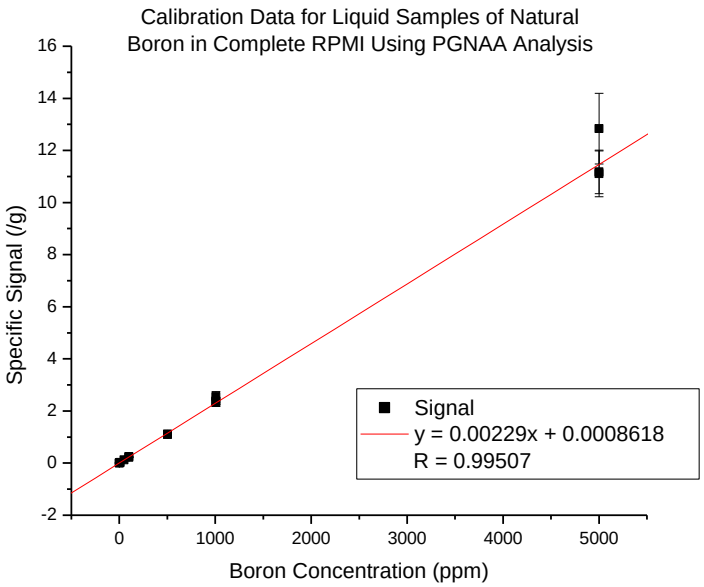

Fig. 7 Calibration curve for elemental boron in complete RPMI. Linear regression, regression equation and correlation coefficient are also shown. (N.B. Error bars for 1000 ppm boron and less are indiscernible from the data points.)

self-shielding effects within the samples below 5000 ppm of natural boron. The minimum detection limit (MDL) representing the nominal 95% confidence interval was calculated as $MDL = 2\sigma_{C_B}$, where $\sigma_{C_B}{}^2$ is the variance of the boron concentration derived from the expansion of the variance in the calibration curve equation (see Section 2.3). Using this metric the MDL values for HPLC water, HBSS and complete RPMI are 2.88 ppm, 3.34 ppm and 1.28 ppm, respectively.

The concentration of boron in the blank for each of the media was determined from the y-intercept of the calibration curves; for HPLC water, HBSS and complete RPMI the values were 0.0044 ± 0.0008 ppm, 0.0034 ± 0.0004 ppm, and 0.0009 ± 0.0005 ppm, respectively. The results were analyzed using a two-

sample Student's t-test. Comparisons indicate no statistically significant difference between HPLC water and HBSS (P>99.0%), HPLC water and RPMI (P>96.1%), nor HBSS and RPMI (P>96.9%). As a result, the conclusion cannot be made that any differing quantities of residual boron exist between the three substrate media.

While the MDL results of this study are in the range of 1-3 ppm, which is in line with the generally accepted detection limit of BP#4 at MNR for boron, this was significantly worse than the results published by both Byun et al. (2004) [0.067 μg] and Crittin et al. (2000) [0.0038 μg].[45,62] In these studies the MDL was calculated as $3\sqrt{N_B}/S \cdot t_m$, where N_B is the sum of the background counts in the ADC channels corresponding to the boron peak, S is the analytical sensitivity in cps/mg (i.e. slope), and t_m is the duration of the background measurement in seconds. Using this definition, the MDL for the calibration in HPLC water is calculated to be 1.67 μg, an improvement compared to the MDL calculated per Equations 5 and 6, albeit still significantly worse than the results of Byun et al. (2004) and Crittin et al. (2000).

The discrepancy between the results herein and the other published studies can be attributed to several factors. While a number of these factors are well defined, the discrepancy cannot be fully explained by them alone. Data for the other factors that may contribute to the discrepancy, however, were not readily

available for comparison. The well-defined factors that contribute to the discrepancy include differences between each study in terms of neutron flux, duration of sample counting/irradiation, and relative efficiency of the detector. The other factors that may contribute to the discrepancy include detector electronics, sample preparation and holder composition, irradiation facility characteristics and geometry, incident neutron energy spectrum and the gamma ray background from construction and shielding materials. These other factors, however, are more speculative because of the unavailability of raw data for direct comparison.

For the well-defined factors contributing to the MDL discrepancy some comparison with respect to the magnitude of their effect can be made. With respect to the neutron flux, for example, Crittin et al. (2000) and Baechler et al. (2002) performed studies at the SINQ spallation source at PSI where the flux was estimated at 1.4 x 10^8 neutrons/cm^2s.[44,62] Byun et al. (2004) performed studies at one of the beam ports of Seoul National University's (SNU) Hanoro reactor where the stated neutron flux at sample position was 7.9 x 10^7 neutrons/cm^2s.[45] As stated in Section 2.1, at 3 MW nominal power, the neutron flux at MNR BP#4 is approximately 4 x 10^7 neutrons/cm^2s, almost half that at SNU and 3.5 times less than that at PSI.[49] Using Poisson counting statistics, it is estimated that the MDL at MNR would be a factor of $\sqrt{2}$ (~1.4) poorer and $\sqrt{3.5}$ (~1.9) poorer than SNU and PSI, respectively, on the basis of neutron flux alone.

Another well-defined factor contributing to the MDL discrepancy is the difference in measurement times. At PSI measurement times varied from several minutes for samples with large quantities of boron to upwards of 46000 seconds in duration for minimally detectable amounts of boron [N.B. results were subsequently normalized to 24 hours by Crittin et al. (2000)].[44,62] At SNU, Byun et al. (2004) reported that samples were counted for 10000 seconds (~2.77 hours).[45] The maximal sample irradiation/counting time in this thesis work was limited to 30 minutes, a factor of several times less than the other studies. This time was selected as a practical counting time with the expectation of counting hundreds of samples in future studies. However, the shorter time obviously leads to a poorer detection limit. On the basis of counting duration alone, it is estimated that the MDL at MNR would be a factor of approximately 2.4 poorer and 6.9 poorer than SNU and PSI, respectively

Finally, of the well-defined factors contributing to the MDL discrepancy is the difference in the relative efficiency of the detector. The HPGe detector used at MNR had a measured certified relative efficiency of 14.4% at 1.33 MeV. In comparison, the relative efficiency at PSI was 36% and that at SNU was 43%.[44,45,62] On the basis of relative efficiency alone, it is estimated that the MDL at MNR would be a factor of approximately 1.7 poorer and 1.6 poorer than SNU and PSI, respectively.

By combining the three well-defined factors discussed above it is possible to gauge the proportion of their contribution to the total discrepancy of the MDL in this work versus that of the others. Combining the well-defined factors accounts for a discrepancy of 5.7 between the MDL at MNR and that at SNU. The reported difference, however, is approximately 25. Therefore, beyond the well-defined factors discussed above there are additional factors which must account for the remaining factor of roughly 4 between the MDL calculated in this work and that at SNU. Similarly, combining the well-defined factors accounts for a discrepancy of approximately 21 between the MDL at MNR and PSI. The reported difference, however, is approximately 440. Therefore, beyond the well-defined factors discussed above there are additional factors which must account for the remaining factor of approximately 21 between the MDL calculated in this work and that at SNU.

One factor which probably contributes to some of the remaining discrepancy between the MDL at MNR versus SNU and PSI is the type of sample containers utilized. The sample containers employed in the studies at PSI and SNU were all made of polytetraflouroethylene (Teflon®) in order to minimize boron background from hydrogen present in low density polyethylene (LDPE).[44,45,62] At MNR all sample holders, including those in this study, are made of LDPE, as other studies and production trace element analysis at MNR have generally not required detection below 1-3 ppm boron. Additionally, in order to

minimize the background contribution from hydrogen further, both Crittin et al. (2000) and Byun et al. (2004) utilized dehydrated samples, thus eliminating any hydrogen present in the samples via aqueous solution.[45,62]

In the absence of raw spectra it is difficult to quantify the additional contribution (versus SNU and PSI) to the background under the boron peak from hydrogen as a result of using an aqueous sample and LDPE container in this work. However, comparing the sensitivity data for the different facilities is instructive in this respect. The sensitivity as measured from the slope of the unnormalized boron signal in this work is 203 cps/mg, which is approximately 5.3 times lower than that at PSI reported by Crittin et al. (2000) [1075 cps/mg] and approximately 10.5 times lower than that from SNU reported by Byun et al. (2004) [2131 cps/mg].[45,62] Based on the well-defined discrepancy factors, a factor of 5.7 difference in sensitivity is predicted between MNR and SNU. The difference between the actual and predicted sensitivity of approximately 1.84 is considerably less than the predicted and measured difference of the MDL (i.e. 5.7). Since a MDL depends on extracting a signal from a background, while sensitivity is a measure of the signal itself, this may suggest that the signal-to-background ratios are significantly poorer for MNR as compared to SNU. Additionally, since the predicted/actual sensitivity (i.e. signal) differences are less than for the MDL differences, this implies the backgrounds are possibly higher at

MNR than at SNU. A similar argument can be made for a comparison of sensitivities and MDLs at PSI.

Additional factors for consideration when comparing the results herein with the results at PSI and SNU are the detection system characteristics. Crittin et al. (2000) also implemented the use of a Compton-suppression (CS) spectrometer, exploiting the use of an array of NaI(Tl)/BGO scintillators and a sophisticated fast electronic signal processing scheme to convert signals only when there was no coincidence between the CS scintillator signal (NaI/BGO) and the time signal of the germanium (within a 400 nanosecond time window).[62] Given that the background signal under the boron peak is presumably mostly due to hydrogen gamma rays which Compton scatter in the detector, then a system which preferentially removes background signal from under the boron peak in the acquired spectrum would be expected to improve the detection limit while not changing the sensitivity.

Other factors for consideration of the differences between the MDL results of the three facilities are the unique characteristics of each irradiation facility. As stated in Section 2.1, the PGNAA facility at MNR utilizes silicon and sapphire beam filters to yield a very pure thermal neutron beam with a cadmium ratio of 148 as measured through gold foil activation.[49] In comparison, Byun et al. (2004) used Bragg diffraction from pyrolytic graphite crystals and applied a focusing

technique with the crystals in order to maximize the flux at the sample position. In this manner a very pure thermal neutron beam with a cadmium ratio of 266 was achieved at SNU.[45] Crittin et al. (2000) on the other hand employed capillary-based neutron focusing optics in order to maximize the flux at the sample position. Although not explicitly reported, it is expected that the cadmium ratio at PSI is much higher than both MNR and SNU due to the inherent quality of the cold neutron beam from the spallation neutron source at SINQ.[62] These factors contribute to a lower mean energy of the neutron spectrum at SNU and PSI which may lead to differences in the mean neutron cross sections and ultimately improve the sensitivity of the PGNAA facilities.

Additionally, both Byun et al. (2004) and Crittin et al. (2000) minimized the use of boronated shielding compounds at the last stages of their irradiation facilities, instead making use of ^{6}LiF for both shielding and detector collimation.[45,62] The MNR PGNAA facility in this study differs in that Boroflex is used for the last stage neutron shielding and collimation for the HPGe detector. The presence of boron in the vicinity of the detector may negatively impact the background boron signal, and thus contribute to a lower signal-to-background ratio for the PGNAA samples.

The combined effect of the various differences between this study and those of Byun et al. (2004) and Crittin et al. (2000) ultimately equates to a

PGNAA facility that is less sensitive and has a poorer detection limit in measuring boron compared to the others. A summary of the experimental differences between this work and those of Byun et al. (2004) and Crittin et al. (2000) is presented in Table 1 below.

Table 1 Comparison of Experimental Differences for Prompt Gamma Neutron Activation Analysis of Boron.

	Byun et al. (SNU)	**Crittin et al. (PSI)**	**This Work (MNR)**
Neutron Source	Reactor	Spallation	Reactor
Neutron Flux (n/cm^{2}s)	7.9×10^7	1.4×10^8	3.98×10^7
Cadmium Ratio	266	Not reported	148
Detector Relative Efficiency (%)	43	36	14.4
Detector Distance (cm)	25	26.5	21.115
Counting Time (s)	≤ 10000	≤ 86400	≤ 1800
Sample Preparation	Dehydrated	Dehydrated	Aqueous
Sample Holder Material	Teflon	Teflon	Polyethylene
Compton Suppression Electronics	No	Yes	No
Sensitivity (cps/mg)	2131	1075	203
MDL (µg)	0.067	0.0038	1.67

2.5 Preliminary Boron Measurements - Conclusion

The MDL of boron in the tested geometry at BP#4 of MNR was in the range of 1-3 ppm. While the MDL of boron for the three solutions was not measured to be as sensitive in this study as those of other studies, the detection limits might be considered reasonable given the fact that future biological studies would test compounds at concentrations ranging up to several thousand ppm. However, in order to improve the detection limit for future studies, longer

counting times, which result in decreased background signal in general, could be used. Additionally, developing sample vials made of Teflon®, which contains no hydrogen, could also aid in improving the MDL of boron. Further biological testing would determine if improvements in the PGNAA setup are merited.

3 Implementation and Testing of MCNP5 on SHARCNET

3.1 MCNP5 on SHARCNET - Introduction and Background

The preliminary investigative analysis of Kreft (2005) compared the measured neutron flux in a stylized leg phantom with the simulated neutron flux in a phantom model using Monte Carlo N-Particle 5 (MCNP5).[57,58] The geometrical volumes, patient setup, and flux tallying of the simulated irradiation facility were not unlike those which would be implemented in practical dose planning calculations of arthritic knee joints of patients. During that work, the duration of simulation calculations was on the order of 24 h in order to generate results with sufficiently acceptable statistical uncertainties (~0.5%). While this was considered acceptable for one-off patient calculations, for optimization of experimental setup this calculation time represented a significant hindrance on productivity.

In an attempt to improve the throughput of Monte Carlo simulation results at McMaster University, execution of MCNP5 on a parallel computing platform was developed in this thesis work. MCNP5 was installed on the Shared Hierarchical Academic Research Computing Network (SHARCNET) (www.sharcnet.ca). SHARCNET is a high-performance computing network comprised of computational computing clusters based at 16 post-secondary

academic institutions in Southern Ontario. The MCNP5 source and executable distribution was compatible with both Parallel Virtual Machine (PVM) (www.epm.ornl.gov/pvm) and Message Passing Interface (MPI) (www.mcs.anl.gov/mpi) implementations.

3.2 MCNP5 on SHARCNET - Materials and Methods

The "wobbe" computing cluster based at McMaster University was designed in particular for the implementation of general applications in MPI and was selected as the optimal candidate cluster given the proximity to administrators and expertise in the area of parallel computing. The wobbe cluster contained a total of 208 64-bit processors (64 dual-core 1.8 GHz AMD Opteron with 4 GB RAM, 32 dual-core 1.8 GHz AMD Opteron with 8 GB RAM, 4 quad-core 2.6 GHz AMD Opteron with 32 GB RAM) with Myrinet and 1 GB ethernet connections. The operating system implemented on the wobbe cluster was Fedora Core 3 (i.e. Linux-based). The MCNP5 MPI-compatible executable was successfully compiled for the 64-bit platform from the source code using the Pathscale compiler with minor modifications to the Make file included with the MCNP5 distribution.

It was necessary in this thesis work to acquire an estimate of the performance enhancement (execution time) of running MCNP5 on locally

accessible parallel computing infrastructure and determine the ideal number of processors for use with varying simulated geometries. Theoretically, as the number of processors utilized for the execution of the simulation doubles, the execution time is halved (Figure 8). However, in practice, the execution time improvement reaches a limit at which point the use of additional processors for the simulation does not reduce the execution time further due to limits imposed by the inter-processor communication capabilities. Plotting the inverse of the time reduction as a function of processors yields the theoretical parallelization performance (Figure 9). In this examination, the optimal practical parallelization performance target of 70% of the theoretical performance was established.

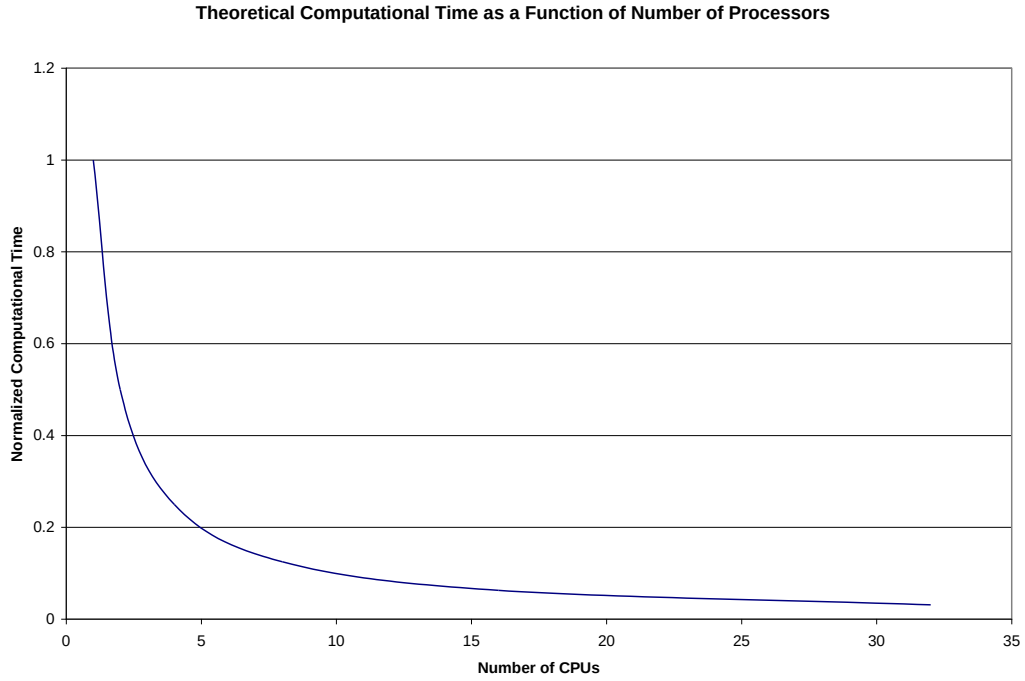

Fig. 8: Theoretical Relative Execution Time as a Function of Processor Number.

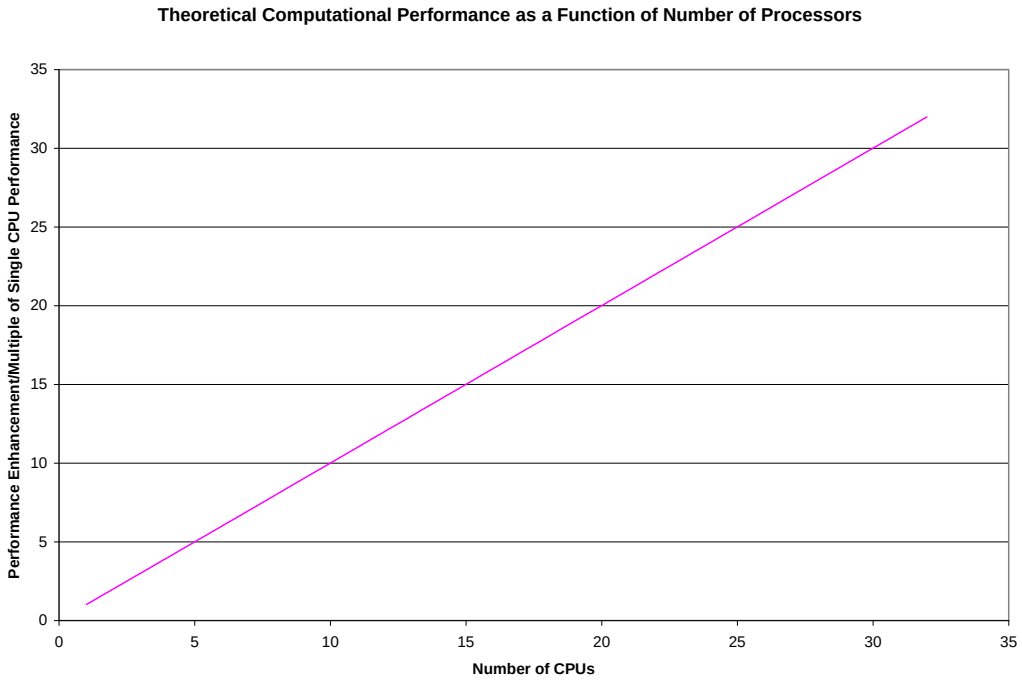

Fig. 9: Theoretical Parallelization Performance as a Function of Processor Number.

The 70% level was considered a compromise between overall speed (i.e. maximum number of processors) and efficiency (e.g. at 50% of theoretical performance half of the potential processor use for other simulations is wasted).

In practical MCNP5 usage, as the geometrical complexity of the simulated model increases so too does the execution time. Hence, it was a natural extension of this experience to test the computational performance enhancement using input files specifying differing geometrical complexities. Three geometrical models were considered for this purpose. The simplest model consisted of a point detector and cell-averaged fluence tally from a 10 cm sphere of radioactive gas. The model of Kreft (2005) was considered to be a moderately complex geometry.[58] In this

model the neutron interaction number on a copper foil at a distal locus of a leg phantom through an HDPE moderator was calculated. Finally, the k-code criticality calculation of the detailed McMaster Nuclear Reactor (MNR) was used to represent the highest level of tested geometrical model complexity.[64]

The method of measurement used for the evaluation of the performance was to perform three separate runs of the same input file for a fixed number of starting particles and document the execution time of the runs. Three time metrics are calculated and displayed upon simulation completion on wobbe: elapsed time, allocated time, and used processor time. The allocated and used times represent the actual duration times of computation. However, since users' productivity is a function of elapsed time, it was the selected metric for evaluation. The average and standard deviation of the three separate runs for each geometry were calculated and plotted as a function of the number of processors used in parallel to generate the execution time graphs. The inverse values of the execution time were then calculated and plotted as a function of the number of processors to generate the performance graphs. Finally, the performance efficiency was plotted and compared to the 70% performance target for the number of processors utilized.

3.3 MCNP5 on SHARCNET – Results and Discussion

Figures 10, 11 and 12 show the elapsed time, performance, and performance efficiency for the simple MCNP5 test geometry. Figures 13, 14 and 15 show the elapsed time, performance, and performance efficiency for the moderately complex MCNP5 test geometry. Finally, Figures 16, 17 and 18 show the elapsed time, performance, and performance efficiency for the complex MCNP5 test geometry.

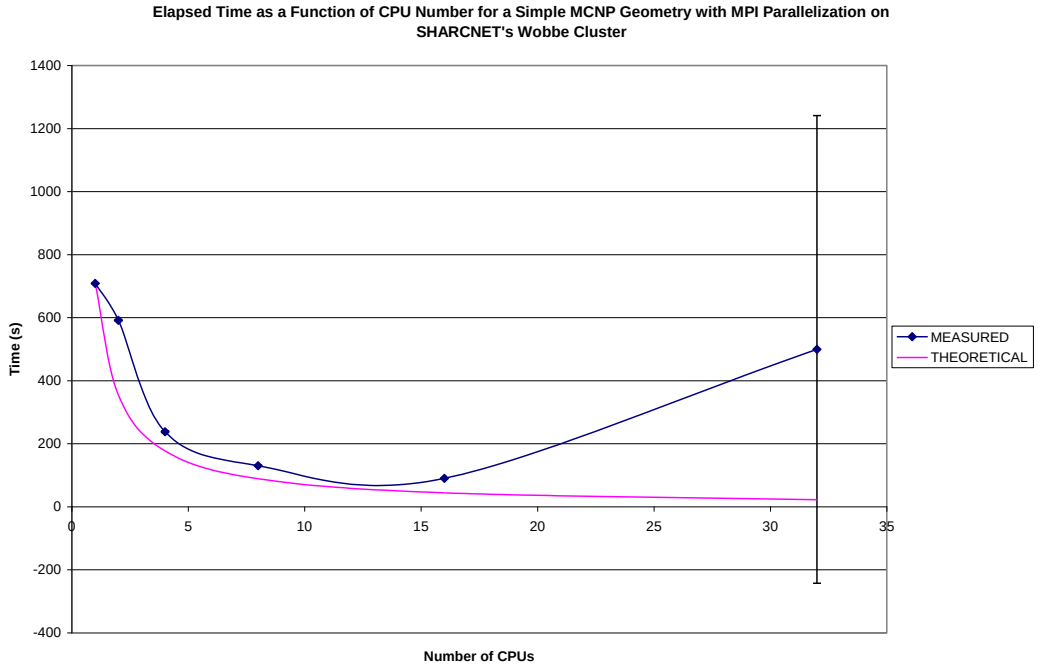

Fig. 10: Simple MCNP5 Test Geometry – Elapsed Time as a Function of Processor Number.

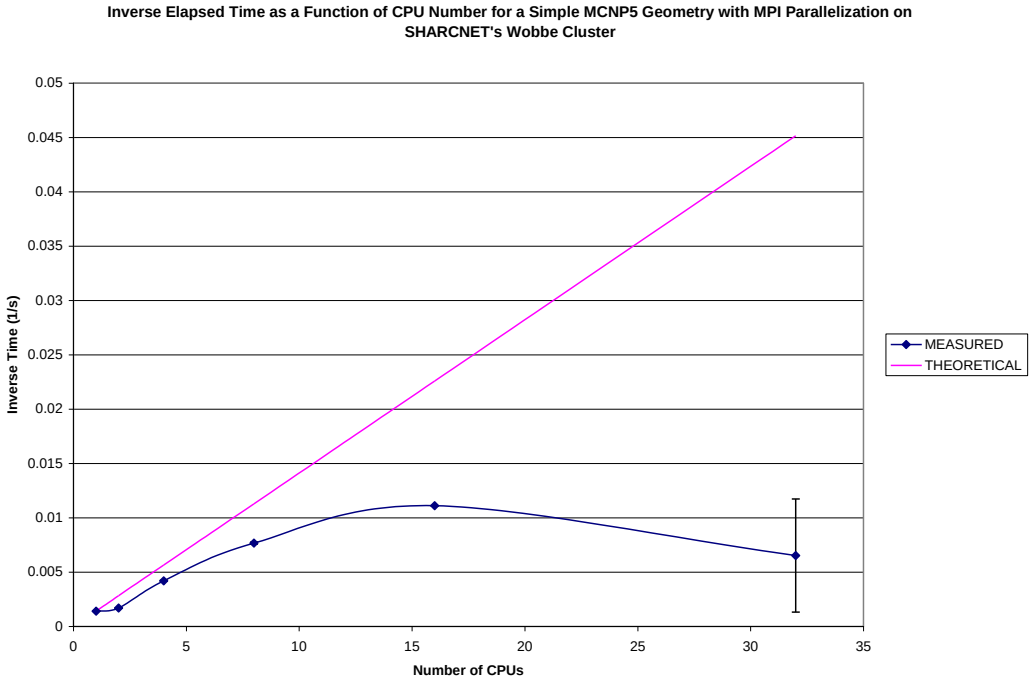

Fig. 11: Simple MCNP5 Test Geometry – Performance as a Function of Processor Number.

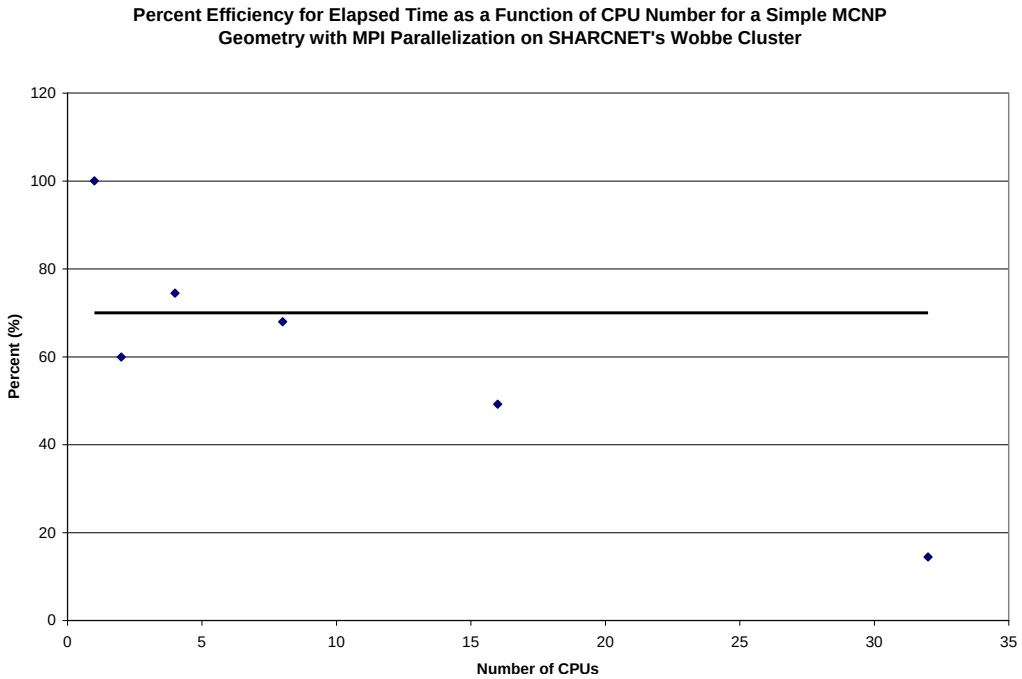

Fig. 12: Simple Complex MCNP5 Test Geometry – Performance Efficiency as a Function of Processor Number.

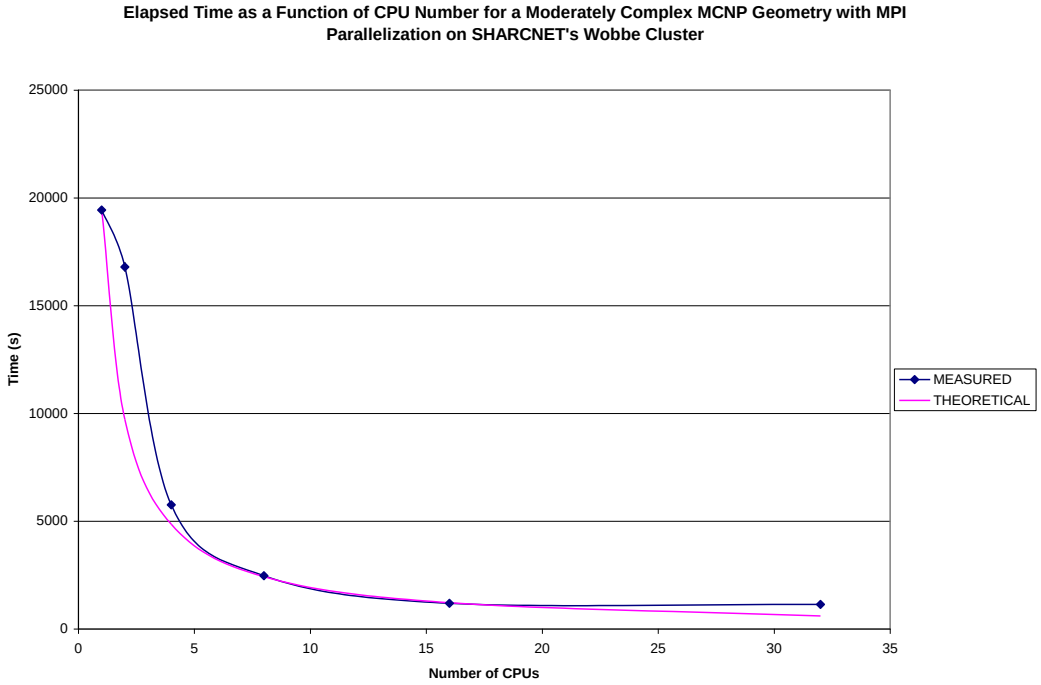

Fig. 13: Moderately Complex MCNP5 Test Geometry – Elapsed Time as a Function of Processor Number.

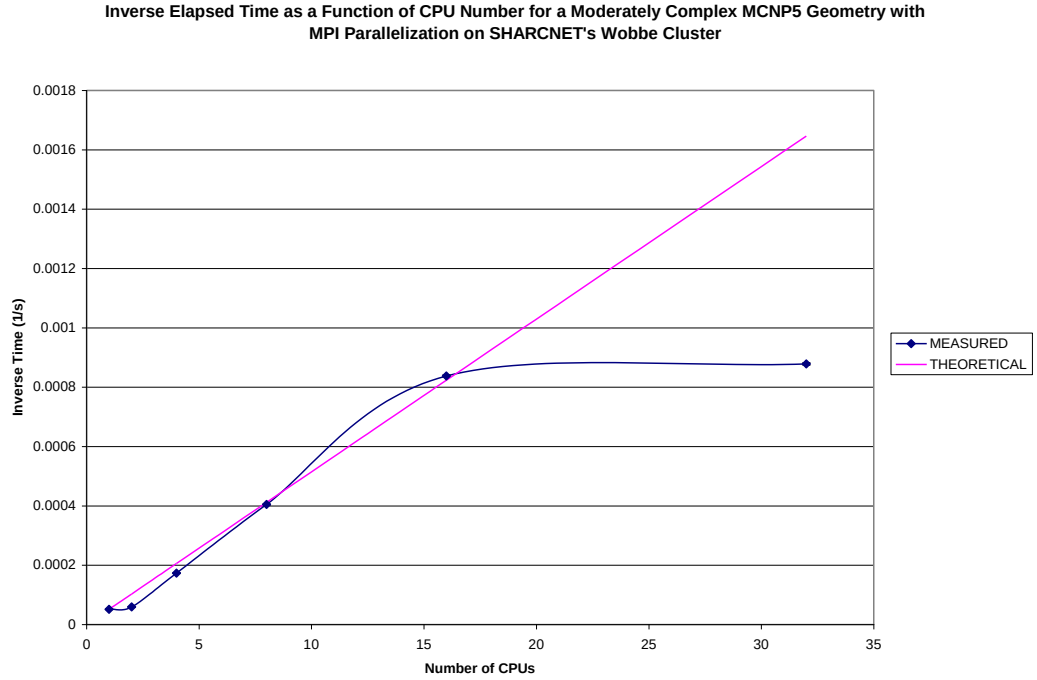

Fig. 14: Moderately Complex MCNP5 Test Geometry – Performance as a Function of Processor Number.

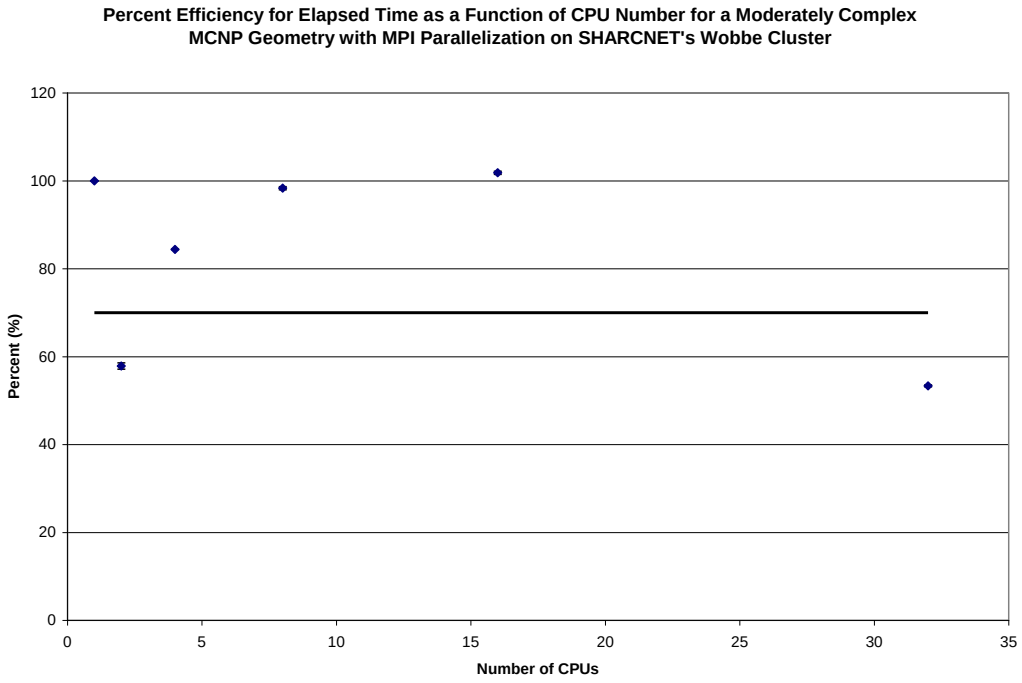

Fig. 15: Moderately Complex MCNP5 Test Geometry – Performance Efficiency as a Function of Processor Number.

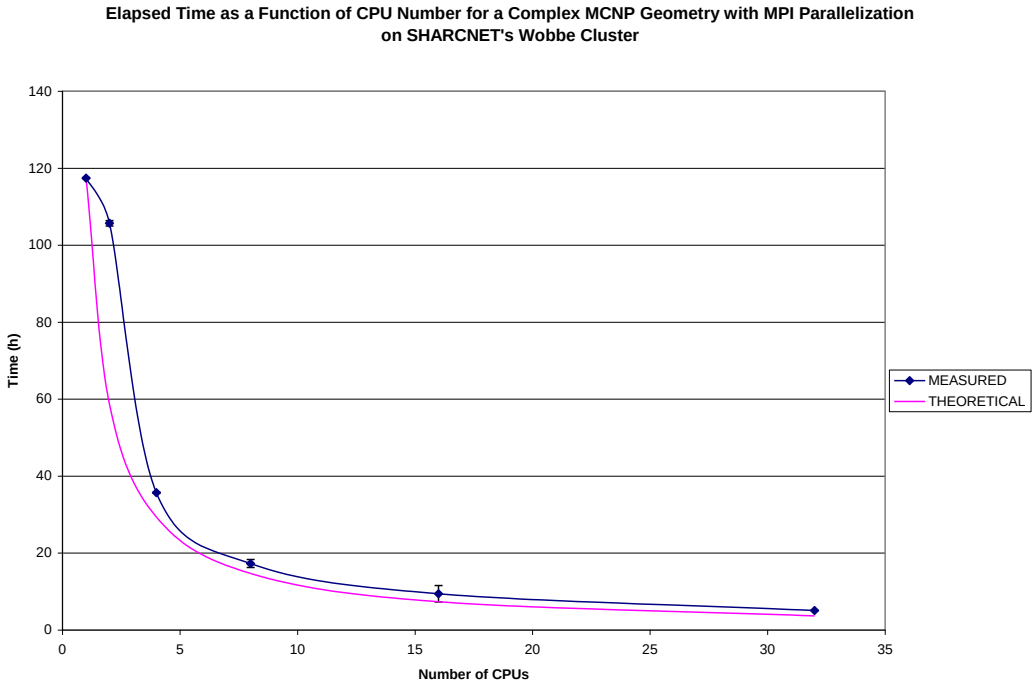

Fig. 16: Complex MCNP5 Test Geometry – Elapsed Time as a Function of Processor Number.

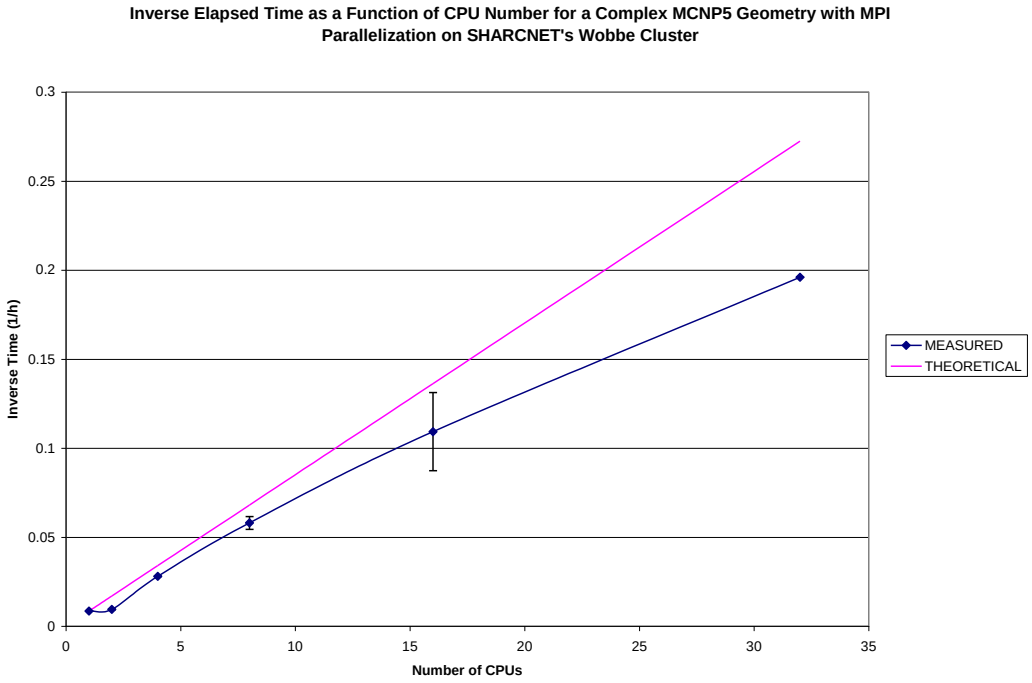

Fig. 17: Complex MCNP5 Test Geometry – Performance as a Function of Processor Number.

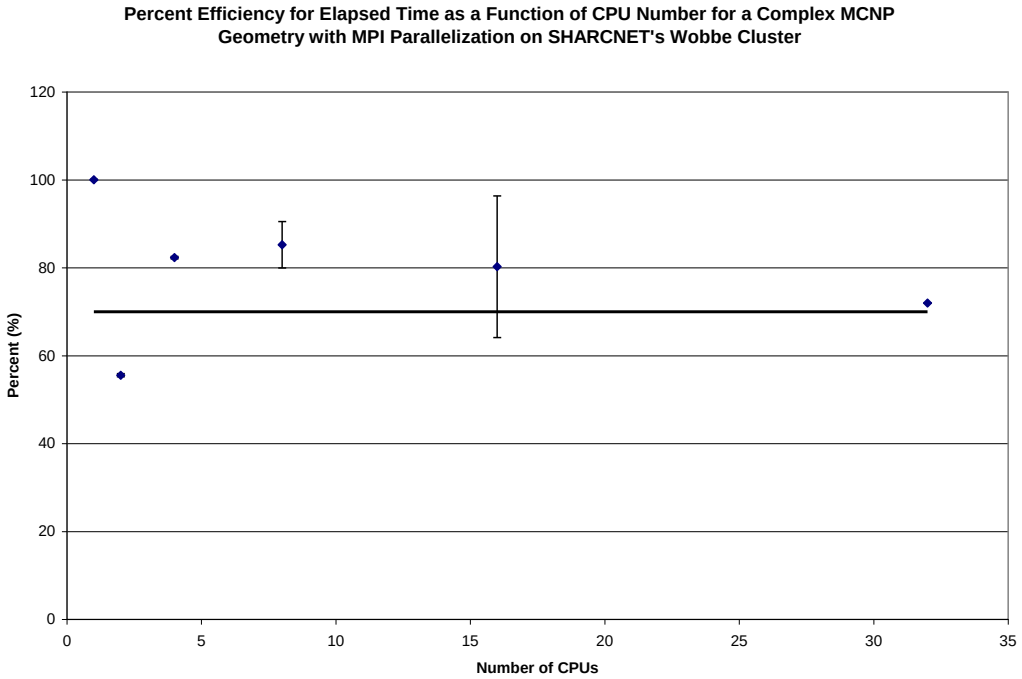

Fig. 18: Complex MCNP5 Test Geometry – Performance Efficiency as a Function of Processor Number.

Figures 10 through 12 indicate that for simple geometrical models, the elapsed time reduction is efficient up to 8 processors. Beyond this number of processors the process of message passing between processors overburdens the computational time. With 32 processors over 80% of the computational capacity of the processors is wasted. For the moderately complex geometry the elapsed time reduction is improved up to 16 processors as evidenced in Figures 13 through 15. With 16 processors the message passing process for the moderately complex model achieves a "sweet spot" resulting in a computational efficiency greater than the theoretical performance based on multiples of the single processor timing. Finally, Figures 16 through 18 demonstrate that excellent performance was achieved throughout the range of processor numbers used for the complex geometrical model.

Although the performance of the MCNP simulations increased with the increase in the number of processors practical limitations were observed during testing. Generally, the number of processors available on wobbe at any given time fluctuates from 0 to 40 due to the high demand of the cluster and user prioritization. If only one run with a complex geometry is required it may be worthwhile to wait for available processors if none are available (i.e. wait in queue). However, if many sets of runs are required, such as for sensitivity studies or model development, reducing the number of processors per run may allow the user to fit within the available processor number and maximize the overall

simulation set performance. For very large sets, such as might be utilized for on-the-fly genetic optimization model development, running all simulations on individual processors without parallelization may be ideal. In the latter case, the ideal SHARCNET cluster designed specifically for high throughput serial jobs is "whale", which has several thousand individual processors.

3.4 MCNP5 on SHARCNET - Conclusion

The Monte Carlo-based neutron transport code MCNP5 was implemented on the SHARCNET "wobbe" cluster as a means of significantly improving computational performance for analysis and evaluation of neutron flux in proposed geometries. Performance improvements on the order of a 10-fold reduction in executable time were successfully demonstrated for typical calculation types (e.g. neutron irradiation of phantom joint and reactor criticality). Although the expected performance improvement was realized, it was also recognized that actual performance improvement depended on availability of processors on the cluster. In practice, cluster use and number of processors should be selected on a case-by-case basis for maximum performance improvement.

4 Preliminary Studies of Biological Effects and Uptake of Boron Compounds

4.1 Biological Effects and Uptake Studies - Introduction and Background

Apoptosis studies have been widely used at McMaster University to quantify the effects of medical imaging and therapeutic radiation on lymphocytes.[33] The general methodology behind such studies involves isolation of lymphocytes from whole blood obtained by venipuncture of human donors, treatment of lymphocytes with both control and prescribed doses of radiation, and observation of the apoptotic response of such cells from which inference is made as to the response *in vivo* of the cells to the same radiation. Additionally, studies might observe other related effects of radiation, such as those by Schnarr (2007) in which the apoptotic response of lymphocytes of cancer patients, who received several "challenge" doses in the process of screening and treatment, was studied to understand how the adaptive response to radiation might mitigate the effects of DNA damage.[33]

While it is generally accepted by biologists that cell death occurs primarily via necrosis and apoptosis, several other pathways for cell death have now been identified including autophagy, mitotic catastrophe, paraptosis, and caspase-independent programmed cell death.[34-38] Necrosis refers to accidental injurious cell death which results in an inflammatory response in normal individuals.

Apoptosis, commonly known as programmed cell death (PCD), on the other hand is a controlled termination of a cell's life which is highlighted by various histological and biochemical changes.[34-38] Changes characteristic of apoptosis include cell shrinkage, an increase in cell density, cell membrane changes including loss of adhesion, DNA condensation and DNA fragmentation.[34-38] Each of these physiological changes is accompanied by biochemical changes for which various compounds are available to detect the presence of these apoptotic signals.[39] While some of these compounds are themselves fluorescent, others can be conjugated to fluorescent chromophores which can then be detected via flow cytometry.[39]

In order to mimic treatment-like conditions, as well as utilize experimental methods that would allow for comparison of results with those of both the MIT group and the PSI group, it was necessary in this thesis work to modify the experimental protocols as prepared by Schnarr (2007). The studies performed by Binello (1995) incubated surgically excised tissues in enriched culture media containing the boronated salt KBH at different conditions.[11] Since the intent of the studies in this and future work at McMaster University was to utilize cells isolated from blood samples, the protocols from Binello were not directly applicable to this thesis work and could not be used herein. The studies performed by Stritt (2001) incubated whole blood cells in enriched culture media containing the boronated salt KBH at different concentrations prior to flow cytometry of the

whole blood samples.[17] This protocol too was not directly applicable to this thesis work since the experimental protocol of Schnarr separated leukocytes from whole blood prior to sample irradiation.[33] Post-irradiation the Schnarr protocol proceeded directly to flow cytometry analysis of cell apoptosis. However, due to the requirement for a period of incubation with boron compounds, as well as subsequent washing of the cells to remove the boronated substrate, it was necessary as part of this thesis to make unique modifications to the Schnarr protocol to incorporate these steps as there was previously no such existing protocol to utilize. Description of the protocol adaptation of previous work to experimental conditions herein follows in this chapter.

The experiments in the studies to follow at McMaster University would use novel organic compounds which led to concern over interaction of the compounds with the various proteins and growth factors found in such enriched media. The preference for the substrate of the compound solutions for cell incubation was a non-toxic, non-reactionary solution such as saline. However, since this type of solution lacked any vital nutrients, it was unknown as to the survival of the cells during the 1 hour incubation period, even in the control saline solution alone. Preliminary experiments were required to both modify the protocol and to test the viability of leukocytes following the interim incubation period in phosphate buffered saline (PBS) to ensure that the novel protocol would prove suitable. Following on the preliminary biological and boron measurement

work, initial studies of the effects of boron compounds on peripheral blood leukocytes were undertaken.

4.2 Developed Protocol for Boron Compound Incubation - Materials and Methods

Blood was taken from three individuals selected randomly from a cohort of volunteers at McMaster University under informed consent. Peripheral blood samples (10 to 20 ml) were obtained via venipuncture by a certified phlebotomist and collected in sodium heparinized Vacutainers® (BD Biosciences, Mississauga, ON, Canada). Blood samples were processed within 2 hours of collection.

Leukocytes were isolated via density gradient centrifugation. Blood samples were inverted several times to ensure homogenous dispersion. Patient blood was gently layered in 3 ml aliquots onto 3 ml of previously aliquoted room temperature Histopaque-1077 (Sigma-Aldrich, Oakville, ON, Canada) in 15 ml centrifuge tubes. The centrifuge tubes were then spun at room temperature for 30 minutes at 300 g, break on high. Following centrifugation, the leukocyte layer was clearly visible approximately half way up the centrifuge tubes. Using a sterilized Pasteur pipette, the blood plasma/Histopaque-1077 mixture above the leukocyte layer was discarded and the leukocyte layer from each centrifuge tube was pooled by transferring to 30 ml of cold PBS in a labeled 50 ml centrifuge tube.

Cells were washed several times to remove the Histopaque-1077. The centrifuge tube was inverted several times to ensure homogenous dispersion. Half the volume of the cell suspension (~ 17 ml) was transferred to an empty labeled 50 ml centrifuge tube. Both centrifuge tubes were topped to 30 ml with cold PBS. The cell suspensions were centrifuged at 0 ºC for 8 minutes at 250 g, break on high. Following centrifugation the supernatant was removed and discarded via pipette. The pellet was resuspended via forceful pipetting. Cold PBS was added to a total volume of 30 ml to one tube and cold complete RPMI 1640 medium (Lonza, Walkersville, MD, USA) [16.4% v/v Fetal Bovine Serum (PAA Laboratories Inc., New Bedford, MA, USA), 0.82% v/v L-glutamine (Lonza, Walkersville, MD, USA), 0.82% v/v Penicillin Streptomycin (Lonza, Walkersville, MD, USA)] was added to a total volume of 30 ml in the other tube. The procedure was repeated once more.

Following the final wash, a cell count was performed on a Z2 Counter (Beckman Coulter, Mississauga, ON, Canada). The cell count was adjusted to 5 x 10^5 cells/ml in each tube with cold PBS in the PBS-labeled tube and cold complete RPMI in the other, and 4 ml of the RPMI cell suspension was transferred to a labeled 25 cm^2 vented-cap tissue culture flask (Becton Dickinson, Franklin Lakes, NJ, USA) and placed on ice. The two 50 ml centrifuge tubes were incubated for 1 hour at 37 ºC in a water bath.

Since the procedure was such as to replicate the incubation of cells with boronated compounds, the cells were washed once again following the 1 hour incubation. Both centrifuge tubes were topped up to 30 ml with their respective solutions. The cells were pelleted at 0 ºC for 8 minutes at 250 g, break on high. Following centrifugation the supernatant was removed and discarded via pipette. The pellet was resuspended via forceful pipetting. Cold PBS was added to a total volume of 30 ml to both tubes. The procedure was repeated, adding cold complete RPMI to a total volume of 30 ml to both tubes following supernatant removal. The washing was again repeated adding cold complete RPMI to a total volume of 10 ml in both centrifuge tubes. The cell count was adjusted to 5×10^5 cells/ml in each tube with cold complete RPMI and 4 ml of each cell suspension was transferred to labeled 25 cm^2 vented-cap tissue culture flasks. The two culture flasks were placed on ice for 15 minutes to equilibrate to 0 ºC. All three culture flasks were incubated at 37 ºC, 95% relative humidity, 5% carbon dioxide for 44 hours.

After the 44 hour incubation period the tissue culture flasks were removed from the incubator. Cells were resuspended using forceful pipetting and washing of the flask walls. Flow cytometry tests were prepared by transferring 0.5 ml aliquots of each sample to 3 ml flow cytometry tubes. The tubes were capped and pelleted at 300 g at room temperature, break on high. Following centrifugation the caps were removed and the tubes were decanted of their supernatant and blotted

in an inverted position on bench towels to remove excess media. To each control tube 500 μL of PBS was added, and to each test tube 500 μL of 0.75 μM propidium iodide (PI) (Sigma-Aldrich, Oakville, ON, Canada) in PBS solution was added.

Samples were analyzed with a Beckman Coulter EPICS® XL Flow Cytometer (Beckman Coulter, Mississauga, ON, Canada). Viability of the cells was assessed using the well-established PI uptake endpoint. Propidium iodide is a flourophore which intercalates with DNA and RNA, enhancing its fluorescence. In isotonic solutions propidium iodide is normally prevented from entering the cell interior by the cell membrane, unless the membrane has been compromised as is the case for necrotic and apoptotic cells.[40]

4.3 Developed Protocol for Boron Compound Incubation - Results and Discussion

The percent uptake of propidium iodide for the three patients are shown in Figure 19 (over). As can be seen, there was little observable difference between the levels of propidium iodide uptake for the cells incubated for 1 hour in PBS and those incubated for 1 hour in complete RPMI. Combining the results for the three patients yielded uptake levels of 2.00 ± 0.53 %, 2.77 ± 0.70 %, and 2.93 ± 0.66 % for standard protocol (SP), complete RPMI incubation and PBS incubation, respectively. The results were analyzed using a paired, two-sample

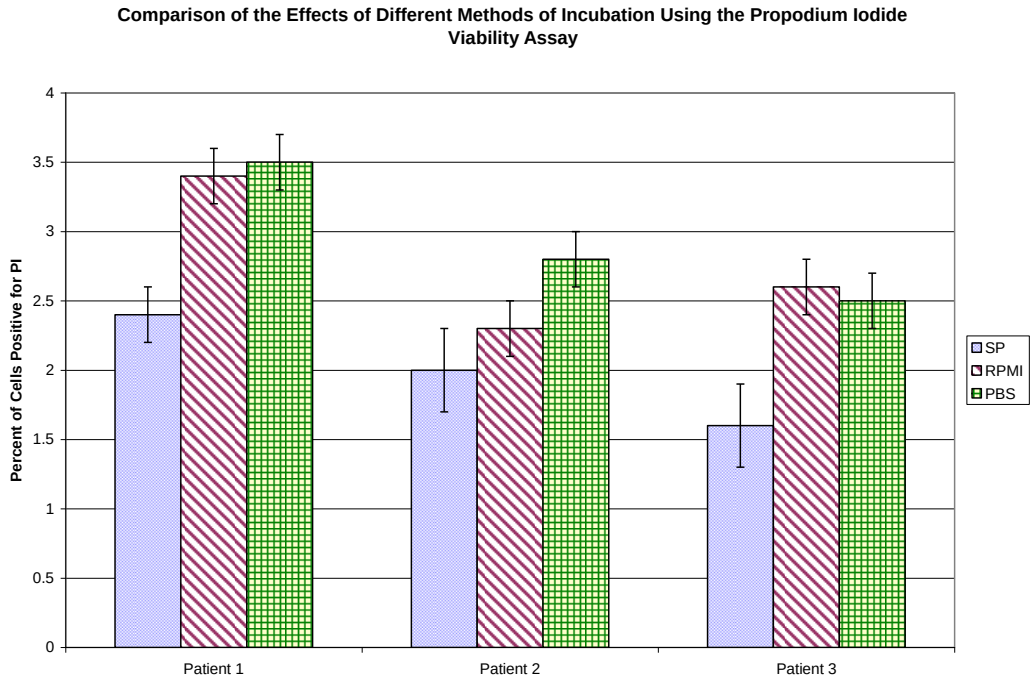

Fig. 19 Propidium Iodide uptake levels are shown as a percentage fraction of the total isolated leukocyte cell population for three volunteer blood donors. SP: standard 44 hour protocol without interim 1 hour incubation, RPMI: cells incubated for 1 hour in complete RPMI before being washed and incubated for 44 hours, PBS: cells incubated for 1 hour in PBS before being washed and incubated for 44 hours.

Student's t-test. Comparisons indicate a statistically significant difference between SP and RPMI (P>95.9%) and SP and PBS (P>99.5%), but no statistically significant difference between PBS and RPMI (P>44.4%), where the confidence level α is 0.05.

Based on the results above it was deemed that interim incubations in either saline solution or complete media would yield similar levels of apoptosis and necrosis and that the interim incubation was not significantly detrimental to the

cells' viability to preclude cellular studies in which cells would be incubated in solution with boronated compounds.

4.4 Biological Effects and Uptake Measurements - Background

Initially, there was a necessity to evaluate a simple compound to determine whether the PGNAA technique tested could be used to evaluate boron compound uptake. The compound selected for this purpose was boric acid. While boric acid is not known to have any functional cellular activity, the availability and low cost of this compound would allow for generous use within the scoping studies proposed.

Following flow cytometry and PGNAA work with boric acid, the desire was to attempt initial studies with the corticosteroid-carborane ester developed by Valliant et al. (2000); the expectation was that this compound could show the same functionality as that of other glucocorticoids with the additional benefit of having a significant fraction of its molecular weight made up of boron.[14] The infeasibility of using this compound in the present studies developed early on, however.

Hydrocortisone and other like glucocorticoids are solubilized in saline solutions via the hydrophilic groups of the esterized forms in which an acetyl

group or succinyl group is functionally reacted at the carboxyl group of the glucocorticoid (e.g. hydrocortisone acetate, hydrocortisone succinate). In the production of corticosteroid-carborane ester, the glucocorticoid is esterized to a highly non-polar carborane ring, which structurally resembles a soccer ball, increasing the hydrophobicity of the glucocorticoid group even further. Thus, in contrast to the acetate or succinate versions of the glucocorticoids, the carborane version is not soluble in water. Various attempts to solubilize the corticosteroid-carborane ester were made, including dissolution in 95% ethyl alcohol, addition of dimethyl sulfoxide in ranging amounts, as well as addition of α-, β-, and γ-cyclodextrins to no avail.

Although successful dissolution of the corticosteroid-carborane ester would likely require encapsulation within liposomes, the desire at this venture was to maintain experimental simplicity. The preference in this respect was to incorporate potentially non-toxic, organic boronated compounds that were water soluble. Three water soluble compounds that fitted these criteria had been recently developed by Andrew Green of the Valliant Group in the Department of Chemistry at McMaster University.[50] The three compounds developed all incorporated the *nido* structure of the carborane ring wherein the closed soccerball-like structure of the carborane ring (*closo*-carborane) is opened to resemble a nest (hence *nido*-carborane) due to the presence of one less boron atom in the structure compared to that of the *closo*-carborane. The compound

selected to be studied first was sodium [7-methyl-(β-D-glucopyranosyloxy)-7,8-dicarba-*nido*-undecaborate(-1)] or "Glucose *Nido*-Borane" (GNB). GNB is essentially D-glucose esterized to a *nido*-carborane ring and has a molecular weight of 348.59 g/mol. This compound was expected to be relatively non-toxic and perhaps have metabolic uptake into the cell due to the glucose functional group, and was the compound which was available in the largest quantity.

4.5 Biological Effects and Uptake Measurements - Materials and Methods

Blood was taken from three individuals selected randomly from a cohort of volunteers at McIARS under informed consent for studies with boric acid. Blood was taken from another individual selected randomly from the same cohort of volunteers, along with two of the patients from the first set of three individuals for studies with GNB. Peripheral blood samples (10 to 20 ml) were obtained via venipuncture by a certified phlebotomist and collected in sodium heparinized Vacutainers® (BD Biosciences, Mississauga, ON, Canada). Blood samples were processed within 2 hours of collection.

Leukocytes were isolated via density gradient centrifugation. Blood samples were inverted several times to ensure homogenous dispersion. Patient blood was gently layered in 3 ml aliquots onto 3 ml of previously aliquoted room temperature Histopaque-1077 (Sigma-Aldrich, Oakville, ON, Canada) in 15 ml

centrifuge tubes. The centrifuge tubes were then spun at room temperature for 30 minutes at 300 g, break on high. Following centrifugation, the leukocyte layer was clearly visible approximately half way up the centrifuge tubes. Using a sterilized Pasteur pipette, the blood plasma/Histopaque-1077 mixture above the leukocyte layer was discarded and the leukocyte layer from each centrifuge tube was pooled by transferring to 30 ml of cold Hank's Balanced Salt Solution (HBSS) (Invitrogen, Burlington, ON, Canada) in a labeled 50 ml centrifuge tube.

Cells were washed several times to remove the Histopaque-1077. The cell suspensions were centrifuged at 0 ºC for 8 minutes at 250 g, break on high. Following centrifugation the supernatant was removed and discarded via pipette. The pellet was resuspended via forceful pipetting. For boric acid studies, cold HBSS was added to a total volume of 30 ml to each tube, while for GNB studies cold complete RPMI 1640 medium (Lonza, Walkersville, MD, USA) [16.4% v/v Fetal Bovine Serum (PAA Laboratories Inc., New Bedford, MA, USA), 0.82% v/v L-glutamine (Lonza, Walkersville, MD, USA), 0.82% v/v Penicillin Streptomycin (Lonza, Walkersville, MD, USA)] was added to a total volume of 30 ml in each tube. The procedure was repeated once more.

Following the final wash, a cell count was performed on a Z2 Counter (Beckman Coulter, Mississauga, ON, Canada). The cell count was adjusted to 1 x 10^6 cells/ml in each tube with cold HBSS for the boric acid studies, and cold

complete RPMI for the GNB studies. An aliquot of 4 ml of each suspension was transferred to a labeled 50 ml centrifuge tube and placed on ice to act as an additional 44 hour control. The remaining cell suspensions were divided into 3 ml aliquots dispensed into labeled 15 ml centrifuge tubes for the boric acid studies and one of the GNB patients, and 2 ml aliquots for the remainder of the GNB studies. Into each tube double the volume of boron compound in HBSS was added at varying concentrations of boron to yield an approximate cell count of 5×10^5 cells/ml. The 15 ml centrifuge tubes were incubated for 1 hour at 37 ºC in a water bath.

Following the interim incubation the cells were inverted several times to ensure homogenous dispersion. From each 15 ml centrifuge tube in the boric acid studies 2 ml aliquots were transferred to labeled flow cytometry tubes. The cytometry tubes were placed on ice. The remaining cells in the 15 ml centrifuge tubes were washed to remove the compound. The 15 ml centrifuge tubes were topped up to 10 ml with HBSS. The cells were pelleted at 0 ºC for 8 minutes at 250 g, break on high. Following centrifugation the supernatant was removed and discarded via pipette. The pellet was resuspended via forceful pipetting. Cold HBSS was added to a total volume of 15 ml to all tubes. The procedure was repeated, adding cold complete RPMI to a total volume of 15 ml to both tubes following supernatant removal. The washing was again repeated adding cold complete RPMI to a total volume of 15 ml in all centrifuge tubes. Each cell

suspension and the 44 hour control sample were transferred to labeled 25 cm^2 vented-cap tissue culture flasks. The culture flasks were placed on ice for 15 minutes to equilibrate to 0 ºC. All culture flasks were incubated at 37ºC, 95% relative humidity, 5% carbon dioxide for 44 hours.

The cell suspensions in the flow cytometry tubes that were placed on ice during the washings were partially prepared for PGNAA. The flow cytometry tubes were capped and pelleted at 300 g at room temperature, break on high. Following centrifugation the caps were removed and the tubes were carefully decanted of their supernatant into empty flow cytometry tubes and tapped several times in inverted position to remove excess media. The decanted tubes were vortexed to resuspend the remaining cells. The tubes containing the decanted material were labeled as "Decant #1" plus the concentration at which they were incubated. The tubes were then capped and stored for PGNAA at a later time. To each of the decanted tubes 2 ml of cold HBSS was added. All tubes were vortexed and pelleted at 300 g room temperature, break on high. Again the contents of the pelleted suspensions were decanted into empty flow cytometry tubes. The decanted tubes were vortexed to resuspend the remaining cells. The tubes containing the decanted material were labeled as "Decant #2" plus the concentration at which they were incubated. Again the tubes were capped and stored for PGNAA at a later time. To each of the decanted tubes 2 ml of High Performance Liquid Chromatography (HPLC) water (Caledon Laboratories Ltd.,

Georgetown, ON, Canada) was added. The filled tubes were vortexed to ensure homogenous dispersion, labeled as "HPLC Cell Remnants" plus the concentration at which they were incubated. Finally, the tubes were capped and stored for PGNAA at a later time.

After the 44 hour incubation period the tissue culture flasks were removed from the incubator. Cells were resuspended using forceful pipetting and washing of the flask walls. Flow cytometry tests were prepared by transferring 0.5 ml aliquots of each sample to 3 ml flow cytometry tubes. Additionally, four control tubes were prepared by transferring 0.5 ml aliquots of the 44 hour control cell suspension to 3 ml flow cytometry tubes. The tubes were capped and pelleted at 300 g at room temperature, break on high. Following centrifugation the caps were removed and the tubes were decanted of their supernatant and blotted in an inverted position on bench towels to remove excess media. To all tubes 100 μL of HBSS was added and to each test tube 10 μL of R-phycoerythrin conjugated IgG2a RMO52 monoclonal antibody (CD14-PE) (Beckman Coulter, Mississauga, ON, Canada) and 10 μL 7-amino-actinomycin D (7-AAD) (Beckman Coulter, Mississauga, ON, Canada) was added. Additionally, 10 μL of CD14-PE was added to one of the control tubes to act as a CD14-PE control and 10 μL of 7AAD was added to one of the control tubes to act as a 7AAD control. All tubes were placed in the dark at room temperature for 15 minutes. To all test tubes 500 μL of 50 nM 3,3'-dihexyloxacarbocyanine iodide (DiOC6) (Sigma-Aldrich, Oakville,

ON, Canada) in distilled water was added. Additionally, 500 μL of 50 nM DiOC6 was added to one of the control tubes to act as a DiOC6 control and 500 μL of HBSS was added to the remaining control tube to act as a cells only control. All tubes were placed in the dark at room temperature for 15 minutes before flow cytometry.

Samples were analyzed with a Beckman Coulter EPICS® XL Flow Cytometer (Beckman Coulter, Mississauga, ON, Canada). Viability of the cells was assessed using the 7AAD uptake endpoint. Similar to propidium iodide, 7-amino-actinomycin D is a flourophore which intercalates with DNA and RNA, enhancing its fluorescence. In isotonic solutions 7AAD is normally prevented from entering the cell interior by the cell membrane, unless the membrane has been compromised, as is the case for necrotic and apoptotic cells.[51] The chemical flourophore DiOC6 is a cationic dye that is taken up strongly by mitochondria due to the high negative potential that these organelles have.[52] During apoptosis, changes in the membrane potential of mitochondria reduce the uptake of DiOC6. Together, 7AAD and DiOC6 act as a multiparameter flow cytometric test of apoptosis.[33]

The cell populations in the samples were separated into two functional groups for purposes of analysis. One of the groups for which gating was performed represented the total of the leukocyte and monocyte/macrophage

populations. These populations were identified by forward and side scatter plots. Additionally, another group for which gating was performed represented the monocytes/macrophages as identified by CD14-PE positive staining. The monoclonal antibody CD14 is known to have a high binding affinity to monocytes and macrophages, but does not bind to lymphocytes.[53]

For boron quantification, cell samples previously stored in flow cytometry tubes following decanting and washing were prepared for PGNAA. Flow cytometry tubes were vortexed to ensure homogenous dispersion of contents within the cell suspensions. Cell suspensions from each tube were transferred into tarred modified 9" LDPE pipettes using thin polyethylene tubing fitted to 22 gauge 3 ml syringes as outlined in Chapter 2. The sample pipettes were weighed and labeled prior to concurrent irradiation and measurement at BP#4 of MNR.

The relative method of measurement was used for boron detection as described in detail in Chapter 2. Briefly, boron peak area was determined using Levenberg-Marquardt and Simplex methods of the built-in non-linear curve fitting routines of Origin 6.0 (Microcal Software, Northampton, MA, USA). The function fitted was the sum of a linear background and the difference of two error functions. For those samples where the substrate was HBSS an additional Gaussian term was modeled to take into account the interfering signal from sodium present in the sample. The hydrogen peak area was determined as the

background corrected Riemann sum of the channel-by-channel data over the range of the peak. The specific signal, defined as the area of the boron peak divided by the area of the hydrogen peak and normalized by the mass of the sample, was used to determine the concentration of boron in the sample by rearranging the linear calibration equation of the respective sample solutions (HBSS or HPLC water).

4.6 Biological Effects and Uptake Measurements - Results and Discussion

Apoptosis levels of the cell populations were determined as those positive for both 7AAD and DiOC6, whose mitochondrial cell membranes had been compromised and whose DNA was fragmented. The apoptosis levels for boric acid are shown in Figures 20 and 21 for lymphocytes and monocytes/macrophages, and CD14+ cells, respectively. Apoptosis levels are shown as a percentage of the total cell population. While a noticeable increasing trend in the apoptosis levels of the total cell population is evident for increasing boric acid concentrations (Figure 20), such a trend is absent or indiscernible from the data obtained for the CD14+ monocyte population (Figure 21). The apoptosis levels, however, increase only in the range of 6% over two orders of magnitude in the treated concentration of boric acid, indicating little toxicity of boric acid at these concentrations using the apoptosis metric. The apoptosis levels for GNB are

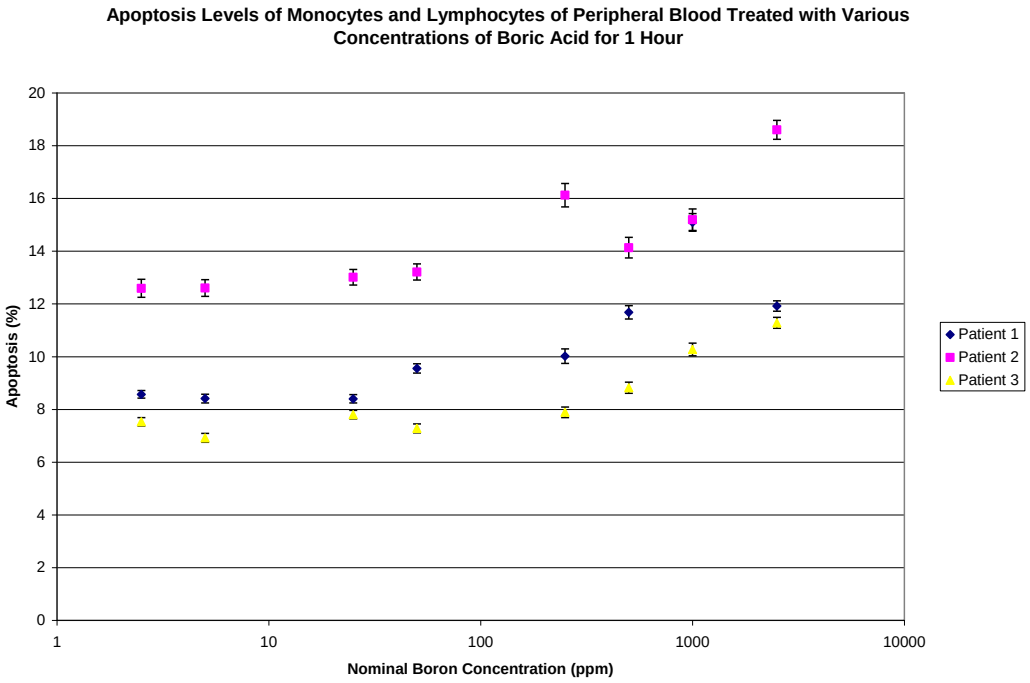

Fig. 20 Apoptosis levels after 44 hours of the cell population identified as both lymphocytes and monocytes by forward and side scatter following incubation for 1 hour with various concentrations of boric acid in Hank's Balanced Salt Solution.

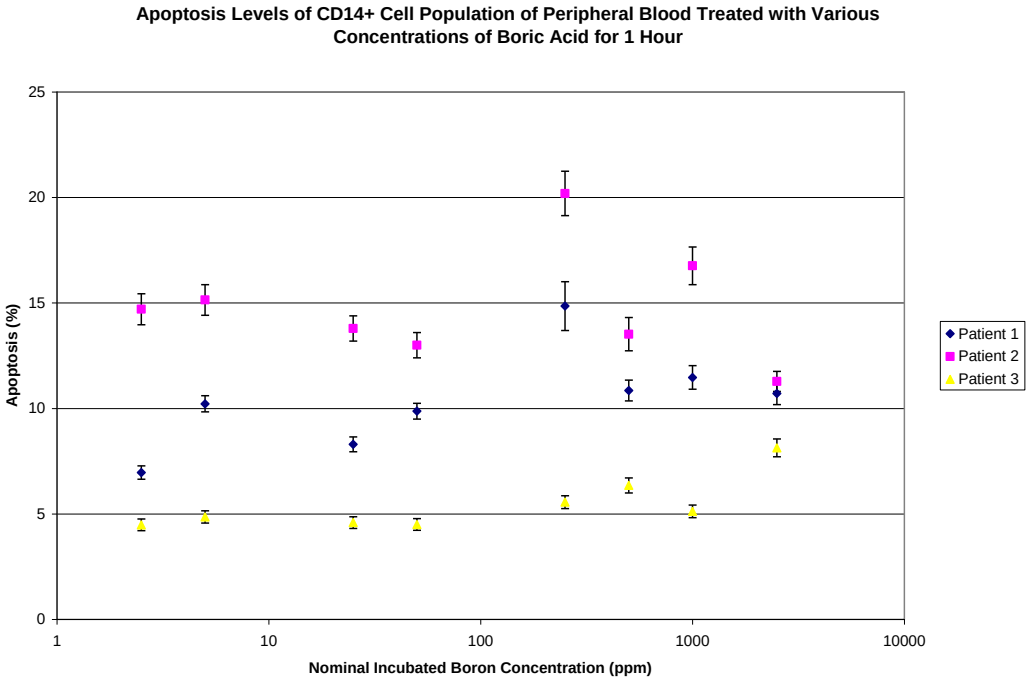

Fig. 21 Apoptosis levels after 44 hours of the cell population identified as monocytes by positive binding to CD14-PE following incubation for 1 hour with various concentrations of boric acid in Hank's Balanced Salt Solution.

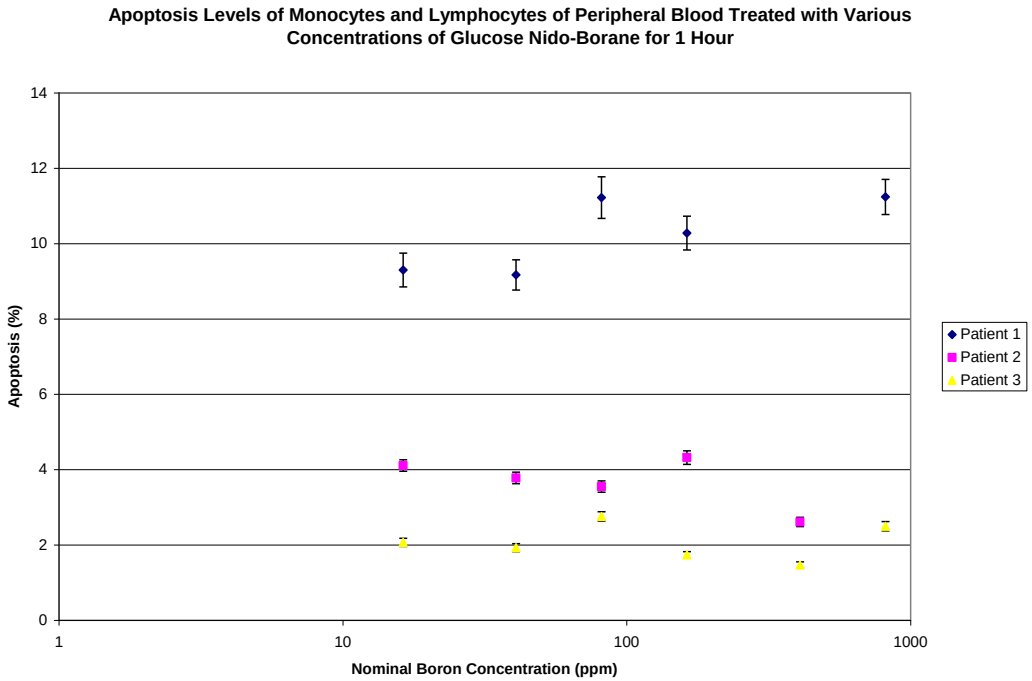

Fig. 22 Apoptosis levels after 44 hours of the cell population identified as both lymphocytes and monocytes by forward and side scatter following incubation for 1 hour with various concentrations of glucose *nido*-borane in Hank's Balanced Salt Solution.

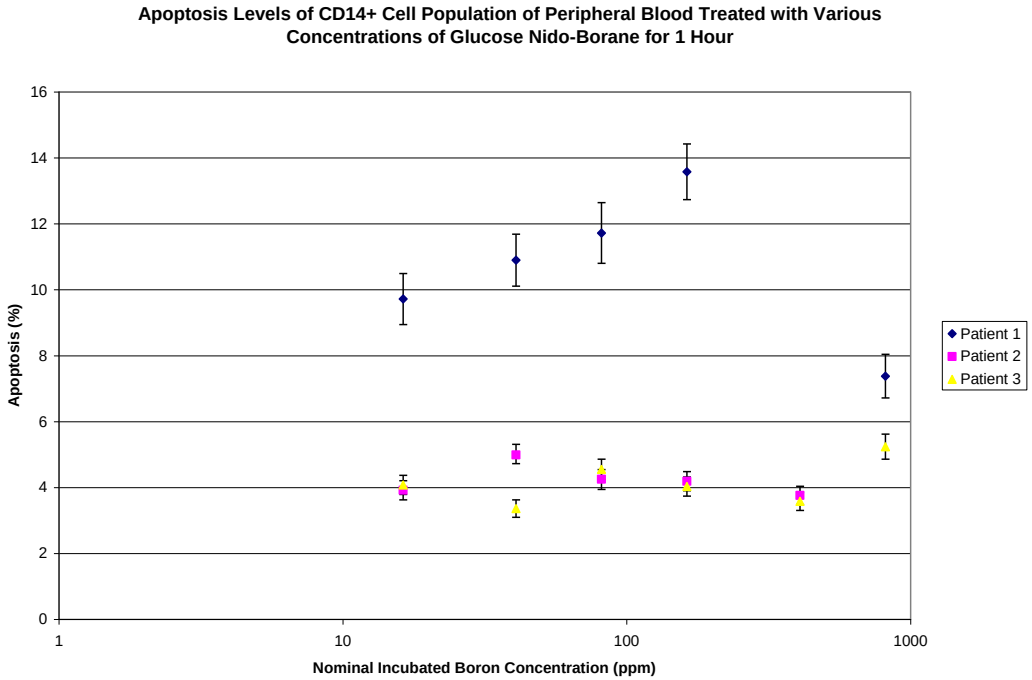

Fig. 23 Apoptosis levels after 44 hours of the cell population identified as monocytes by positive binding to CD14-PE following incubation for 1 hour with various concentrations of glucose *nido*-borane in Hank's Balanced Salt Solution.

shown in Figures 22 and 23 for lymphocytes and monocytes/macrophages, and CD14+ cells, respectively.

With the exception of the slight increase of roughly 2% apoptosis for Patient 1 in the total cell population (Figure 22), the apoptosis levels in both the total cell population and the CD14+ monocytes do not indicate any detrimental toxicity from GNB. Apoptosis levels for the range of GNB concentrations tested for Patients 2 and 3 (the same as Patients 2 and 3 for boric acid in Figures 20 and 21) indicate that the compound is no more toxic than boric acid at the same levels of boron. Of particular interest in two of the data series is the indication that at higher doses of GNB treatment apoptosis levels decrease compared to those at doses in the range of several ppm (Figure 22 Patient 2 and Figure 23 Patient 1).

Upon further literature review, several studies have indicated that the CD14 molecule plays a vital role in the apoptosis response of monocytes.[20,54-56] In particular, the expression of CD14 is down-regulated during apoptosis. The implication is that identifying the apoptotic response of the monocyte population by the expression of CD14 is inappropriate. This might explain the difference in responses to the two cell populations for boric acid above. Since the total cell population of monocytes, macrophages and lymphocytes was identified by forward scatter, this population could have correctly incorporated the apoptotic response of the compromised monocytes. On the other hand, gating for CD14+

monocytes may have discounted those monocytes which were in fact undergoing apoptosis and would have otherwise been detected as expressing uptake of both 7AAD and DiOC6.

Prompt gamma neutron activation analysis of the cells and washings was performed to determine whether uptake of boric acid could be measured by this technique in cognizance of the limit of detection as determined in Chapter 2. The decanted supernatant from each cell washing was measured in addition to the final washed isolated cells in order to observe the effects of the washing process on the boron concentration and provide additional insight into the overall process that might contribute to future process improvement. Sample data for Patient 1 are shown for Decant #1, Decant #2 and Remnants in HPLC water in Figures 24, 25 and 26 respectively. A sample boron spectrum for the 2500 ppm Decant #2 sample for Patient 1 with sample fitted parameters is shown in Figure 27. Figure 24 shows data typical of all 3 patients in that the incubating solution maintains the linearity of the boron signal and that dilutions during biological preparation prior to incubation were consistent relative to all sample concentrations. Figure 25 for Patient 1, also typical of all patient data, indicates that the HBSS wash is diluted inconsistently and that unspecific binding of the boron solution to the cells may interfere with the final boron concentration of the HBSS washing solution. Finally, Figure 26 shows clearly that the boron signal from the remnant cells

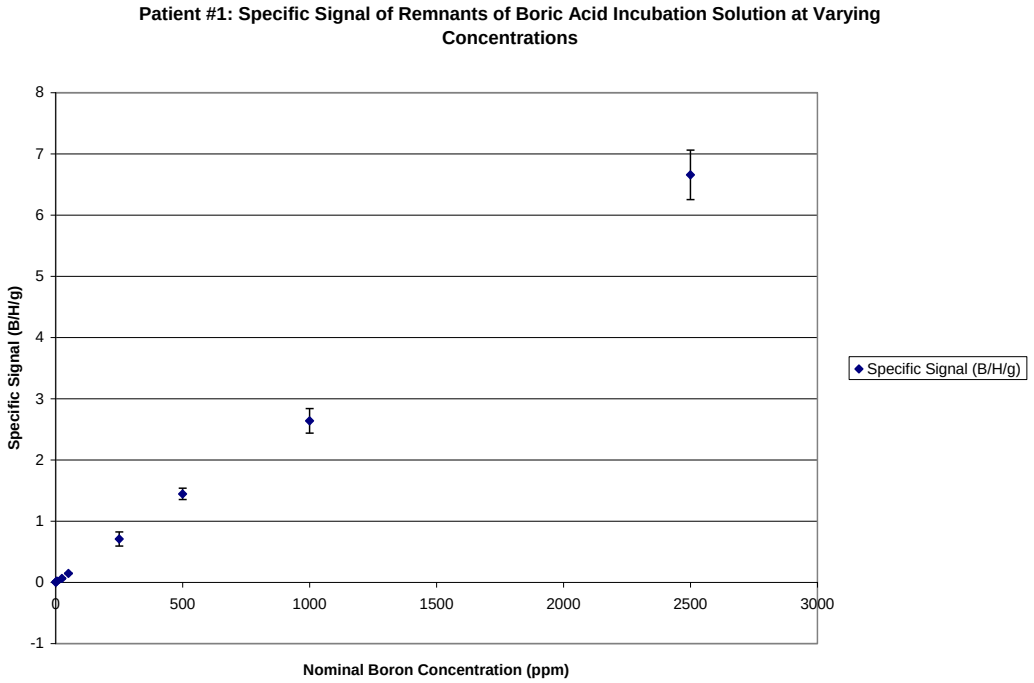

Fig. 24 Measurements of the PGNAA boron signal from decanted boric acid solution following centrifugation of the cells post 1 hour incubation for Patient 1.

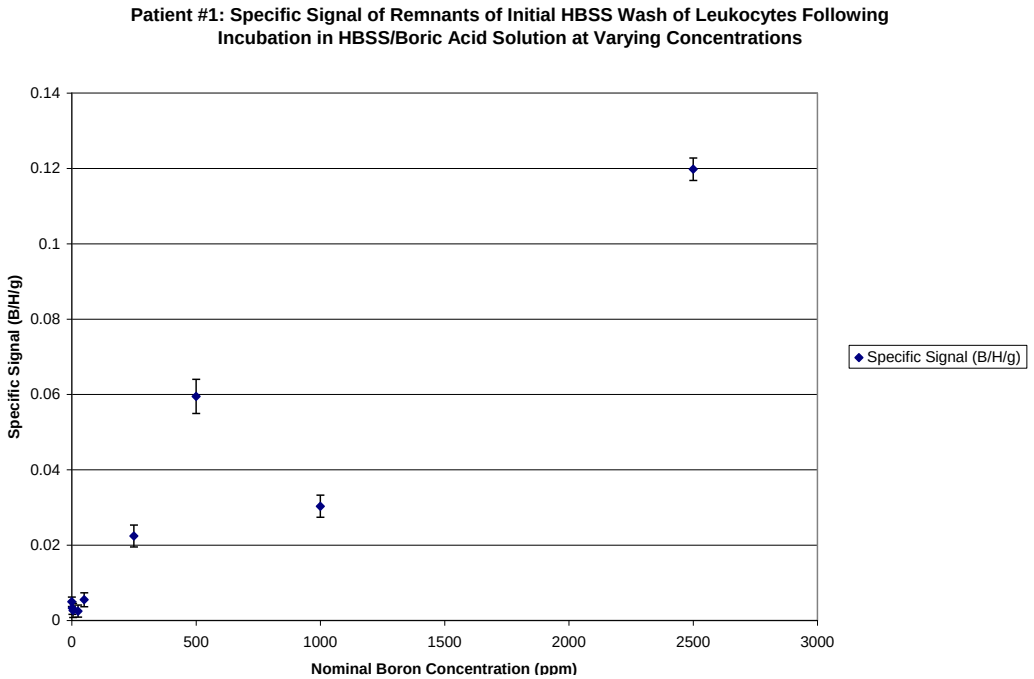

Fig. 25 Measurements of the PGNAA boron signal from decanted HBSS washing solution following centrifugation of the cells post 1 hour incubation for Patient 1.

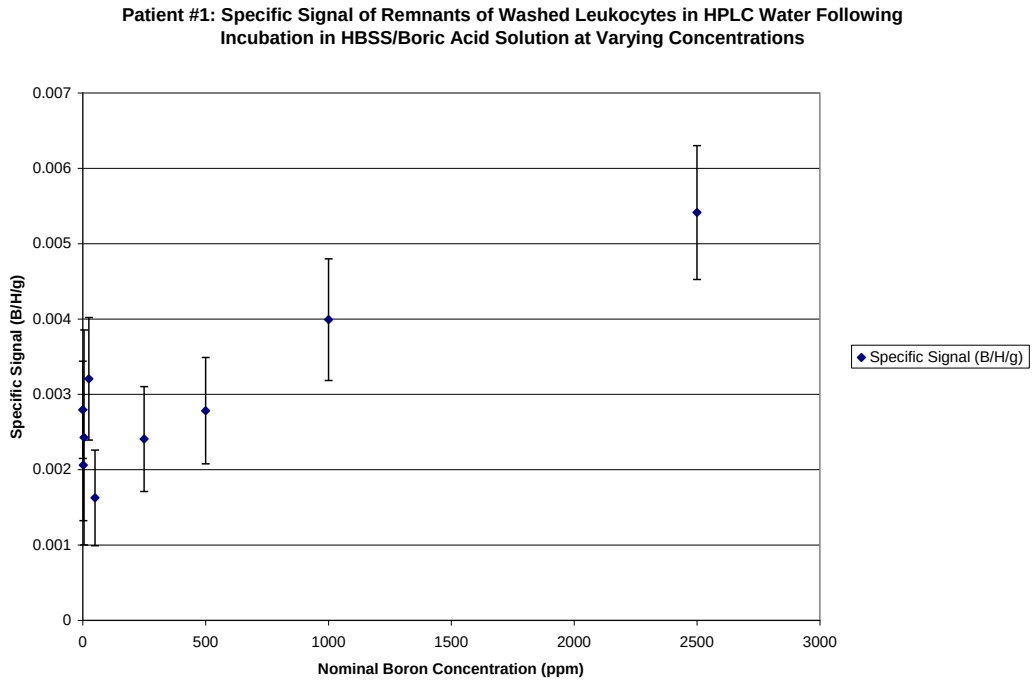

Fig. 26 Measurements of the PGNAA boron signal from the cell remnants in HPLC water following washing with HBSS post 1 hour incubation for Patient 1.

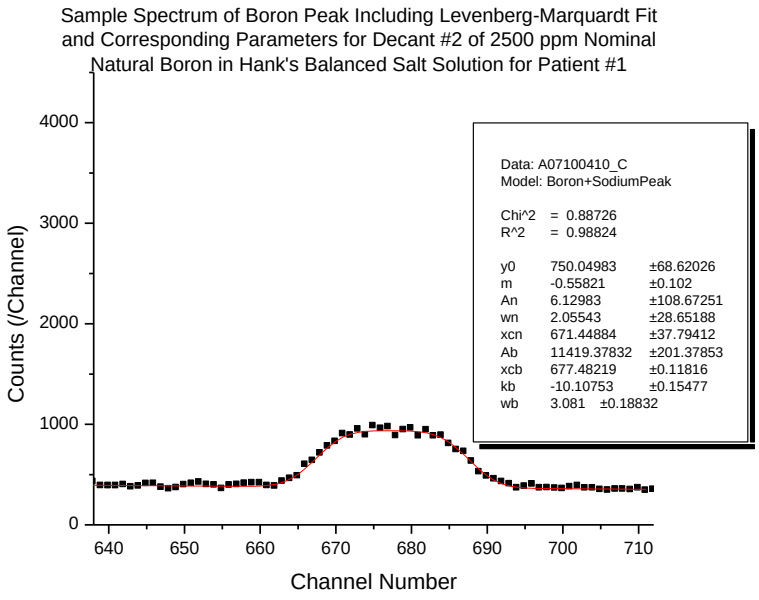

Fig. 27 A sample spectrum over the range of the boron peak for Decant #2 of 2500 ppm nominal elemental boron in Hank's Balanced Salt Solution (HBSS) for Patient #1. Corresponding parameter values are also shown.

cannot be distinguished from other signals over a wide range of boron concentrations.

While it appears based on the data of Figure 26 that the boron specific signal can be determined at the highest incubated concentration of 2500 ppm, review of the final calculation of the boron concentrations in Table 2 (over) from all of the patients indicates that the boron signal is below the detection limit calculated in previous experiments as described in Chapter 2. Although the boron concentration of the final solution was below the detection limit and, therefore, the result cannot be experimentally quantified, the result of 0.9 ± 0.2 ppm is distinguishable from the control signal and the technique has the potential to be used should either the detection limit be reduced further or the experimental method of incubating and washing be somehow improved. The resultant concentration is consistent with the result for potassium dodecahydro-dodecaborate (KBH) determined by N. Stritt at PSI when treating lymphocytes.[17] The challenge with the current experimental method, as with that at PSI, is that while the washing procedure is necessary to remove unspecifically bound boron, the methodology ultimately leads to loss of the boron compound due to simple diffusion.

Table 2 Summary of boron concentration measurements for patients and controls of incubated solutions, washings and remnants of cells following 1 hour incubation with boric acid.

Sample	Nominal Boron Concentration (ppm)		PATIENTS Measured Boron (ppm)	± (ppm)		CONTROLS Measured Boron (ppm)	± (ppm)
DECANT #1							
HBSS Decant #1	0		-0.2	0.4		0	0.3
2.5 ppm Decant #1	2.5		2.4	0.4		2.4	0.4
5 ppm Decant #1	5		5.4	0.4		5.2	0.4
25 ppm Decant #1	25		30.3	0.9		25.7	0.8
50 ppm Decant #1	50		59.1	1		55.4	1
250 ppm Decant #1	250		298	8		291	9
500 ppm Decant #1	500		605	15		564	13
1000 ppm Decant #1	1000		1191	30		1137	33
2500 ppm Decant #1	2500		2903	73		2782	90
DECANT #2			**PATIENTS**			**CONTROLS**	
HBSS Decant #2	0		0.6	0.4		0.7	0.3
2.5 ppm Decant #2	2.5		-0.2	0.5		0.6	0.6
5 ppm Decant #2	5		0	0.3		0.4	0.3
25 ppm Decant #2	25		0.1	0.5		-0.5	0.4
50 ppm Decant #2	50		1.2	0.4		0.2	0.4
250 ppm Decant #2	250		8.8	0.6		2.5	0.6
500 ppm Decant #2	500		15.5	0.6		5.9	0.3
1000 ppm Decant #2	1000		23.2	0.7		10.4	0.6
2500 ppm Decant #2	2500		63.8	0.9		31.3	0.8
REMNANTS			**PATIENTS**			**CONTROLS**	
HBSS in HPLC Water	0		-0.7	0.3		-0.8	0.3
2.5 ppm in HPLC Water	2.5		-0.4	0.3		-0.7	0.2
5 ppm in HPLC Water	5		-0.5	0.3		-1	0.2
25 ppm in HPLC Water	25		-0.3	0.3		-1.1	0.2
50 ppm in HPLC Water	50		-1	0.2		-1	0.2
250 ppm in HPLC Water	250		-0.8	0.2		-0.9	0.2
500 ppm in HPLC Water	500		-0.2	0.3		-0.6	0.3
1000 ppm in HPLC Water	1000		0.1	0.3		-0.6	0.2
2500 ppm in HPLC Water	2500		0.9	0.2		-0.3	0.3

The same procedure for decanting and washing was carried out for one of the patients following incubation with GNB at 1630 ppm natural boron (data not shown). The signal from the cell remnants in HPLC was also below the detection limit and was indistinguishable from the control signal, indicating that GNB also diffused rapidly out of the cell and could not be measured using the current experimental technique. In light of the limited quantities of this compound

available, further measurements using this technique were not performed and the compound was used only for the apoptosis measurements as shown above.

4.7 Biological Effects and Uptake Studies - Conclusion

Preliminary apoptosis studies indicate that both boric acid and glucose *nido*-borane are not toxic with respect to this metric and future studies should utilize the highest possible concentrations to maximize the possibility of detection using PGNAA. While monocytes are a critical target in rheumatoid arthritis and their response to neutron treatments should be measured, CD14 antibodies should not be used to isolate this population during flow cytometry when apoptosis is the metric of choice. Using the experimental method of washing the cells with fresh media/saline solution allows for diffusion of the water-soluble boron compounds out of the cells, reducing the boron concentration below the detection limit for PGNAA. Therefore, determination of uptake of water-soluble boron compounds using the methods as outlined is not feasible when utilizing PGNAA as the method of boron measurement.

5 Development and Testing of Automated PGNAA of Lyophilized Samples

5.1 Automated PGNAA of Lyophilized Samples - Introduction

Based on the findings of Chapters 2 and 4 it was evident that the methodology employed for detection of boron uptake in the biological samples would prove inadequate to quantify the levels of boron present in the samples. The issues highlighted in Section 2.5 regarding the boron detection technique included the necessity to increase the counting time to several hours and to increase the sample flux, if possible, via changes in sample holder material, sample irradiation geometry, addition of neutron reflectors, or an increase in reactor power. Regarding biological sample preparation, Section 4.7 highlighted the fact that the isolation of cells containing the tested boron compound would require an alternate method which does not include washing of the cells with fresh media.

The samples analyzed in the previous chapters were of media in liquid form contained within modified LDPE disposable transfer pipettes. This sample setup was convenient for both sample preparation (since it did not require a priori drying of the media) and prompt gamma measurement (since it minimized the number of layers of material between the neutron beam and the sample). However, the use of liquid samples required the manual insertion of the samples

into the neutron beam. While this was not an unreasonable task when the counting time was on the order of minutes, this posed a practical challenge for increasing the time interval to several hours. The intent of the method of biological boron measurement was ultimately for hundreds of samples to be analyzed. It would be impractical for a technician to change samples manually every 4 hours, 3 times per day, on a daily basis.

5.2 Automation of PGNAA Rabbit System - Materials and Methods

In general, as discussed in Section 2.1, the Centre for Neutron Activation Analysis (CNAA) at MNR utilizes a pneumatically driven sample delivery system ("Rabbit System") to position sealed cylindrical LDPE sample carriers containing the sample material into the neutron beam for prompt gamma neutron activation analysis. This system might be considered to be semi-automated in that several samples are loaded into a cartridge prior to the start of measurement allowing for minimal downtime between sample measurements.

The PGNAA setup at MNR consists of two independent personal computers (PCs) that possess software with which the user interacts to perform the analysis. One PC ("PC-A") consists of the software executable which controls the Rabbit System by activating an array of actuators and switches through an Opto 22 communication network. The user interacts with the graphical user

interface (GUI) via logically organized menus and buttons by left-clicking on the mouse. The other PC ("PC-B") consists of the Aptec spectral acquisition software and MCA card which interface with the HPGE gamma detection apparatus (Figure 3). The normal procedure to perform a single count cycle consists of 1) sending the sample to the beam by clicking a mouse button on PC-A, 2) starting counting for a preset time interval by depressing a keyboard button on PC-B, 3) saving the spectrum to file on PC-B, and 4) clearing the sample from the beam and sending it to temporary waste by clicking a mouse button on PC-A.

While the PGNAA setup allows for relatively rapid sample changes at the neutron beam line, it does not preclude the requirement of an operator to interact with the software of both PCs to complete the analysis of each sample. Thus, the existing system did not remove the impracticality faced with the manual sample loading used in prior chapters for count times of several hours. However, if these independent software programs could be interfaced on a single PC to act automatically in a coordinated fashion, removing the need for a user, then sample counting intervals could be selected completely independently of user availability.

The hardware used in the PC consisted of a Pentium® P54CS 200 MHz chipset with 32 MB of RAM, an Intel 82430FX Pentium® Processor to PCI bridge, and an Intel 82371FB PCI to ISA bridge. The hard disk was a 2.93 GB Generic IDE Disk Type 46 with a FAT32 file system. Additional hardware

included a Toshiba CD-ROM XM-6102B CD-ROM drive, a Generic NEC 3.5 inch floppy drive, an Aptec MCArd AHV Version 7.04.00.03 (Canberra Co., Meriden, CT), and an Opto 22 serial communication card (Opto 22, Temecula, CA, USA). The operating system used with this platform was Windows 95 (Microsoft Co., Redmond, WA).

The spectral acquisition software was upgraded from Aptec 5.11 Release 9 (Chapters 2 and 4) to Aptec 6.31 Release 11 (Aptec Engineering Limited, Canberra Co., Meriden, CT). The components in this software package included the Aptec MCA Application Multchannel Analyzer ("MCA"), Aptec Supervisor Application Automation Control ("Supervisor"), and Aptec MCArdWin Application MCArd DDE Server.

The automated Rabbit System control software was developed using Microsoft Visual Basic 6.0 for 32-bit architecture. Communication to the Opto22 controller was achieved using manufacturer supplied interfacing modules. The Rabbit System control software that was modified was originally created (November 1999) and updated (July 2007) by John Avelar, Senior Engineer of MNR, to function with the reconfigured Opto 22 communication board.

The intention of the software modification was to implement additional functionality to previously existing Rabbit System software. As such, preexisting

functionality (i.e. user operated sample control) was desired to be kept. Therefore, the new automatic sample changing and spectral acquisition feature was created as an add-on package consisting of new forms and modules, with modifications to existing modules to handle these new features. The user would be given the option upon logging in to the software of specifying whether they would like to use the standard "Manual" mode or the new "Auto" mode.

In order to perform the sample changing and spectral acquisition, several pieces of input would initially be required from the user including the number of samples to count and the counting time interval to apply to each sample. The additional input required would be the name of a "Jobfile". The Jobfile is a type of input file used by the Supervisor application which loads headers and regions of interest (ROIs) from a previously existing spectrum (.s0) file. Additionally, the Jobfile contains the preset counting time interval which must be set to the same value as that provided as input to the Rabbit System software. Therefore, the normal process of operation would be for the user to setup and save a Jobfile with the specific acquisition parameters required, start the Rabbit System software, enter into Auto mode and provide as input the Jobfile filename, the corresponding preset counting time specified in the Jobfile, and the number of samples to be counted.

The general hours of operation of MNR are from 9 a.m. to 11 p.m. Monday to Friday. However, actual full power is not always achieved on the hour at 9 a.m. each morning and is often delayed depending on preconditions of operation. This is particularly true on the first day of operation each week. The same can be true for shutdown each evening. Therefore, it would be required to implement a logical condition which halts execution of the sample changing and counting routine between the hours when MNR is not operating. In order to preclude errant counting during hours within which MNR should be operating but may be delayed, a 12 hour operating window between the hours of 10 a.m. and 10 p.m. from Monday to Friday was specified internally in the software. This would permit three 4-hour sample counts to be performed each day on an automated basis. By querying the internal OS system clock from the Visual Basic executable, logical tests could be performed and decisions made based on whether or not the present time and day are within the specified window of operation.

The sending and clearing of the sample to and from the sample position at the beam line consists of interfacing with the previously existing module of the Rabbit System software. Upon sending of the sample and pausing for a 10 second buffer period to allow the sample to reach the position in the beam line, the Supervisor application is executed from within the Rabbit System software to load the specified Jobfile and count the sample. Once the preset time has elapsed, the sample is cleared from the beam line and the software pauses for a 10 second

buffer period to allow the sample to reach the waste bin. If the number of samples

Fig. 28 Algorithm Flow Chart of Automatic Rabbit System Software Component.

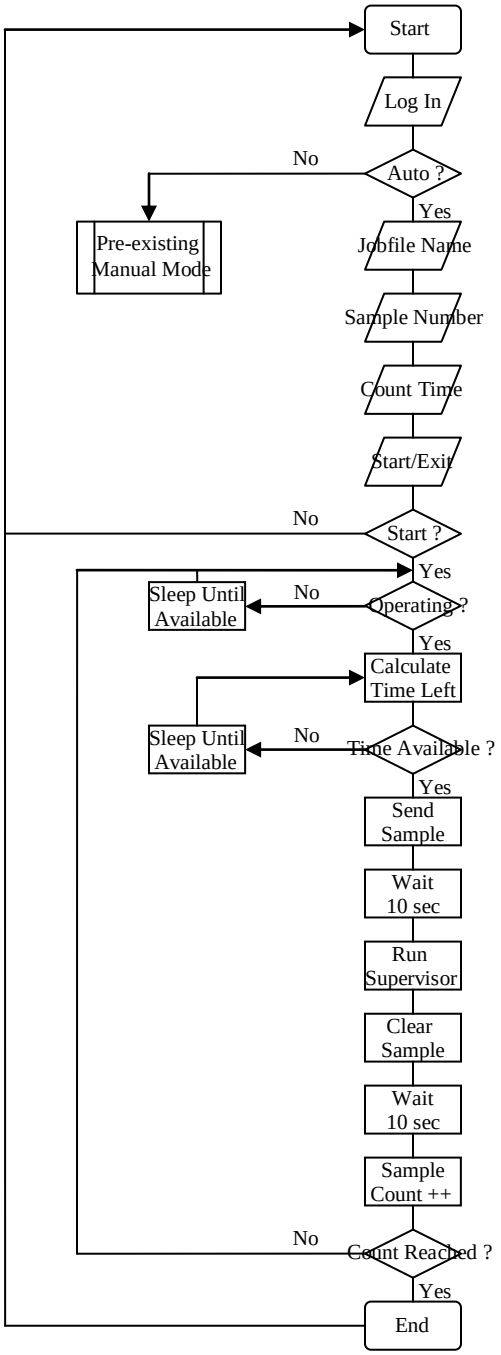

counted is less than the number of samples requested to be counted by the user, and the count time does not lead to counting during off-hours of operation, the process is repeated. Otherwise, the process terminates successfully. Figure 28 shows an algorithm flow chart of the processes and logic described above.

5.3 Automation of PGNAA Rabbit System - Results and Discussion

The new automated add-on feature to the Rabbit System was developed and implemented in this thesis work to interface with the previously existing Opto 22 control algorithm without eliminating the option to execute the Rabbit System manually, if so desired. Using "Shell and Wait" execution statements from within the Auto module, the Supervisor application was successfully run in a systematic way to perform spectral acquisition. The autosave feature in the Supervisor application allowed for hundreds of consecutive samples to be executed by incrementing an integer number appended to the file name. Although the user is presently required to keep a record of which sample corresponds to which integer filename, it is not unduly difficult to keep track of the sample numbers (samples are frequently assigned integer sample numbers by experimenters anyhow). The sample ID numbers can easily be coordinated to match up with the file names generated by the Supervisor application if so desired. Figures 29 through 38 show screen shots of the GUI forms with which the user interacts to initiate automated sample counting.

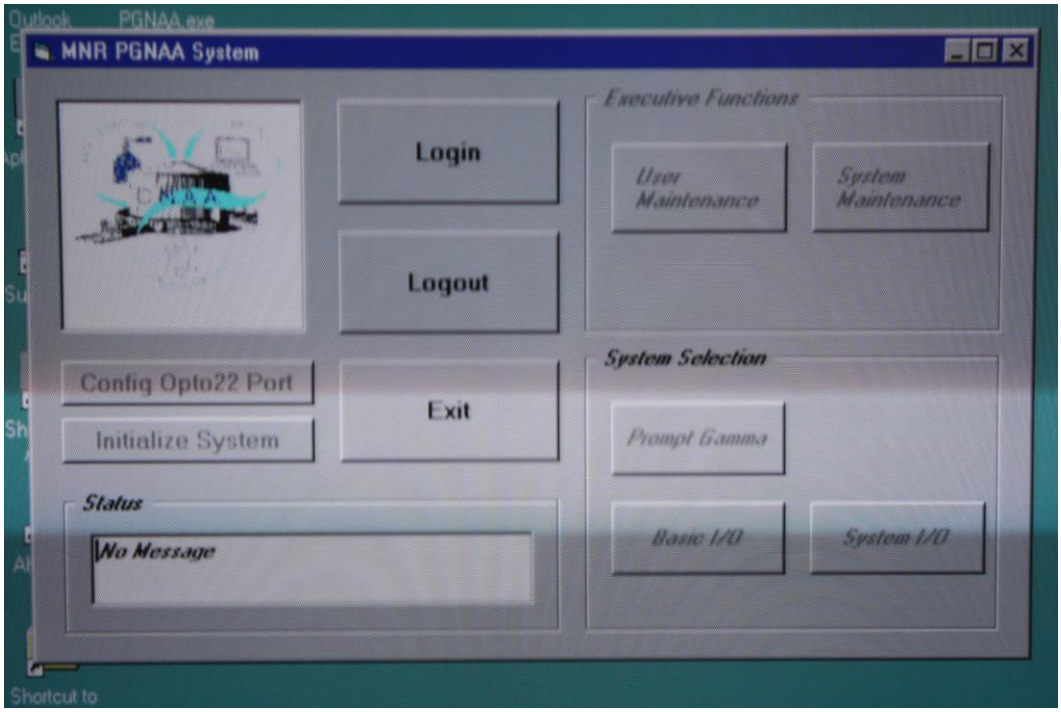

Fig. 29 Initial GUI form seen by the user of the Rabbit System software upon execution of the executable. The user would normally proceed by clicking the "Login" mouse button.

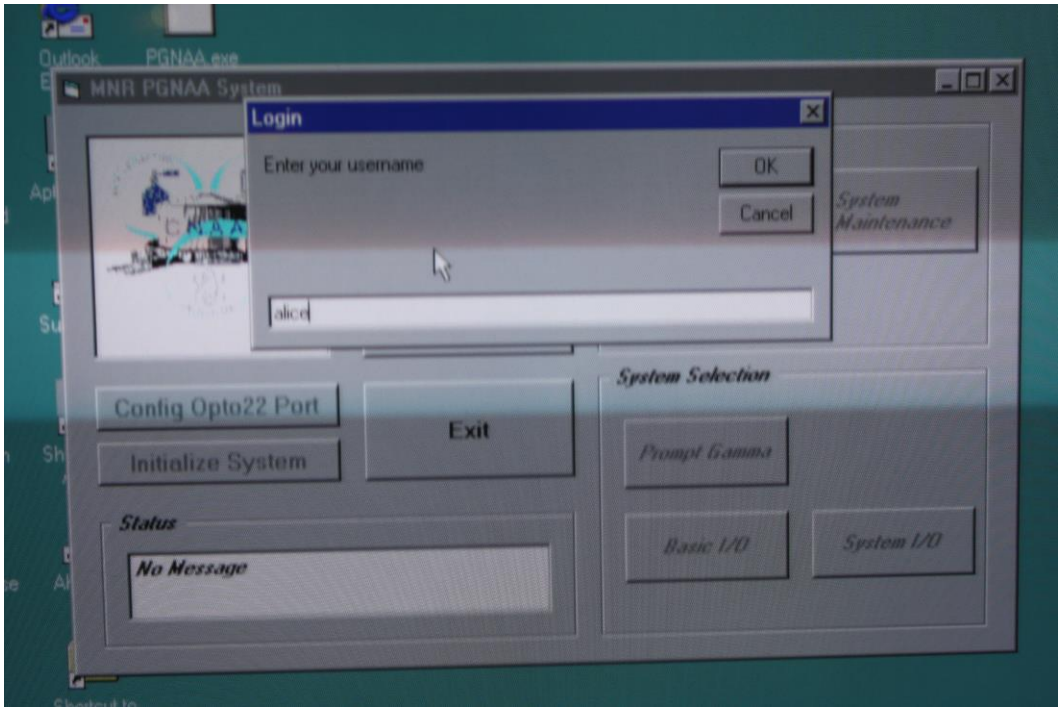

Fig. 30 Upon clicking the "Login" mouse button the user is prompted to enter their username, which must be a previously assigned authorized individual at CNAA.

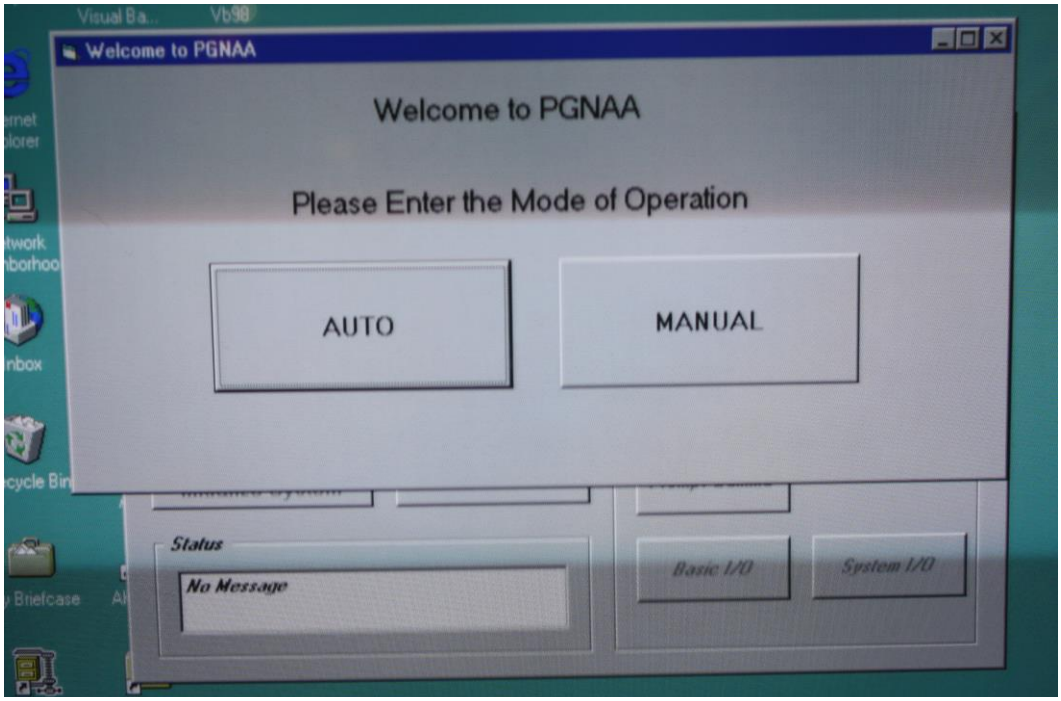

Fig. 31 Upon logging into the program, the user is prompted to select a mode of operation. Selecting the "MANUAL" option results in the standard user driven operation of the Rabbit System.

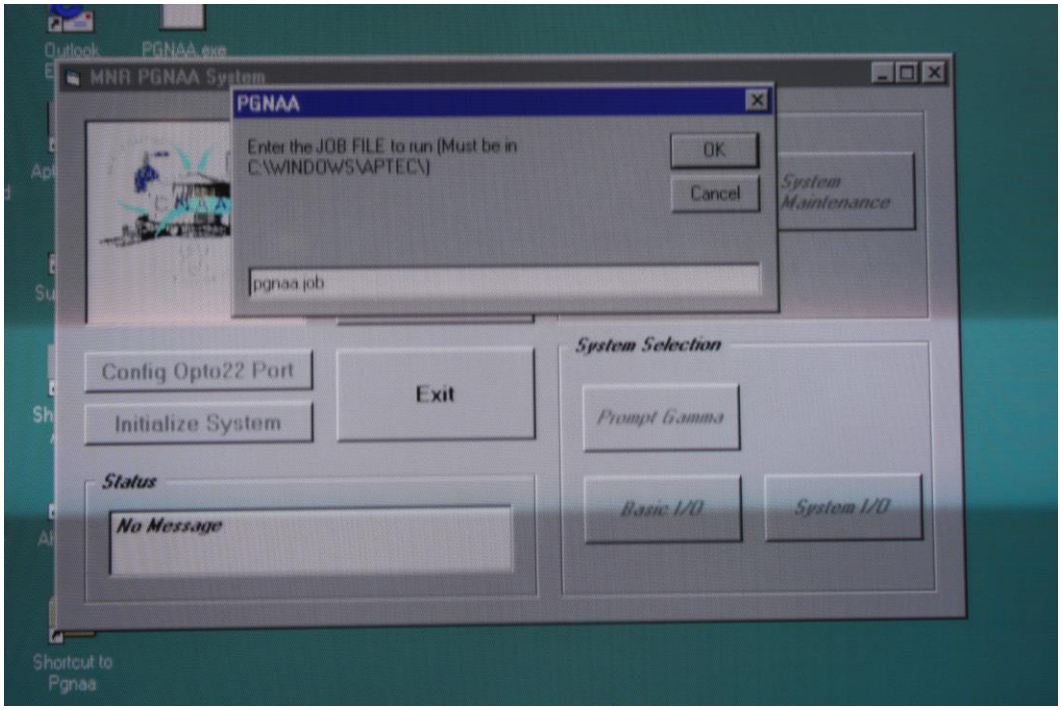

Fig. 32 Upon selecting the "AUTO" option, the user is prompted to enter the name of a Jobfile. The location of the file must be in the C:\WINDOWS\APTEC directory. Should the file not exist, the user is notified and given the option to re-enter the name of the Jobfile or exit the program.

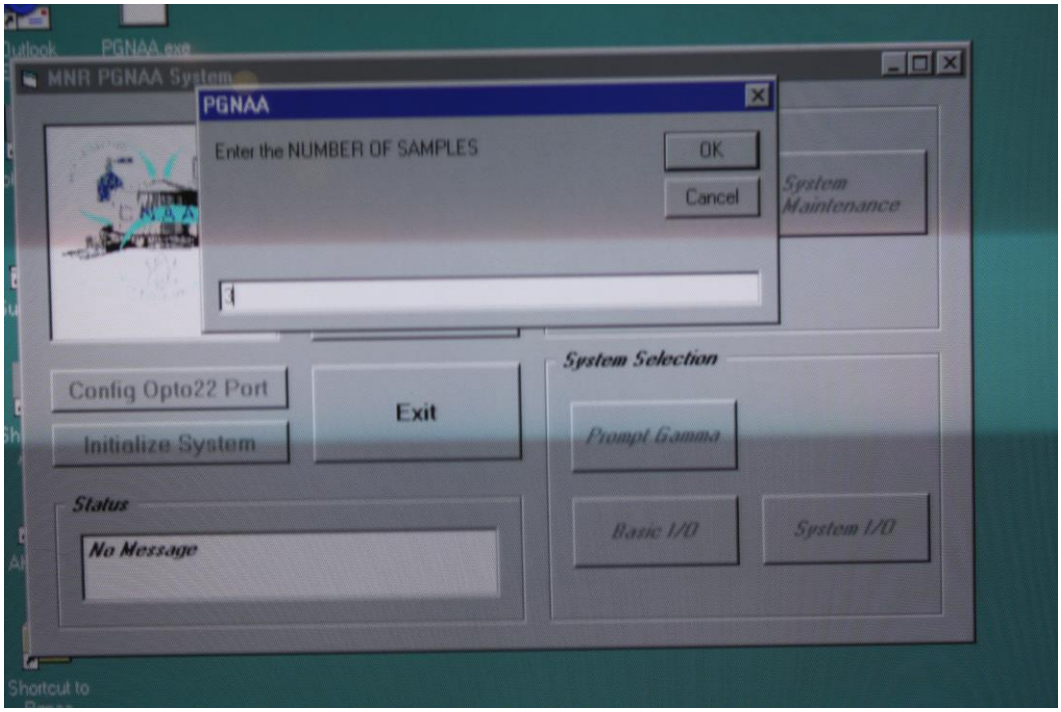

Fig. 33 The user is next prompted to enter the number of samples to be counted.

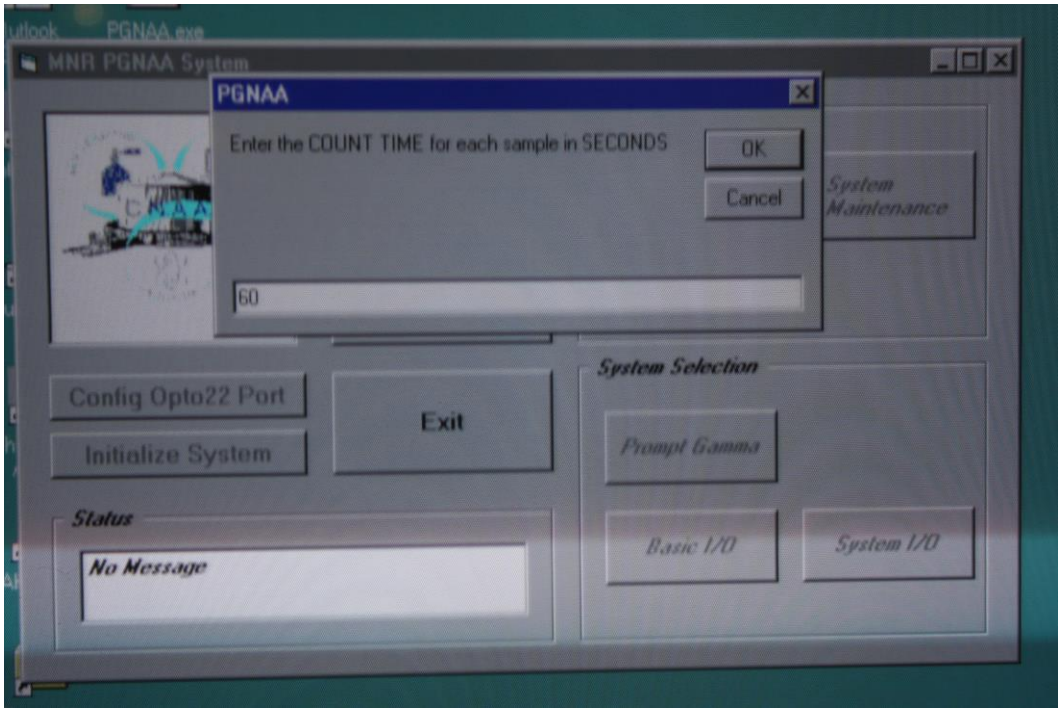

Fig. 34 The user is next prompted to enter the count time for each sample in seconds.

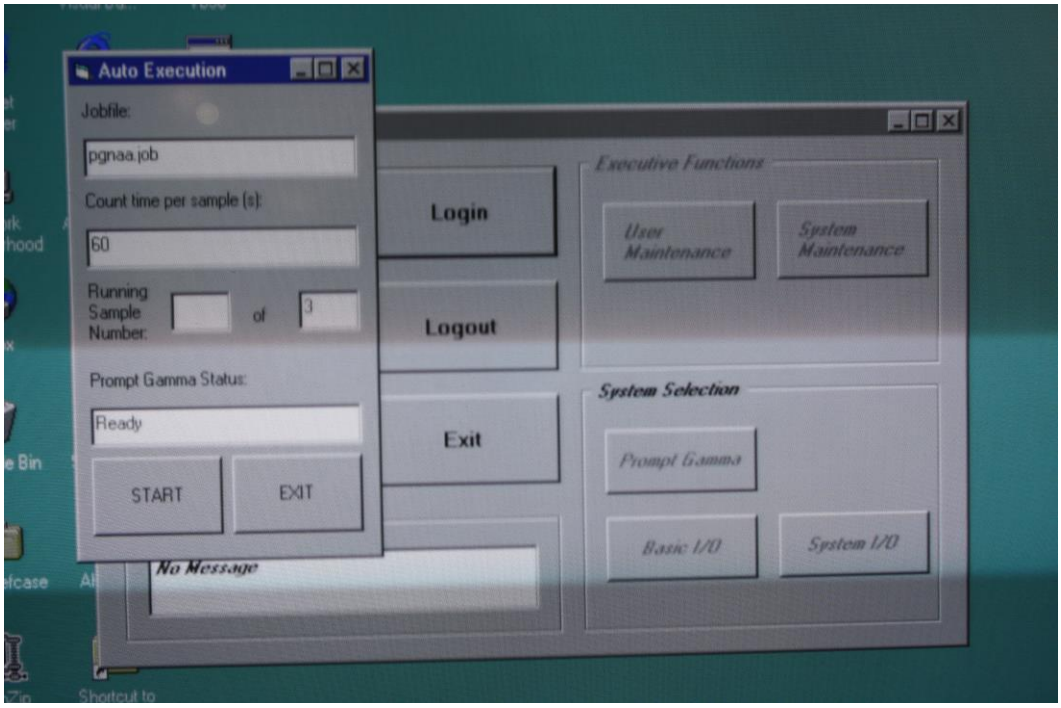

Fig. 35 The user is finally presented with the Auto Mode status form. Upon clicking on the "START" mouse button the automated system routine begins measuring the requested number of samples.

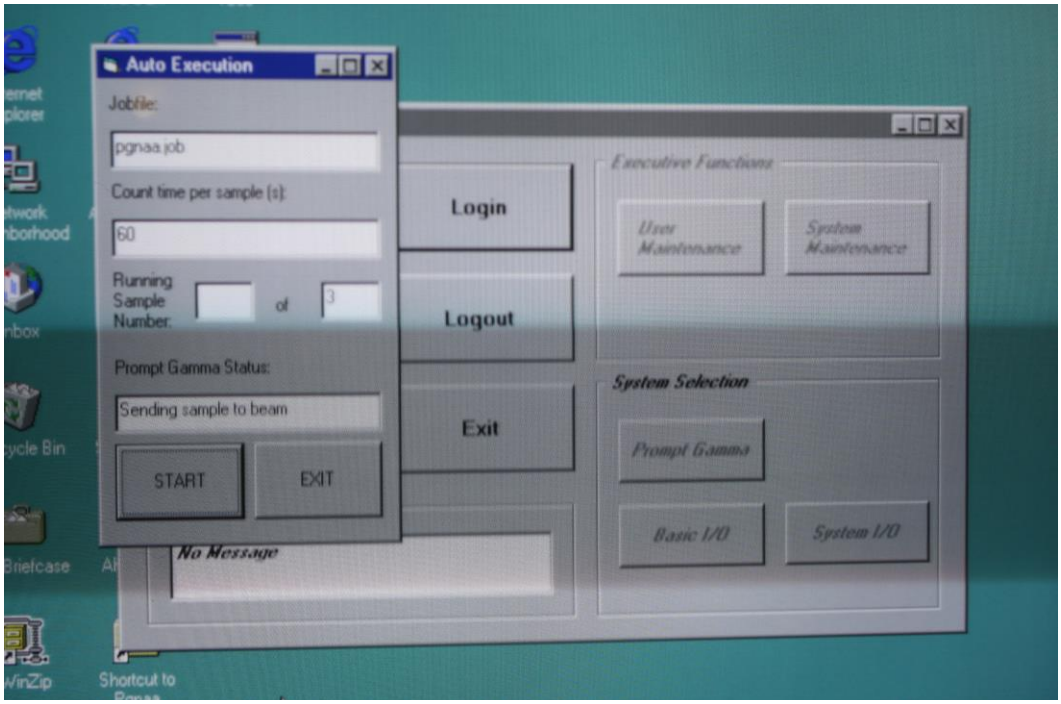

Fig. 36 The user is provided with status messages throughout the course of execution of the automated routine. Sample counting is performed within the hours of operation, defined to be from 10 a.m. to 10 p.m., Monday to Friday. During off hours the routine halts until the following day at 10 a.m., or until Monday at 10 a.m. if the time of execution is later than 10 p.m. on Friday.

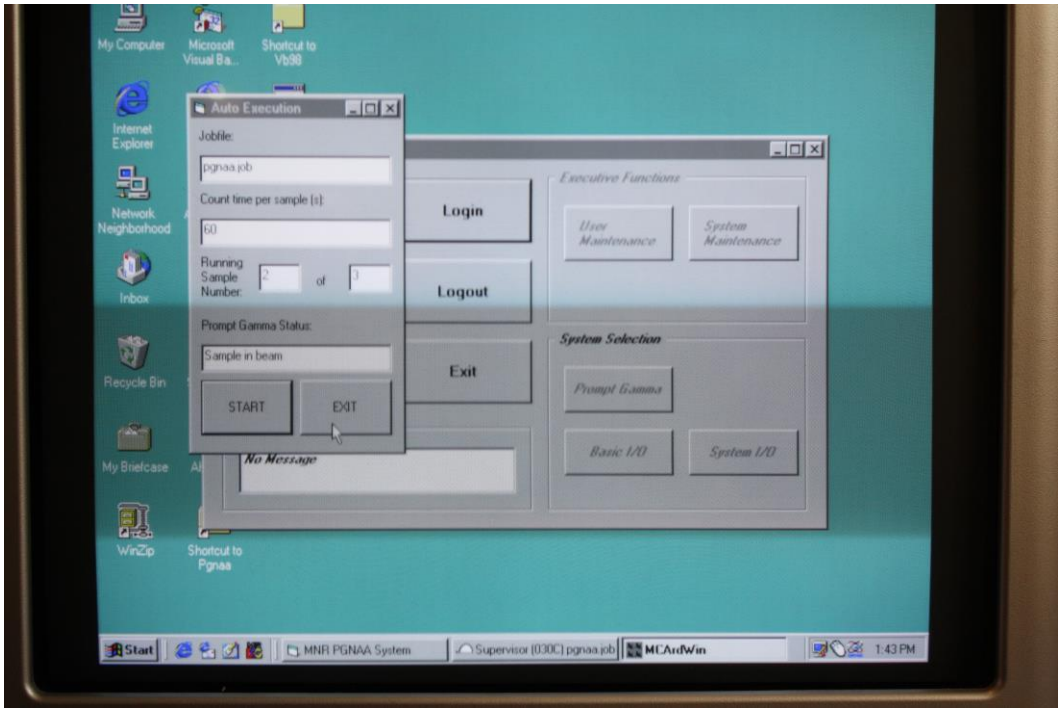

Fig. 37 While the Supervisor and MCA applications are running (during sample measurement) the programs are minimized on the Windows toolbar.

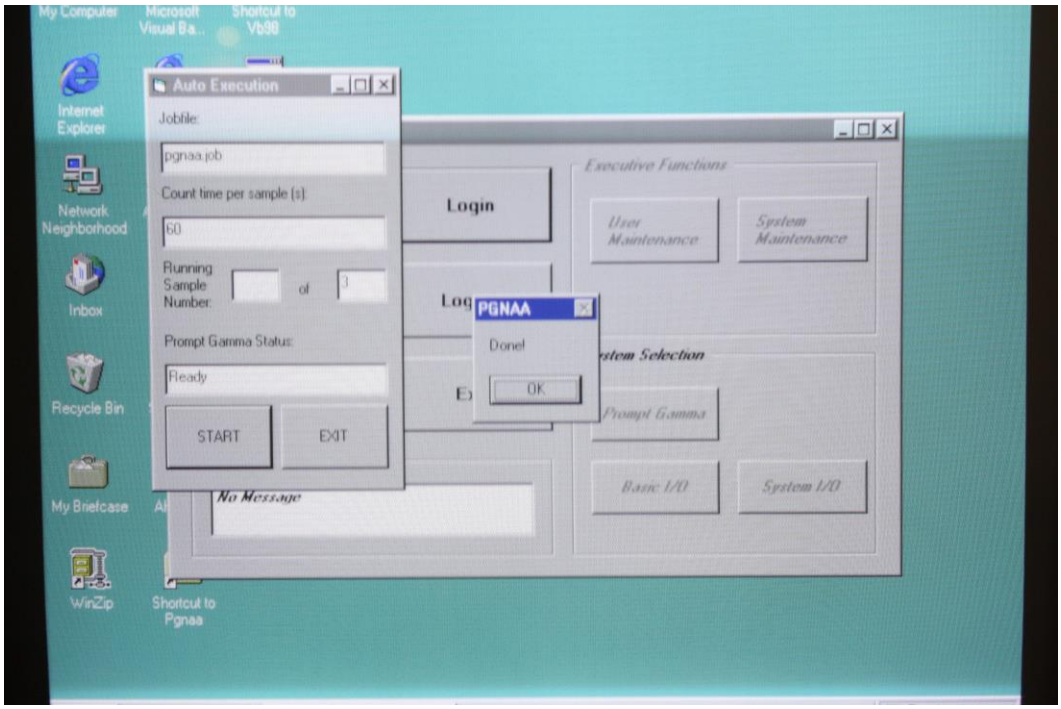

Fig. 38 Upon completion of counting all samples specified, the user is notified and given the option to start another count with the same inputs (START) or exit to return to the initial GUI form (Figure 29).

5.4 Development of Lyophilized Sample Measurements - Background

Automation of the PGNAA site at MNR allowed for the loading of multiple samples (>30) into a cartridge, inputting the measurement specifics into the user prompts, and running the software package automatically to count all samples without further need of interaction. Although this process significantly decreases user interaction time and allows for maximum flexibility of available beam time for sample analysis, it does require prior preparation of the samples. Aqueous samples could not be used with the standard PGNAA vials due to leakage concerns, restricting the samples to those which were dehydrated. Such sample dehydration was previously done indirectly at MNR by aliquoting sample liquid onto filter papers which were dried and then subsequently inserted into "Rabbit System" vials. However, due to the volume of sample liquid this would prove impractical in this application and an alternative method of dehydration was proposed and ultimately used.

A convenient and rapid method that was utilized to achieve dehydration of samples was lyophilization or "freeze-drying". Lyophilization functions by reducing the temperature and pressure of the sample (e.g. water for aqueous solutions) below the triple point at which the three phases of the solute coexist. These conditions permit the sublimation of the solute molecules directly from the solid state to the gaseous state. The process involves first freezing the samples

with dry ice or liquid nitrogen, and placing the samples into a glass flask which is then attached to the vacuum port of a lyophilizer. With the aid of a vacuum pump the lyophilizer maintains the pressure and temperature below the triple point of water in order for sublimation to occur. Lyophilization is used on a regular basis in chemistry research laboratories at McMaster University in order to dehydrate samples rapidly for quantitative analysis in less than 24 hours from the time of compound generation.

The successful automation of the PGNAA site allowed for the investigation of boron detection based on the findings of Chapters 2 and 4; namely the necessity to increase the counting time to several hours and to increase the sample flux potentially via changes in sample holder material. With the automated PGNAA site the use of the traditional sealed cylindrical polyethylene vials was required for the samples to be transported through the half inch diameter plastic tubing which comprises the "Rabbit System".

The use of the new experimental setup utilizing polyethylene vials containing the lyophilized boron-containing material in itself required evaluation via determination of the minimum detectable limit (MDL). However, in the process of evaluation it was also appropriate to, at the same time, investigate the experimental setup using an alternate material for the sample carriers and compare the performance against the polyethylene vials. As previously discussed

in Chapter 2, Teflon® is commonly used at research facilities worldwide as a sample carrier due to the lack of hydrogen in its elemental composition and was an obvious selection for an alternate sample carrier material. Prior to experimental testing and comparison it was first required to design and manufacture vials made from Teflon® in this thesis work.

The standard polyethylene vials used at the PGNAA facility are manufactured en masse from low cost, low density polyethylene (LDPE) at a cost of less than $0.10 per vial. Upon loading of the sample material, the vials are heat-sealed, enclosing the sample material within the cavity of the vial. Due to the particular natural properties of Teflon® it would prove difficult to heat seal vials made from Teflon® in the same manner as the LDPE vials. Additionally, due to the customized nature of the fabrication request and the cost of Teflon® material itself, the cost of the Teflon® vials was on the order of $25 per vial. Therefore, it was determined early on that, due to the cost and material properties, the Teflon® vials would be required to be resealable and reusable.

5.5 Lyophilized Sample Measurements - Materials and Methods

Standard “Rabbit System” vials used regularly by the Centre for Neutron Activation Analysis were utilized as the nominal polyethylene vials. The vials, made of low density polyethylene (LDPE), are custom fabricated to specification

by Adanac Air Tube Systems Limited (Saint-Lambert, Quebec). The vials consisted of an open-top cylindrical container of approximately 1.6 cm^3 and a flat, disk-like lid which fits into the container portion. The lid is heat-sealed to the container using a modified soldering element, enclosing the sample material within the cavity of the vial. The outer diameter of the vials was 0.460 inches and the wall thickness of the vials was 0.048 inches. The axial length of the vials was approximately 0.993 inches including the cap when inserted and heat-sealed. The optimized cylindrical shape and dimensions allow for effective pneumatically-driven transport of the vials through the 0.5 inch inner diameter "Rabbit System" tubing while permitting maximum sample volume.

Teflon® vials were custom fabricated to specification from virgin Teflon® bar by Fine CANCRO Machining Company Limited (Ancaster, Ontario). Material properties of the Teflon® bar included a specific gravity of 2.16, tensile strength of 3000 PSI, and shore D hardness of 54. The Teflon® bar was machined to a hollow cylindrical tube with one end closed. The open end of the cylindrical tube was machined to a 32-pitch threaded grooving to accept a mated screw-on cap. The mated cap was also machined from Teflon® bar with a 32-pitch threaded grooving. The overall dimensions of the Teflon® vials were selected to match those of the LDPE vials with an outer diameter of 0.460 inches, a wall thickness of 0.048 inches and axial length of 0.993 inches including the cap when fully screwed into the vial. The overall inner volume was approximately

1.5 cm^3, slightly less than that of the LDPE vials due to the thickness of the screw-on cap. The final design offered resealable vials which would adequately contain dried sample material but allow for easy washing to ensure reusability for boron-containing samples.

Boron calibration standards were prepared with water as the substrate solution. A 5000 ppm elemental boron stock solution was first prepared by dissolving 2.85885 g of boric acid (National Institute of Standards and Technology, Washington, D.C.) in 100 ml of HPLC water (Caledon Laboratories Ltd., Georgetown, ON). Calibration standards of 100, 50, 10, 5, and 1 ppm elemental boron resulted from dilutions of the stock solution. All dilutions were prepared using analytical balance and volumetric flask and resulted in errors of less than 1%.

Samples for each boron concentration were prepared by aliquoting 1.5 ml of each standard solution to LDPE vials and 1.4 ml of each standard solution to Teflon® vials. Additionally, 0 ppm blanks were included for calibration purposes by using HPLC water alone. All samples were weighed in vials which were weighed and tarred prior to aliquoting. Samples for each standard concentration were triplicated to account for uncertainty in the experimental process. Samples were then allowed to freeze overnight in a -20°C freezer. Following freezing, the open top of each vial was wrapped with lint-free tissue wipes (Kimwipes,

Kimtech Science, Kimberly-Clark Inc., Mississauga, ON) and tape to prevent unintentional aerial dispersion through the top opening of the vial due to the suction force of the vacuum during lyophilzation. Samples were lyophilized in a Virtis 3.3-373500 Benchtop Vacu-Freeze Dryer (Cambridge Scientific, Cambridge, MA) and Edwards Model RVS A653-01-905 (Edwards High Vacuum International, Crawley, Sussex, UK).

The experimental analysis of Chapter 2 indicated that while adequate for the purposes of normalizing the boron signal, the spectral hydrogen peak at 2.2 MeV, which arose from both the LDPE sample containers and the surrounding shielding, was distorted leading to poor fitting results that contributed unnecessarily to the uncertainty in the measurements. Additionally, since Teflon® lacks hydrogen in the elemental composition of the structural unit comprising the polymer, the normalizing signal from hydrogen between the LDPE and Teflon® vials would be inconsistent. Therefore, gadolinium standards were used to generate the normalizing signal for the boron peaks of the standards (see Section 6.3 below for further discussion). Gadolinium standard solution of 250 ppm was prepared by diluting stock 1000 ug/mL gadolinium atomic absorption solution (#207136, Sigma-Aldrich, Oakville, ON) with HPLC water (Caledon Laboratories Ltd., Georgetown, ON) using an analytical balance and volumetric flask. Gadolinium-enriched sample vial inserts were prepared by aliquoting 100 µL of the 250 ppm standard solution onto suspended #1 Whatman filter papers

(Whatman International Ltd., Maidstone, England). The filter papers were suspended on glass flasks to minimize absorption of the gadolinium onto other surfaces. The wetted filter papers were then allowed to dry overnight. Once dried, the gadolinium-enriched filter papers were folded four times and inserted into the lyophilized sample vials prior to sealing the vials. Finally, the LDPE vials were heat sealed using a modified soldering iron and the Teflon® vials were sealed by screwing on the mated screw-on caps.

The prompt gamma detection system was the same as that described in Chapter 2 and included an Ortec GMX-13180 Hyper-Germanium Photon Detector System (Ortec Inc., Oak Ridge, Tennessee), Canberra Model 2020 Spectroscopy Amplifier (Canberra Co., Meriden, CT), ND581 Analogue-to-Digital Convertor and ND599 Loss-Free Counting System (Nuclear Data Inc., Schaumburg, IL), and Aptec MCArd AHV Version 7.04.00.03 (Canberra Co., Meriden, CT). Spectrum collection software employed was Aptec 6.31 Release 11 (Aptec Engineering Limited, Canberra Co., Meriden, CT). The Auto-PGNAA execution system described in Section 5.2 was utilized to submit samples automatically within the normal full-power operating hours of the McMaster Nuclear Reactor. Sample irradiation and concurrent spectrum collection was performed for 4 hour time intervals for all boron samples and background counts. The sample collection preset was gated for live-time with all samples yielding a dead-time ratio of less than or equal to 0.3%.

5.6 Lyophilized Sample Measurements - Data Analysis

The relative method of measurement was employed to analyze the specific quantities of boron as was performed in Chapter 2. However, as discussed in Section 5.5 above, the spectral line that was proportional to the neutron flux was selected from the gadolinium signal generated by the gadolinium vial inserts. The peak area of that signal was used as the normalizing factor. The normalized signal for various standard boron concentrations was then plotted against the known boron concentration, from which the MDL and relative vial performance could be determined. The spectral line chosen was the 185 keV gamma ray of gadolinium, which arises from the (n,γ) reaction on ^{157}Gd. Finally, calibration data were generated in which the B/Gd signal were further normalized to account for the mass of the samples.

Analysis of the boron peak was performed using Origin 6.0 (Microcal Software, Northampton, MA, USA). The function fitted over the range of the boron peak was the following:

$$F(E) = F_{Bckg}(E) + F(E)_B \tag{11}$$

where $F_{Bckg}(E)$ is the function of the background signal and $F_B(E)$ is the

function of the boron peak. The background signal was modeled as a simple linear function:

$$F_{Bckg}(E) = aE + b \tag{12}$$

where a is the slope and b is the y-intercept of the background signal. The boron peak was modeled as the difference of two error functions:

$$F_B(E) = \frac{A_B}{4}\{erf\,\frac{(E - E_{0,B} + k_B)}{\sigma_B\sqrt{2}} - erf\,\frac{(E - E_{0,B} - k_B)}{\sigma_B\sqrt{2}}\} \tag{13}$$

where A_B is the area of the boron peak solved for via non-linear curve fitting routines with Origin 6.0, $E_{B,0}$ is the central energy of the boron peak, and k_B and σ_B are additional fitting parameters. The gadolinium peak was modeled as a simple Gaussian function:

$$F_{Gd}(E) = \frac{A_{Gd}}{w_{Gd}\sqrt{\frac{\pi}{2}}} e^{-2\frac{(E-E_{0,Gd})^2}{w_{Gd}^2}} \tag{14}$$

where A_{Gd} is the area of the gadolinium peak, $E_{0,Gd}$ is the central energy of the gadolinium peak, and w_{Gd} is the width of the Gaussian-shaped peak. Peak fitting

and parameter analysis was accomplished using Origin 6.0's built-in non-linear Levenberg-Marquardt curve fitting routine using statistical weighting.

5.7 Development of Lyophilized Sample Measurements - MCNP Analysis

As a prelude to the experimental measurement and data analysis described above, computational simulation of the geometry and physical interactions was undertaken to provide additional insight into the evaluation of the Teflon® vials as compared to the LDPE vials. This computational simulation was performed using Monte Carlo N-Particle Version 5 (MCNP5).[57] Briefly, MCNP5 simulates the transport and interaction of nuclear particles through user-defined geometries and materials using Monte Carlo statistical methods and is a benchmark software tool used worldwide in the areas of medical physics, radiation shielding, nuclear criticality and detector design, to name a few.

The MCNP5 model developed was based on a previous model of the PGNAA facility by Atanakovic.[49] The model defines the walls, experiment table, shielding, and detector of BP#4 at the McMaster Nuclear Reactor and is shown in Figures 39 through 42. The neutron source at the beam port window was modeled as a mono-directional planar source 2 inches high by 1 inch wide with a Maxwellian energy distribution at room temperature, centered about the mid-point of Figure 42. The sample vial was modeled as a hollow cylinder closed at both

ends with length of 0.993 inches, outer diameter of 0.460 inches, and wall and end thickness of 0.048 inches. The Teflon® Rabbit System guide tube was modeled as a 12" vertical section about the mid-plane of the vial. The vial and guide tube as modeled are shown in Figures 43 and 44.

The MCNP5 simulations were comprised of two sets: the sample vial made of LDPE and the sample vial made of Teflon®. The composition of LDPE was simplified to that of the repeating units of the polymer, namely $(C_2H_4)_n$ with a

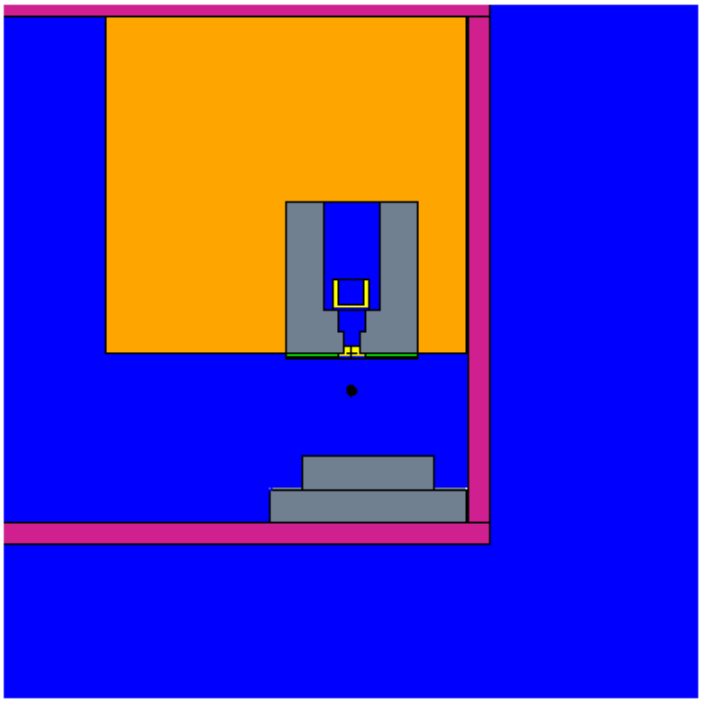

Fig. 39 Birds-eye-view of MCNP5 model of BP#4 of the McMaster Nuclear Reactor, centered about the origin of the model at the face of the detector. The model shows the wax shielding (orange), concrete walls (magenta), lead shielding (grey) and surrounding air (blue). The sample is shown just below the detector along the neutron beamline located at the right concrete wall.

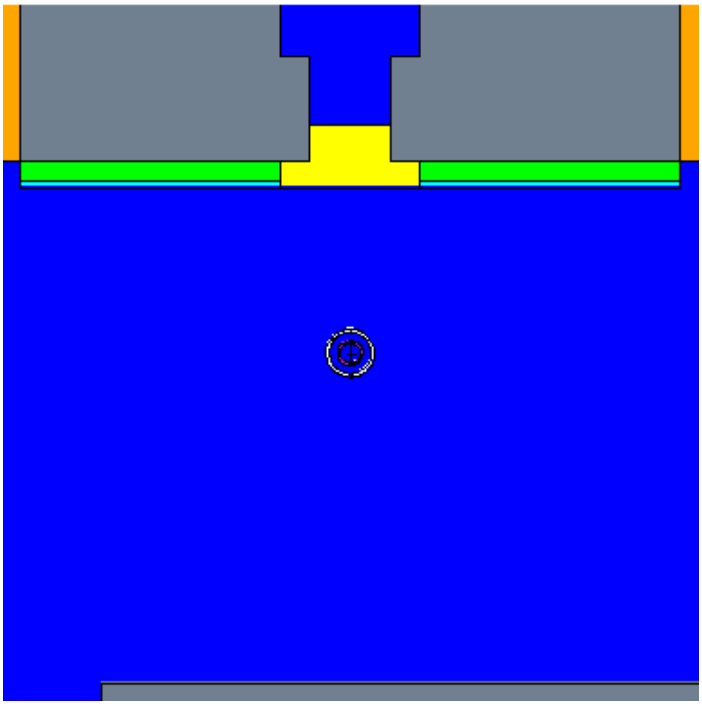

Fig. 40 Close-up of birds-eye-view of MCNP5 model shown in Figure 39, centered about the origin of the sample vial. The sample vial and Teflon® guide tube are discernable.

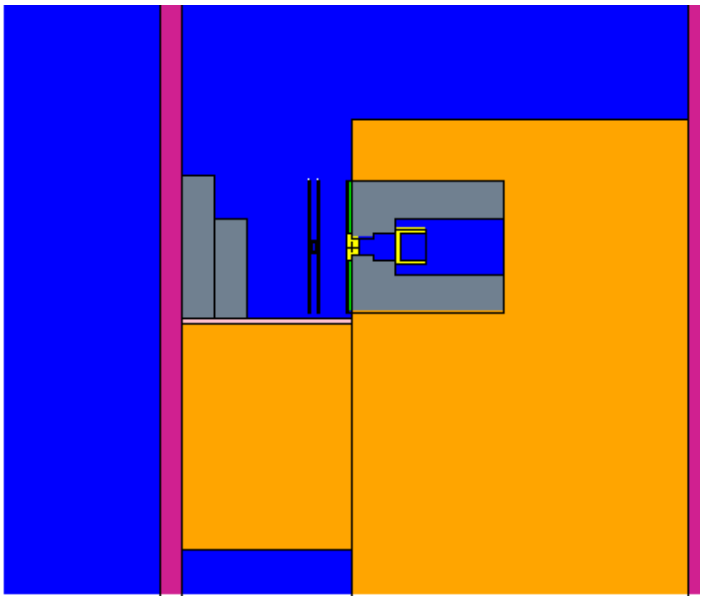

Fig. 41 Beams-eye-view of MCNP5 model of BP#4 of the McMaster Nuclear Reactor, centered about the origin of the model at the face of the detector. The model shows the wax shielding (orange), concrete walls (magenta), lead shielding (grey) and surrounding air (blue). The sample is shown just left of the detector along the neutron beamline located into the page.

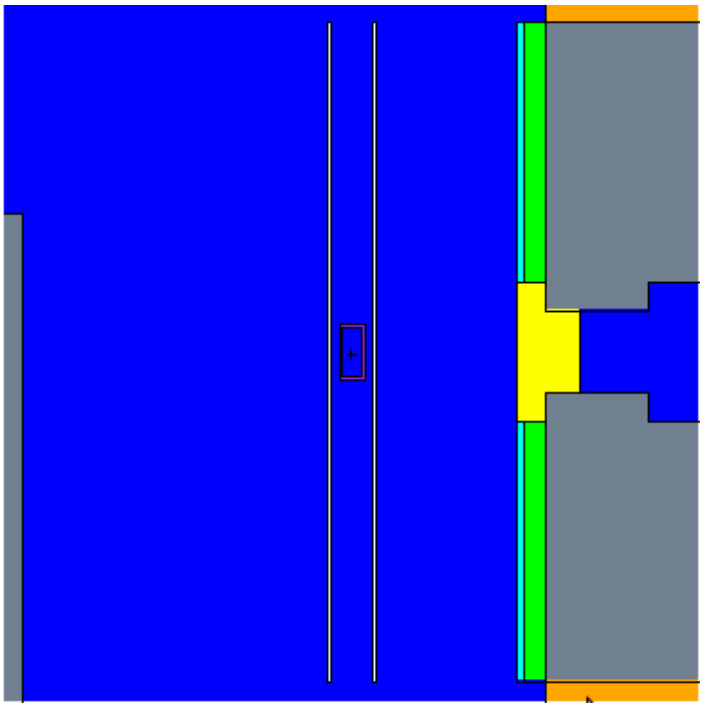

Fig. 42 Close-up of beams-eye-view of MCNP5 model shown in Figure 41, centered about the neutron beam line and origin of the sample vial. The sample vial and Teflon® guide tube are discernable.

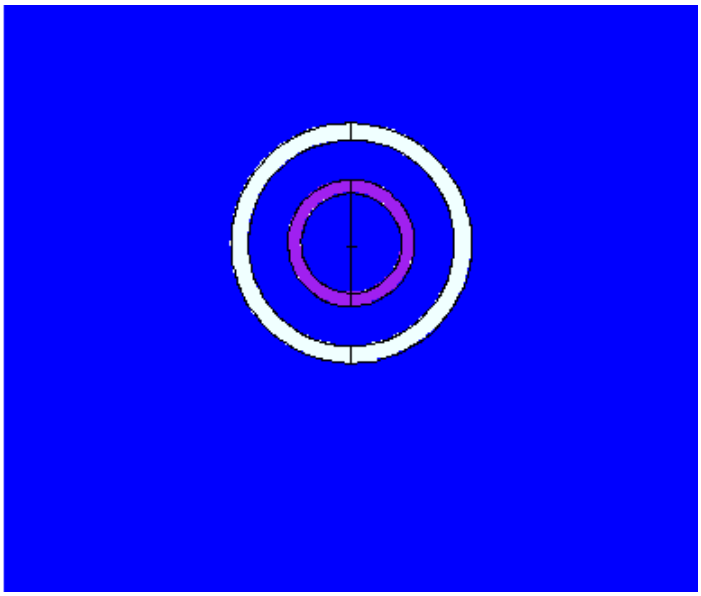

Fig. 43 Birds-eye-view of MCNP5 model of sample vial and Teflon® guide tube showing the segregated halves of the modeled volumes: front half (right of vial) and left half (left of vial). (N.B. Neutron beam incident direction is from right to left of the figure.)

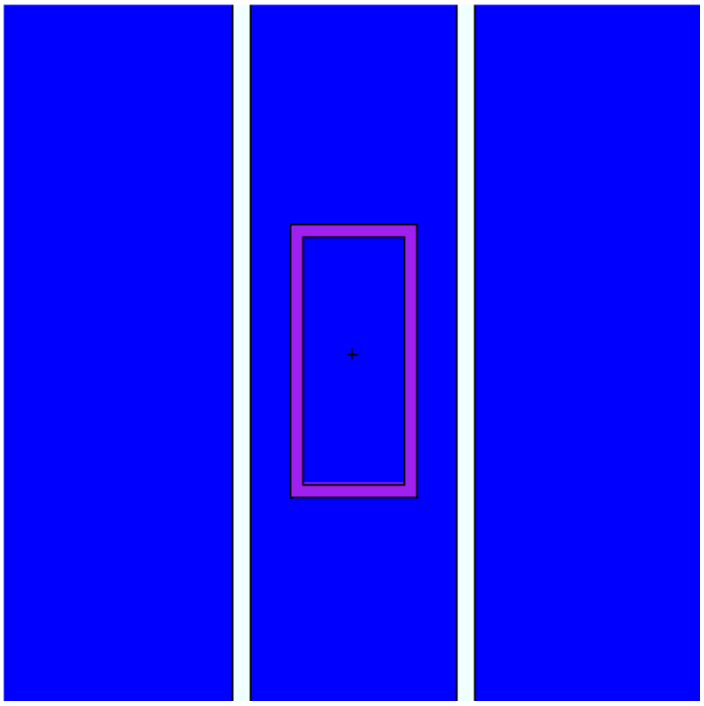

Fig. 44 Beams-eye-view of MCNP5 model of sample vial and Teflon® guide tube.

density of 0.92 g/cm^3. The composition of Teflon® was also simplified to that of the repeating units of the polymer, namely $(C_2F_4)_n$ with a density of 2.2 g/cm^3.

Cross-section data for materials were specified to be taken largely from the ENDF/B-VII.0 Nuclear Data Library at 293.6 K, and otherwise from ENDF/B-V/VI.0.[59] Additionally, for the modeled LDPE sample vial, thermal scattering of neutrons from hydrogen was accounted for using the S(α,β) thermal scattering treatment, where the scattering properties were for hydrogen in polyethylene at room temperature. However, due to the lack of hydrogen in the

elemental composition of Teflon®, the free gas thermal neutron treatment was utilized for the modeled Teflon® sample vial.

The MCNP5 simulations were executed for 100 million starting source particles and resulted in errors of less than 0.03% with statistical metrics ensuring validity of the results (e.g. near constant FOM and slope of Pareto function equal to 10). The figures-of-merit for the simulation-based comparison of the LDPE and Teflon® vials were the F4 cell-averaged flux tally in the inner sample space of the vial and the F4-based capture tally in the vial itself. The normalized tally results were scaled to a neutron flux of 4×10^7 neutrons/cm^{2}s at the beam port exit of BP#4 of the McMaster Nuclear Reactor.

Based on the MCNP model described, the simulated neutron flux within the inner vial cavity of the LDPE vial is $2.9045 \pm 0.0009 \times 10^7$ neutrons/cm^{2}s, while for the Teflon® vial it is $2.7165 \pm 0.0005 \times 10^7$ neutrons/cm^{2}s, yielding a LDPE to Teflon® neutron flux ratio of 1.0692 ± 0.0004. The LDPE to Teflon® neutron capture ratio is 45.48 ± 0.02. The latter result arises from the fact that over 99% of neutron captures in LDPE occur in hydrogen. In Teflon® nearly 85% of neutron captures occur in fluorine. However, due to the larger neutron capture cross section in hydrogen compared to fluorine, the relative capture ratio of hydrogen versus fluorine is nearly 55:1. These results indicate that although the neutron flux is roughly the same between the two vial compositions, the detected

signal from the hydrogen is much larger for LDPE than for Teflon® resulting in a more significant background signal of the overall gamma spectrum from which to extract the boron signal and reducing the sensitivity for boron in LDPE.

5.8 Lyophilized Sample Measurements - Results and Discussion

Sample boron spectra for a lyophilized 10 ppm boron calibration standard in HPLC water for both LDPE and Teflon® vials are shown in Figure 45 below. Calibration graphs for elemental boron in HPLC water for LDPE and Teflon® vials are shown over in Figures 46 and 47, respectively. Regression analysis was performed using the built-in linear fitting routine of Origin 6.0 with error

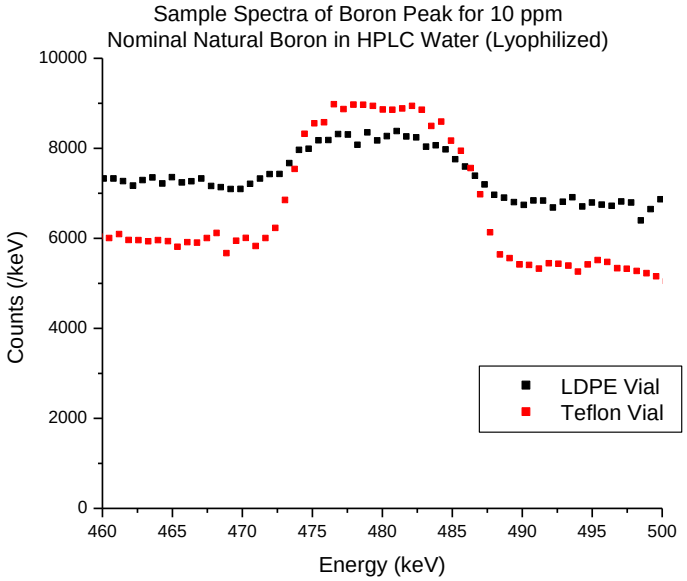

Fig. 45 Sample spectra over the range of the boron peak for the lyophilized 10 ppm nominal elemental boron in HPLC.

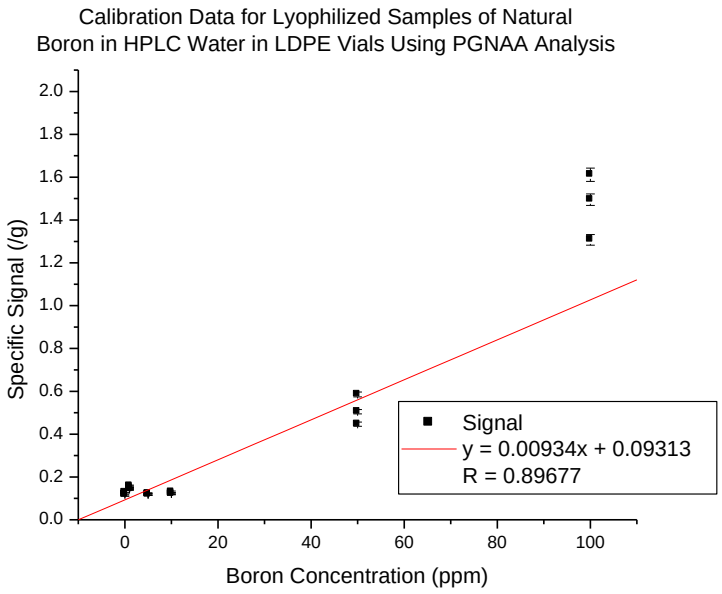

Fig. 46 Calibration curve for lyophilized elemental boron in HPLC water in LDPE vials. Linear regression, regression equation and correlation coefficient are also shown.
(N.B. Error bars for 50 ppm boron and less are indiscernible from the data points)

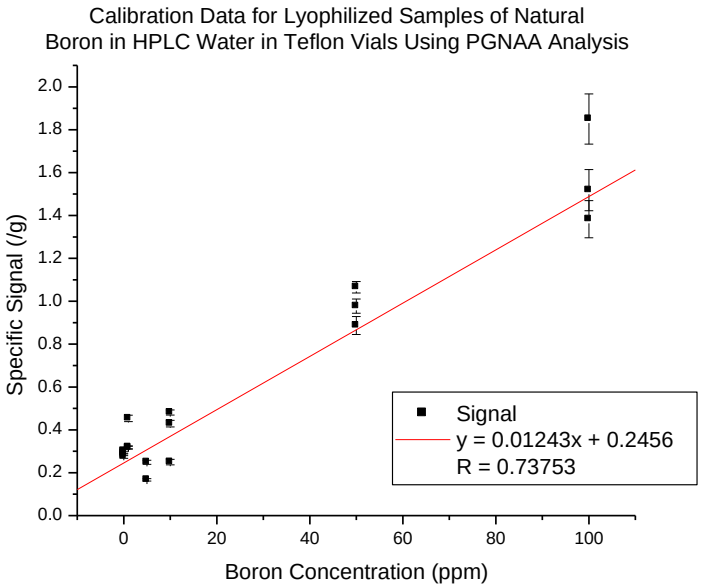

Fig. 47 Calibration curve for lyophilized elemental boron in HPLC water in Teflon® vials. Linear regression, regression equation and correlation coefficient are also shown. (N.B. Error bars for 10 ppm boron and less are indiscernible from the data points)

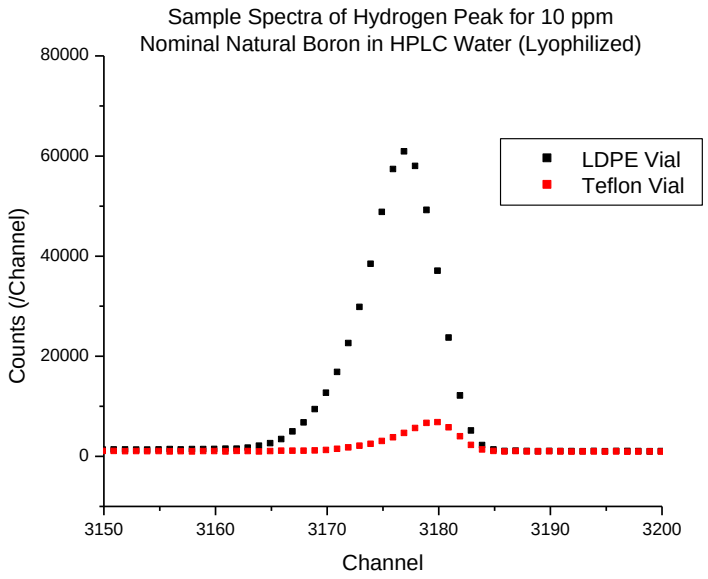

Fig. 48 Sample spectra over the range of the hydrogen peak for the lyophilized 10 ppm nominal elemental boron in HPLC.

weighting. Sample spectra of the hydrogen signal in LDPE and Teflon® vials are shown above in Figure 48.

The correlation coefficients of the results for boron in LDPE and Teflon® vials were 0.89677 and 0.73753, respectively, indicating that the response was not strongly linear over the range of boron concentrations tested. Despite the poorer correlation coefficient using the Teflon® vials, the obvious anomaly using the LDPE vials was the non-linearity of the data points at 100 ppm elemental boron. Additionally, in comparison to the results of Chapter 2, the variation in the data points for each measured concentration is large. The minimum detection limit (MDL), which represents the 95% confidence interval of the limit of detectable

boron concentration, was determined to be 3.56 ppm and 10.11 ppm for the LDPE and Teflon® vials, respectively.

Comparing these MDL values with those calculated in Chapter 2 indicates that the lyophilized sample method is not more sensitive than the liquid sample method utilized in Chapter 2, despite using a largely increased counting time of 4 hours. That said the results shown in Figures 46 and 47 themselves demonstrate an inherent problem with the experimental setup in that the signal values had large deviations. Additionally, considering that the linear trend of the data should pass through the cluster of data points at 100 ppm for LDPE vials, and recognizing that below 50 ppm the data points are substantially constant with near-zero slope, the evidence suggests that the lyophilized substrate of the sample was highly volatile and indeed a large fraction of sample may have been lost between the lyophilization process and sample preparation, despite taking all precautions to avoid such an occurrence.

During the lyophilization process the samples are exposed to a strong vacuum for a period of up to 24 hours. Given the fact that the mass of substrate left following lyophilization in the vials was on the order of nanograms it is reasonable to suspect that some of the dehydrated sample material may have been lost. This could have been due to either the vacuum forces during lyophilization itself or post-lyophilization, from either accidental mechanical manipulation or

exposure to air streams surrounding the vials during manual handling. Thus, in order to prevent such sample loss, in using the lyophilization method of sample preparation the extracted boron solution should first be uniformly dispersed in a solution with quantifiable amounts of signal unspecific substrate. Based on the results of Chapter 2 and initial testing, lyophilized RPMI may indeed be such a solution due to the fact that, when lyophilized, a considerable amount of powdered residue remains while still providing levels of boron detectability close to HPLC water.

Comparing the 100 ppm results of the LDPE and Teflon® vial measurements, the MCNP5 results of near equal neutron flux within the vial cavity between the two vial types are substantiated. Based on the sample spectra shown in Figure 48, the hydrogen signal using the LDPE vials is significantly higher than that generated when using Teflon® vials. Integrating the spectra and correcting for the background signal, the ratio of hydrogen captures in LDPE to Teflon® is 12.43 ± 0.01, corroborating the results obtained using the simplified MCNP5 model in Section 4.7. As discussed in Section 4.7, the effect of the increased hydrogen signal is indeed a higher background signal using LDPE vials versus Teflon® vials as evident in Figure 45.

5.9 Automated PGNAA of Lyophilized Samples - Conclusion

The MDL of boron in the tested geometry at BP#4 of MNR using the LDPE and Teflon® vials was not more sensitive than that of the liquid sample methods described in Chapter 2, despite a significantly increased counting time. However, the variability and non-linearity of the calibration measurements indicate that the preparation technique itself leads to discrepancies in the measured amounts of sample material and reduces the sensitivity of the experimental setup. In order to improve the detection limit the boron sample solution should be combined with a matrix containing solution such as RPMI to increase the amount of lyophilized material following lyophilization of the sample solution, thus preventing aerial dispersion of the boron containing compound. The measured results were well aligned with those predicted by MCNP5 simulations. However, the apparent advantage of using Teflon® over LDPE was not elucidated in the experimental results due to reasons discussed above.

6 Development and Testing of Improved Lyophilized Sample Measurements

6.1 Improved Lyophilized Samples - Introduction and Background

The unsuccessful effort to improve the minimum detectable limit (MDL) for boron at the PGNAA site in Chapter 5 indicated that an alternate sample preparation method would be required. The results indicated that large discrepancies in the measured amounts of boron were likely due to the loss of sample material in the process of preparation and that prior to lyophilization the boron sample solution should be combined with a matrix containing solution such as RPMI 1640 medium. The result would be an increase in the final lyophilized material from nanograms to hundredths of a gram; enough to potentially prevent aerial dispersion during sample preparation.

The results of Chapter 5 showed that the cell washing method to remove unspecifically bound boron led to the loss of the boron compound due to simple diffusion. This result predicated the need for an alternate method of cell washing/isolation that does not include washing of the cells with fresh media. One such method was utilized by Capala et al. for the evaluation of cellular boron uptake of BNCT agents.[60] Cells were separated from the cell culture media containing boron using a rapid oil filtration procedure originally developed by Wohlheuter et al.[61]

The rapid oil filtration procedure relies on the difference in specific gravities of three compounds: 1 M trichloroacetic acid (TCA), a mixture of silicone oil and light mineral oil (9:1), and the cell culture medium containing boron and treated cells. The three compounds were layered as follows: 750 µL of TCA, 750 µL of oil mixture, and up to 250 µL of medium containing a known number of cells. The liquid compounds were layered in 2 mL centrifuge tubes and centrifuged for 2 min at 12000 rpm. This resulted in the rapid penetration of the cells through the oil layer. The oil mixture acted to separate the cells from the boronated medium and removed any unspecifically bound boron from the cells. The cells were lysed in the TCA layer; however, this was irrelevant for the purpose of boron quantification. The boron containing TCA layer was then removed via syringe by piercing the centrifuge tube, and followed by analysis using direct-current plasma atomic emission spectroscopy (DCP-AES).

The rapid oil filtration procedure could be used as the proposed alternate method of cell separation as stated above. The procedure could be capitalized upon in order to improve the quantification of boron with PGNAA. By adding RPMI 1640 medium to the extracted TCA layer, the resulting compound would provide a sufficient amount of lyophilized material remaining in the vials following lyophilization. In order to avoid any potential damage to the vials, the acidity of the resulting compound could be further neutralized with a base to yield

a salt that would further increase the overall material remaining in the vials post-lyophilization.

Prior to future evaluation of the rapid oil filtration procedure for the application of potential BNCS agents with leukocytes, calibration and determination of the MDL for the proposed improved lyophilization substrate at the PGNAA site was required to be performed. In Chapter 5, the difference between the MDL of the LDPE and Teflon® measurements was evident. However, since the results were questionable amid the issue of aerial dispersion of boron material the results were unreliable for comparing the two materials. Both the MCNP results and measured spectral response (see Figure 45) were shown to be the best in Teflon® and corroborated by the practice of the comparable studies by Byun et al. (2004) and Baechler et al. (2002) at SNU and PSI, respectively.[44,45] For this reason, only Teflon® vials were used for the purpose of evaluating the improved lyophilized sample measurements.

6.2 Development of Improved Lyophilized Samples - Materials and Methods

Boron calibration standards were prepared with a mixture of aqueous trichloroacetic acid, aqueous potassium hydroxide and cell culture medium. A nominal 1 M solution of trichloroacetic acid was prepared by dissolving 16.33945 g of trichloroacetic acid crystals (Anachemia Canada Inc., Montreal,

QC, Canada) in 100 mL of HPLC water (Caledon Laboratories Ltd., Georgetown, ON, Canada). A nominal 10 M solution of potassium hydroxide base was prepared by dissolving 56.11255 g of potassium hydroxide flakes (Caledon Laboratories Ltd., Georgetown, ON, Canada) in 100 mL of HPLC water. The acid/base/medium mixture was prepared by combining 7.5 mL of the 1 M trichloroacetic acid solution, 0.825 mL of the 10 M potassium hydroxide solution, and 7.5 mL of RPMI 1640 medium. A 5000 ppm elemental boron stock solution of the acid/base/medium mixture, hereon referred to as "TPR mixture", was first prepared by dissolving 0.29455 g of boric acid (National Institute of Standards and Technology, Washington, D.C.) in 10 mL of the TPR mixture. Calibration standards of 100, 50, 10, 5, 1 and 0.5 ppm elemental boron resulted from dilutions of the stock solution. All dilutions were prepared using analytical balance and volumetric flask and resulted in errors of less than 1%.

Preliminary test samples of the lyophilized TPR mixture demonstrated a need to reduce the total volume of solution aliquoted into the vials as was used for the Chapter 5 studies. The lyophilization process caused the volumetric expansion of the substrate TPR mixture salt to grow over the vial opening leading to sample loss (Figure 49, over). This is hypothesized to have resulted from a combination of the effect of the suction force from the lyophilizer vacuum and the crystallization under vacuum during lyophilization (dehydration). In order to

Fig. 49 Example of a polyethylene vial showing crystalline overgrowth of the lyophilized TPR-based boron sample material.

prevent this crystalline overgrowth the total volume of solution aliquoted into the vials was reduced from 1.4 ml, as was used in Chapter 5, to 1.1 ml.

Samples for each boron concentration were prepared by aliquoting the 1.1 mL of each standard solution into Teflon® vials. Additionally, 0 ppm blanks were included for calibration purposes by using TPR mixture alone. All samples were weighed in vials which were weighed and tarred prior to aliquoting. Samples for each standard concentration were triplicated to account for uncertainty in the experimental process. Samples were then allowed to freeze overnight in a -20°C freezer. As an additional measure to prevent unintentional aerial dispersion and crystalline overgrowth of the substrate during lyophilization, after freezing a

circular piece of #1 Whatman filter paper (Whatman International Ltd., Maidstone, England) was inserted onto the surface of the frozen sample mixture and the open top of each vial was wrapped with a #1 Whatman filter paper, affixed with a twist-tie. Samples were lyophilized in a Virtis 3.3-373500 Benchtop Vacu-Freeze Dryer (Cambridge Scientific, Cambridge, MA) fitted with an Edwards Model RVS A653-01-905 (Edwards High Vacuum International, Crawley, Sussex, UK).

The automated prompt gamma detection system was the same as that described in Chapter 5. Sample irradiation and concurrent spectrum collection was performed for 4 hour time intervals for all boron samples and background counts. Sample collection preset was gated for live-time with all samples yielding a dead-time ratio of less than or equal to 0.3%. Data analysis for the boron signal was the same as that described in Section 5.6. The boron signal was normalized using the hydrogen peak signal and sample mass, and plotted against the sample boron concentration to yield the requisite calibration curve. Analysis of the hydrogen peak was performed using Origin 6.0 (Microcal, Software, Northampton, MA, USA). The built-in Gram-Charlier peak function was used for fitting the hydrogen peak:

$$F_H(E) = b + \frac{A_H}{w_H\sqrt{2\pi}} e^{\frac{-z^2}{2}} \left(1 + \sum_{i=3}^{4} \frac{a_i}{i!} \mathrm{H}_i(z)\right) \qquad (15)$$

$$z = \frac{E - E_{0,H}}{w_H}$$

$$\mathrm{H}_3 = z^3 - 3z$$

$$\mathrm{H}_4 = z^4 - 6z^3 + 3$$

where b is the y-intercept of the background signal, A_H is the area of the hydrogen peak, $E_{0,H}$ is the central energy of the hydrogen peak, w_H is the half-width of the peak, and a_3 and a_4 are additional fitting parameters. As can be seen in Figure 48 in Chapter 5, the hydrogen peak has a characteristically skewed tail. Attempts to fit this peak with numerous functions including a skewed normal distribution failed to yield adequate fitting and corresponding statistics of the data. However, the Gram-Charlier function, intended for fitting gas chromatography data that have similar characteristic tails to the hydrogen peak, provided good fitting (R^2>0.98) and met the requirements for permitting rapid data analysis while maintaining minimal propagated error. All peak fitting and parameter analysis was accomplished using Origin 6.0's built-in non-linear Levenberg-Marquardt curve fitting routine using statistical weighting.

6.3 Development of Improved Lyophilized Samples - Results and Discussion

Sample boron and hydrogen spectra for a lyophilized 10 ppm boron calibration standard in TPR mixture showing sample fitted parameters are shown

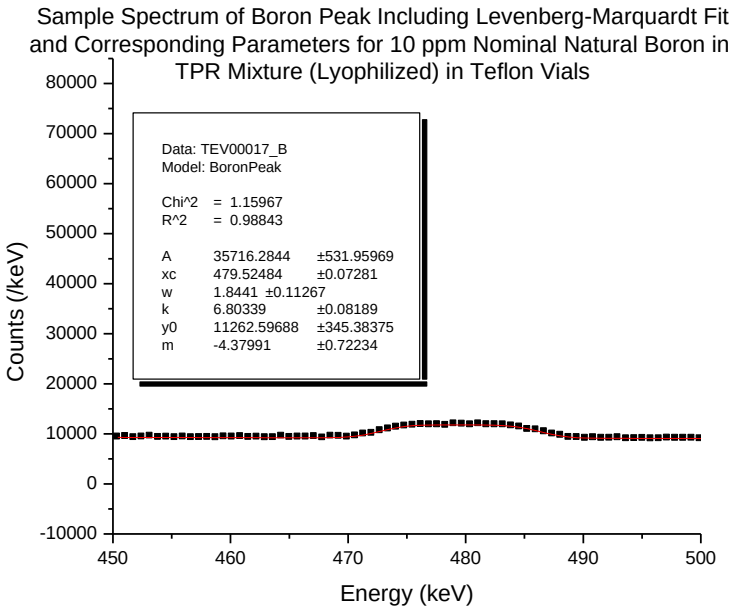

Fig. 50 Sample spectrum over the range of the boron peak for the lyophilized 10 ppm nominal elemental boron in TPR mixture.

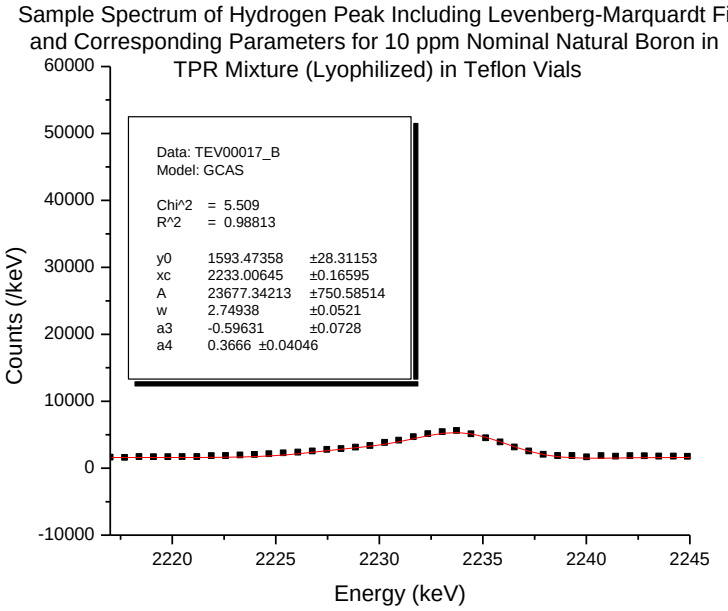

Fig. 51 Sample spectrum over the range of the hydrogen peak for the lyophilized 10 ppm nominal elemental boron in TPR mixture.

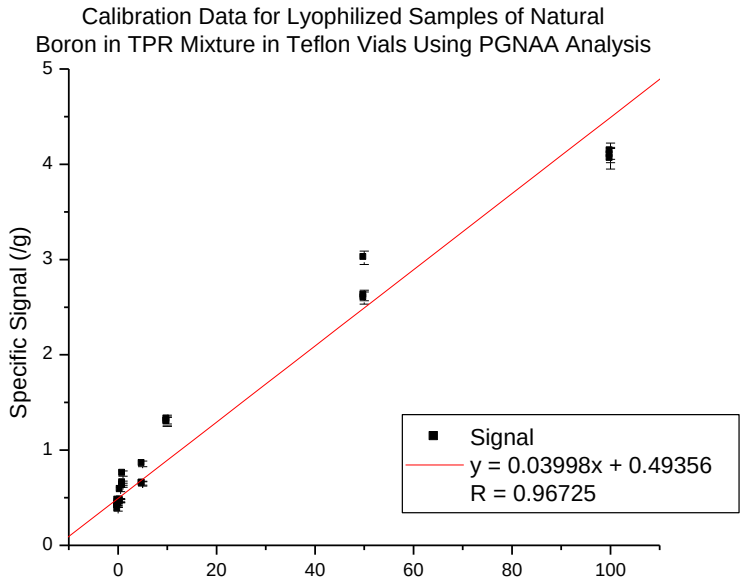

Fig. 52 Calibration curve for lyophilized elemental boron in TPR mixture in Teflon® vials. Linear regression, regression equation and correlation coefficient are also shown.

in Figures 50 and 51 (previous). The calibration graph for elemental boron in TPR mixture for Teflon® vials is shown below in Figure 52. Regression analysis was performed using the built-in linear fitting routine of Origin 6.0 with error weighting. The correlation coefficient of the results for boron in the TPR mixture in Teflon® vials was 0.96725. This represented a significant improvement in linearity over the range of boron concentrations tested versus the findings of Chapter 5 in Teflon® wherein the correlation coefficient was 0.73753. However, this value was not as robust as that for the RPMI-based liquid samples calculated in Chapter 2 (0.99507). The minimum detection limit (MDL) representing the nominal 95% confidence interval was calculated as $MDL = 2\sigma_{C_B}$, where $\sigma_{C_B}{}^2$ is the variance of the boron concentration derived from the expansion of the

variance in the calibration curve equation (see Section 2.3). Using this metric the MDL value was calculated to be 2.70 ppm. Therefore, the MDL was improved versus that for both LDPE and Teflon® in Chapter 5 (3.56 and 10.11, respectively).

The MDL value indicates that the PGNAA method using Teflon® vials with TPR mixture substrate is more sensitive than that using Teflon® vials with HPLC water-based solutions as hypothesized. Therefore, the suggestion in Chapter 5 that a large fraction of sample may have been lost between the lyophilization process and sample preparation is corroborated by the results obtained herein. Additionally, as demonstrated by the improved linearity and correlation, the use of TPR mixture substrate does improve the inherent problem with the experimental setup in Chapter 5 wherein the signal values had large deviations.

Using the conservative definition as specified in Section 2.3 (Equations 5 and 6), the MDL value using the TPR mixture substrate indicates that the lyophilized sample method is not more sensitive than the liquid sample method utilized in Chapter 2 for complete RPMI (1.28 ppm vs. 2.70 ppm). On the other hand, if one applies the less conservative definition of MDL as $3\sqrt{N_B}/S \cdot t_m$ (see Section 2.4) as was utilized by Byun et al. (2004) and Crittin et al. (2000), the MDL was actually improved compared to the complete RPMI results in Chapter 2

(1.36 μg vs. 1.78 μg). However, both results indicate that the detection limit is insufficiently low to meet the requirements for quantifying boron content in the biological samples as proposed in this thesis work. Therefore, further improvements to the overall PGNAA irradiation facility and detection system are required in future studies.

6.4 Development of Improved Lyophilized Samples - Conclusion

The MDL of boron in the tested geometry at BP#4 of MNR using the Teflon® vials with TPR mixture substrate was more sensitive than that of the Teflon® vials with HPLC water described in Chapter 5, but not more sensitive than that of the liquid sample methods described in Chapter 2. The results in this study indicate that ultimately in order to improve the MDL of boron significantly major changes to the PGNAA irradiation facility and detection system are required such as to increase the boron signal and reduce the overall background count rate.

7 General Discussion and Final Conclusion

7.1 General Discussion

The work described in this thesis has completed interdisciplinary scoping studies towards a testing process for boron compounds generated for the purpose of boron neutron capture synovectomy (BNCS). The studies in general have shown promise for the implementation of such a process at McMaster University. However, the investigation has highlighted some of the limitations encountered during the studies, some of which require resolution in the future prior to implementation of such a process.

With respect to treatment of cells with boron compounds, it was found that standard protocols used for leukocyte apoptosis studies could be successfully modified to treat cells with the compounds followed by flow cytometry analysis to determine the impact of those compounds on the viability of the cells. One of the limitations encountered was that of cell subtype labeling and the impact from apoptotic processes, in particular on the expression of CD14 in monocytes as described in Chapter 4. This highlighted the need for careful evaluation in the future of potential cell labeling antibodies. Another limitation encountered in these studies was the rapid diffusion of boron compounds out of the cells and the need for an alternate method of separation of the cells from the treated medium.

This limitation was determined to have been successfully resolved by Capala et al. (1996) for similar studies with respect to boron neutron capture therapy compounds by utilizing a rapid oil filtration process.[60] The assumption in this work (for the purpose of PGNAA measurement of boron) was that this same process could be successfully applied to leukocytes for compounds geared towards BNCS. However, this assumption needs to be confirmed via experimentation in the future in order to implement the overall testing process successfully.

With respect to boron measurements, the prompt gamma neutron activation analysis (PGNAA) site was successfully modified to accommodate liquid sample irradiation for maximum volumes of 2.3 mL. The manual site allowed for the simple manual interchange of samples without the need for disassembly of the irradiation cavity surrounding the neutron beam port. Measurements of boron in these liquid samples were shown to have a minimum detectable limit (MDL) on the order of 1-3 ppm. However, based on preliminary uptake studies conducted in this work, as well as the results of Baechler et al. (2002) and Byun et al. (2004), it is estimated that an improvement of the MDL of an order of magnitude is required in order to support future boron compound testing.[44,45]

Numerous improvements in the detection setup were implemented in order to attempt to improve the MDL: lyophilization of the sample material was implemented to remove contribution to the hydrogen signal and allow for automated sample loading via the McMaster Nuclear Reactor (MNR) "Rabbit System"; the "Rabbit System" was automated to allow for practical 4 hour counting durations that would exploit the daily operation time of MNR; new Teflon® "Rabbit" vials were designed and manufactured to further reduce the background signal from hydrogen versus the standard LDPE vials; a non-specific substrate conducive with the rapid oil filtration process was utilized for lyophilization of boronated samples. While these changes did lead to improved ease of use, reduced background and improved boron signal, they failed to reduce the MDL of boron below the nominal 1 ppm mark.

While some of the improvements implemented in this thesis work include the implementation of dried samples and Teflon® sample holders, which attempt to reduce the background signal in the boron peak, future studies will have to address the issue of the high background in order to further reduce the MDL by implementing gamma spectroscopy improvements. In comparison with the studies of Baechler et al. (2002) and Byun et al. (2004) one noticeable difference, which affects the MDL, is the overall detection efficiency of the HPGE detector.[44,45] Those studies incorporated detectors with relative efficiencies in the range of 40% in contrast with the relative efficiency of 14.4% used herein. While the sample-

to-detector distance of ~21cm compared well against the distance of ~25 cm used in the other studies, future improvements may also include a further reduced sample-to-detector distance, if feasible, in order to improve the absolute detection efficiency.

In an attempt to reduce the background signal in the boron peak a careful review of contributing signal from boron incorporated in shielding materials should be investigated. As an example, reducing the use of boronated shielding material (e.g. Boraflex) and possibly replacing with lithium fluoride (^{6}LiF) tiles may successfully further reduce the overall boron peak background. Future improvements should also take advantage of advances in detection system electronics. More sophisticated detection schemes and electronics, such as the use of a bismuth germinate (BGO) Compton suppression spectrometer, have been shown to reduce spectra background significantly, and was successfully used at PSI for enhanced PGNAA detection and was a recommended future improvement at SNU.[44,45] Together with future use of dried samples and Teflon® sample holders that reduce the hydrogen signal, the largest single contributor to the Compton background, these suggested improvements could reduce the overall background signal and improve the MDL to the required levels for successful PGNAA studies of biological samples for boron content as proposed in thesis work.

The signal strength in gamma spectroscopy is ultimately proportional to the source strength, or activity. For PGNAA of boron, where the decay half-life can be ignored due to the prompt nature of gamma emission, the activity is equal to the rate of interaction defined as follows:

$$R = N\sigma\varphi \tag{16}$$

where N is the number of target atoms, σ is average activation cross section, and φ is the average neutron fluence rate. Since the cross section is an inherent property of ^{10}B, the only fundamental factors that can be increased are the total number of target atoms and the neutron fluence rate. The increase in the number of target atoms can be accomplished by increasing the total sample mass.

Through the course of implementing and improving the final lyophilized sample method for PGNAA of boron, the total final sample volume analyzed, and therefore mass analyzed, was reduced. Future work should, therefore, utilize an increased sample mass in order to increase the total boron signal. As discussed above, the liquid sample setup allowed for a maximum sample volume of 2.3 mL. The sample volumes tested in Chapter 2 were close to this limit (~2.1 mL). One means of increasing the total sample mass is to simply increase the size of the sample container and use more sample volume. However, this may prove impractical due to the nature of the manual apparatus as well as availability of

larger containers. In order to exploit the advantages gained from this work with regards to signal improvement, it is recommended instead that multiple series of sample dehydrations using the TPR mixture substrate with Teflon® vials be investigated in the future. While lyophilization resulted in crystalline overgrowth of the salt (caused by high vacuum), preliminary trials of simple evaporation have shown that the dehydrated substrate remains well contained with reduced total sample substrate volume within the vials (Figure 53). Therefore, successive

Fig. 53 Example of a polyethylene vial showing crystallized TPR-based boron sample material dried via dehydrator.

dehydrations of reduced aliquots should allow for an increased overall sample mass (i.e. 1.4 mL, 1.1 mL, 0.8 mL, 0.5 mL, 0.2 mL). In order to accelerate evaporation a standard food dehydrator might be utilized for this purpose. In this manner the overall tested sample volume would be effectively doubled (~2.1 mL

to 4 mL). The limitation to implementing this, however, in practical use may be the availability of sufficient oil-filtered sample material.

With respect to increasing the neutron fluence rate, one common means in neutron beam applications is via the use of neutron reflecting materials, such as graphite or beryllium, adjacent to and behind the target position. While this could successfully increase the neutron fluence rate, it could also adversely affect the detector performance as a result of neutron activation of the detector crystal. Therefore, prior to implementation at Beam Port #4, the addition of reflectors should be carefully analyzed, for example with MCNP5, and tested in order to assess the cost versus benefit to the overall performance.

An alternate means of increasing the neutron fluence rate that may prove to be more advantageous for this particular application is the use of a neutron focusing optical lens. The past decade has seen the advent and growing use of these devices which act by exploiting the property of total external reflection of low energy neutrons to channel the neutrons down hollow filaments of boron-free glass. When combined and oriented in a geometric nature so as to focus the neutrons, the macroscopic effect of these filaments is to generate a neutron density at the focal point that is 1-3 orders of magnitude larger than the nominal neutron field strength. Indeed the use of a polycapillary neutron lens was successfully used for cold neutrons by Crittin et al. (2000) at PSI to achieve a gain

of 16, and by Chen-Mayer et al. (1997) at NIST to achieve a gain of 60 with a corresponding factor of 20 improvement in the detection limit.[62,63] However, due to the prohibitive cost associated with implementing such a device (>$10k), all other means of improving the detection limit should be explored first. Figure 54 shows a schematic of the proposed upgrades to the PGNAA facility at BP#4 showing major components.

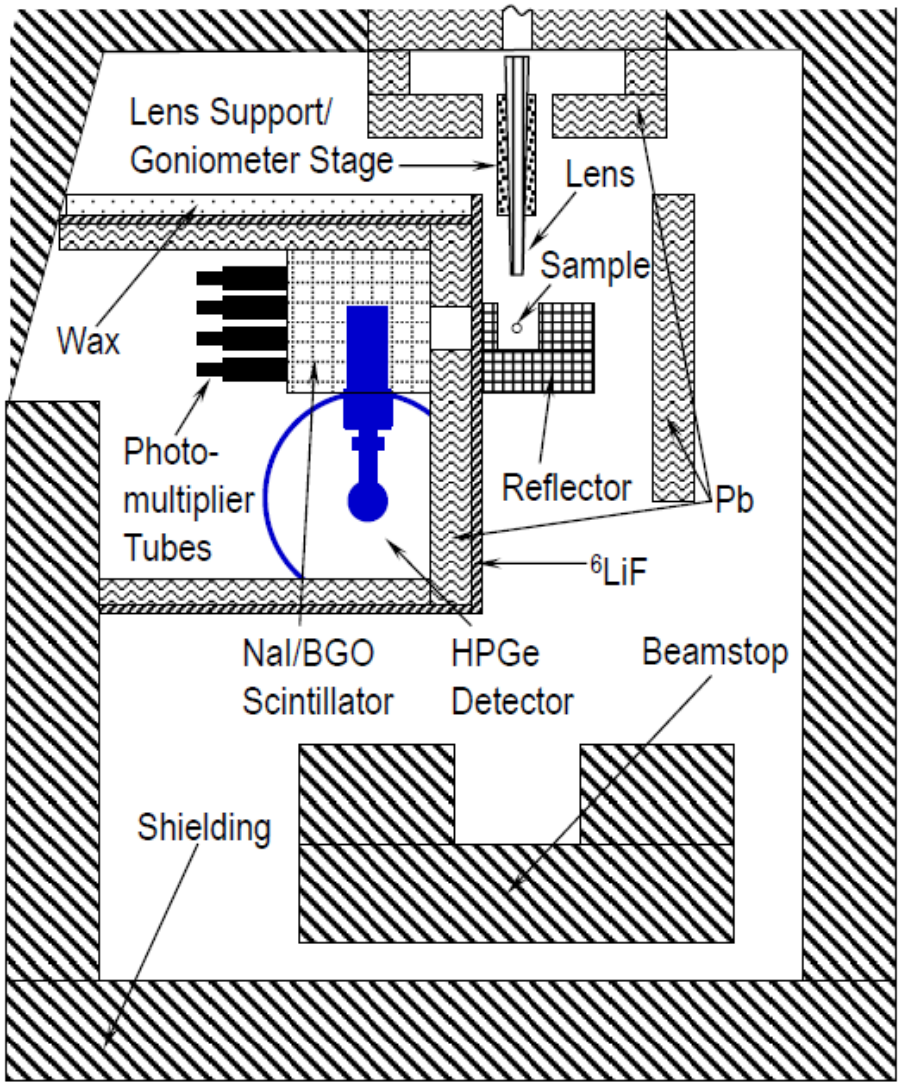

Fig. 54 Plan view schematic of the proposed upgrades to the MNR PGNAA facility at BP#4 showing major components.

7.2 Final Conclusion

Studies laying the ground work for a testing process for boron compounds with potential use in boron neutron capture synovectomy have been completed. It is envisioned that the final testing process will utilize elements investigated and described in this work: leukocytes shall be isolated from human donors via histopaque gradient isolation and treated with potential boron compounds; a portion of the treated cells and media shall be retained and analyzed for background toxicity via flowcytometry; a portion of the treated cells and media shall be isolated for boron uptake measurements via the rapid oil filtration process; the isolated remnants shall be treated with KOH and RPMI-1640 to yield the TPR mixture; the sample remnants in TPR mixture shall be dehydrated in Teflon® vials; PGNAA of the Teflon® vials via the "Rabbit System" shall be performed to measure the cellular uptake of the boron compound. In this manner, candidate compounds can be selected for future treatment and irradiation, followed by incubation and flowcytometry analysis to determine the relative effectiveness of the compounds for further animal studies.

References

1. 1. Gary S. Firestein, "Rheumatoid Arthritis." Kelley's Textbook of Internal Medicine, 4th Ed. edited by David H. Humes et al., Philadelphia: Lippincott, Williams, and Wilkins, pp 1347-1359 (2000)
2. David M. Lee and Michael E. Weinblatt, "Rheumatoid arthritis." The Lancet. Vol. 358, pp 903-911 (2001)
3. Gary S. Firestein, "Rheumatoid Arthritis." Kelley's Textbook of Rheumatology, 7th Ed. edited by E. D. Harris et al, Elsevier Saunders, pp 996-1100 (2005)
4. Ernest H. S. Choy and Gabriel S. Panayi, "Mechanisms of Disease: Cytokine Pathways and Joint Inflammation in Rheumatoid Arthritis." New England Journal of Medicine. Vol. 344, pp 907-916 (2001)
5. J. C. Yanch et al., "Boron neutron capture synovectomy: Treatment of rheumatoid arthritis based on the $^{10}B(n,\alpha)^{7}Li$ nuclear reaction." Medical Physics. Vol. 26, pp 364-375 (1999)
6. F. Marques et al., "Symposium on radioactive colloids in the treatment of arthritis." Annals of the Rheumatic Diseases. Vol. 32, (suppl.):3-9 (1973)
7. M. Oka, "Radiation synovectomy of the rheumatoid knee with Yttrium 90." Annals of Clinical Research. Vol. 7, pp 205-210 (1975)
8. H. Deckart et al., "Radiosynovectomy of the knee-joint with ^{198}Aucolloid, ^{90}Y-ferric hydrate colloid, and ^{186}Re-sulphide colloid." Radiobiologia, Radiotherapia. Vol. 2, pp 363-370 (1979)
9. Gordon L. Locher, "Biologic effects and therapeutic possibilities of neutrons." American Journal of Roentgenology. Vol. 36:1 (1936)
10. R. G. Zamenhof et al., "Boron neutron capture therapy and radiation synovectomy research at the Massachusetts Institute of Technology Research Reactor". Nuclear Science and Engineering. Vol. 110:4; DOE Project, American Nuclear Society (1992)
11. Emanuela Binello, "In Vitro Analysis of Boron-10 Uptake and Neutron Beam Design for Boron Neutron Capture Synovectomy." Master of Science Thesis, Department of Nuclear Engineering, Massachusetts Institute of Technology (1995)
12. D. P. Gierga, J. C. Yanch, and R E. Shefer, "Development and construction of a neutron beam line for accelerator-based boron neutron capture synovectomy." Medical Physics. Vol. 27, pp 203-214 (2000)
13. S. Shortkroff et al., "Dose reponse of the AIA rabbit stifle to boron neutron capture Synovectomy." Nuclear Medicine and Biology. Vol. 31, p. 663-670 (2004)
14. John F. Valliant et al., "The synthesis of corticosteroid-carborane esters for the treatment of rheumatoid arthritis via boron neutron capture synovectomy." Tetrahedron Letters. Vol. 41, pp 1355-1358 (2000)
15. Scott McMaster, Manager, Tandem Accelerator Building, Personal Communication, June 2006

16. L. S. Johnson et al., "Temporal and Spatial Distribution of Boron Uptake in Excised Human Synovium." The Sixth International Symposium on Neutron Capture Therapy for Cancer. Kobe, Japan (1994)
17. Nicolas Stritt, "Boron uptake in cells: A study about the kinetics of boron uptake in cells, neutron-induced cell death (apoptosis) and neutron-induced cell cycle arrest." Diploma-Thesis, NDS Medizin Physik, ETH Zurich (2001)
18. N. E. A. Crompton et al., "Biomedical Research with the Neutron Capture Radiography Facility." NR-Workshop 2001. Paul Scherrer Institut (2001)
19. W. E. Wolcott, "Regeneration of the Synovial Membrane Following Typical Synovectomy." J Bone Joint Surg Am. Vol. 9 pp 67-78 (1927)
20. N. Kawanaka et al., "CD14+,CD16+ Blood Monocytes and Joint Inflammation in Rheumatoid Arthritis." Arthritis and Rheumatism. Vol. 46 No. 10, pp 2578-2586 (2002)
21. U. Mueller-Ladner et al., "Activation of synoviocytes." Current Opinion in Rheumatology. Vol. 12 pp 186-194 (2000)
22. C. Ospelt et al., "Synovial Activation in Rheumatoid Arthritis." Frontiers in Bioscience. Vol. 9 pp 2323-2334 (2004)
23. F. Buttgereit et al., "Glucocorticoids in the Treatment of Rheumatic Diseases: An Update on the Mechanisms of Action." Arthritis and Rheumatism. Vol. 50 No. 11, pp 3480-3417 (2004)
24. D.T. Boumpas et al., "Glucocorticoid Therapy for Immune-mediated Diseases: Basic and Clinical Correlates." Annals of Internal Medicine. Vol. 119 No. 12, pp 1198-1208 (1993)
25. M. Schmidt et al., "Glucocorticoids Induce Apoptosis in Human Monocytes: Potential Role of IL-1β." The Journal of Immunology. Vol. 163, pp 3484-3490 (1999)
26. J.J. Rinehart et al., "Corticosteroid Alteration of Human Monocyte to Macrophage Differentiation." Journal of Immunology. Vol. 129 No. 4, pp 1436-1440 (1982)
27. J.M. Metselaar et al., "Complete Remission of Experimental Arthritis by Joint Targeting of Glucocorticoids With Long-Circulating Liposomes." Arthritis and Rheumatism. Vol. 48 No. 7, pp 2059-2066 (2003)
28. J.M. Metselaar et al., "Liposomal targeting of glucocorticoids to synovial lining cells strongly increases therapeutic benefit in collagen type II arthritis." Annals of the Rheumatic Diseases. Vol. 63, pp 348-353 (2004)
29. P. Barrera et al., "Synovial Macrophage Depletion with Clodronate-Containing Liposomes in Rheumatoid Arthritis." Arthritis and Rheumatism. Vol. 43 No. 9, pp 1951-1959 (2000)
30. P. van Lent et al., "Local removal of phagocytotic synovial lining cells by clodronate-liposomes decreases cartilage destruction during collagen type II arthritis." Annals of the Rheumatic Diseases. Vol. 57, pp 408-413 (1998)
31. R.A. Watson-Clark et al., "Model studies directed towards the application of boron neutron capture therapy to rheumatoid arthritis: Boron delivery by

liposomes in rat collagen-induced arthritis." Proceedings of the National Academy of Sciences USA: Medical Sciences. Vol. 95, pp 2531-2534 (1998)
32. P. van Lent et al., "Selective elimination of synovial macrophages by boron neutron capture therapy prevents onset of murine experimental arthritis." Journal of Controlled Release: *Proceedings of the Ninth European Symposium on Controlled Drug Deliver* Vol. 116 Iss. 2, pp e106-e107 (2006)
33. Kara Schnarr, "The Effects of Medical Imaging and Therapeutic Radiation on Lymphocytes on Cancer Patients." Doctor of Philosophy Thesis, Department of Medical Physics and Applied Radiation Sciences, McMaster University (2007)
34. David Hockenbery, "Review: Defining Apoptosis." American Journal of Pathology. Vol. 146 No. 1, pp 16-19 (1995)
35. R.E. Ellis et al., "Mechanisms and Functions of Cell Death." Annual Reviews in Cell Biology. Vol. 7, pp 663-698 (1991)
36. Guido Majno and Isabelle Joris, "Review: Apoptosis, Oncosis, and Necrosis – An Overview of Cell Death." American Jounral of Pathology. Vol. 146 No. 1, pp 3-15 (1995)
37. A.B. Kane, "Commentary: Redefining Cell Death." American Jounral of Pathology. Vol. 146 No. 1, pp 1-2 (1995)
38. L.E. Broeker et al, "Cell Death Independent of Caspases: A Review." Clinical Cancer Research. Vol. 11 No. 9, pp 3155-3162 (2005)
39. Lorna Ryan, "Apoptosis Measured By Flow Cytometry As A Biological Dosimeter – Comparison of Assays and Effectiveness of 280 keV Neutrons" Master of Science Thesis, Department of Medical Physics and Applied Radiation Sciences, McMaster University (2004)
40. Awtar Krishan, "Rapid Flow Cytoflourometric Analysis of Mammalian Cell Cycle by Propidium Iodide Staining." The Journal of Cell Biology. Vol. 66, pp 188-193 (1975)
41. Scott McMaster, Manager, Tandem Accelerator Building, Personal Communication, June 2006
42. Yakov Kapusta, Director of Research and Development ICP MS and General Manager, Geochronology and Isotopic Geochemistry, Activation Laboratories Ltd., Ancaster, Ontario, Personal Communication, April 2008
43. "Current status of neutron capture therapy." International Atomic Energy Agency IAEA-TECDOC-1223. Austria, May (2001)
44. S. Baechler et al., "Prompt gamma-ray activation analysis for determination of boron in aqueous solutions." Nuclear Instruments and Methods in Physics Research A. Vol. 488, pp 410-418 (2002)
45. S.H. Byun et al., "Prompt gamma activation analysis of boron in reference materials using diffracted polychromatic neutron beam." Nuclear Instruments and Methods in Physics Research B. Vol. 213, pp 535-539 (2004)
46. M. Magara and C. Yonezawa, "Decomposition of gamma-ray spectra including the Doppler-broadened peak for boron determination.", Nuclear Instruments and Methods in Physics Research. Vol. 411, pp 130-136 (1998)

47. M.T. Flanagan (2004), “Michael Thomas Flanagan's Java Scientific Library”. Retrieved June 27, 2008, from Michael Thomas Flanagan's Java Scientific Library Web site: http://www.ee.ucl.ac.uk/~mflanaga/java/
48. J.C. Miller and J.N. Miller, “Errors in instrumental analysis; regression and correlation.” Statistics for Analytical Chemistry. 3rd Ed., pp 101-141, Ellis Horwood and PTR Prentice Hall, Toronto (1993)
49. Jovica Atanackovic, “Optimization of the Prompt Gamma Site at the McMaster Nuclear Reactor for In Vivo Neutron Activation Analysis”, Master of Science Thesis, Department of Medical Physics and Applied Radiation Sciences, McMaster University (2004)
50. Andrew Green, “The Synthesis and Characterization of Carborane and Metallocarborane-Carbohydrate Conjugates”, Doctor of Philosophy Thesis, Department of Chemistry, McMaster University (2008)
51. Beckman Coulter , “7-AAD Viability Dye.”, Reference Document I-A07704 2008-06-10_GB, Retrieved August 19, 2008, from Beckman Coulter Customer Support Information for Use for 7AAD Web site: http://www.beckmancoulter.com/CustomerSupport/IFU/ivdd/A07704%202008-06-10_GB.pdf
52. K. Hertveldt et al., "Technical Report: Flow cytometry as a quantitative and sensitive method to evaluate low dose radiation induced apoptosis in vitro in human peripheral blood lymphocytes" International Journal of Radiation Biology Vol. 71 No. 4 pp 429-433 (1997)
53. Beckman Coulter , “IOTest® CD14-PE Viability Dye.”, Reference Document I-IMO650U 2008-06-09_GB, Retrieved August 19, 2008, from Beckman Coulter Customer Support Information for Use for CD14-PE Web site: http://www.beckmancoulter.com/CustomerSupport/IFU/ivdd/IM0650U%202006-06-09.pdf
54. H. Liu et al., “Regulation of Mcl-1 Expression in Rheumatoid Arthritis Synovial Macrophages.” Arthritis and Rheumatism. Vol. 54 No. 10, pp 3174-3181 (2006)
55. S. Heidenreich et al., “Regulation of Human Monocyte Apoptosis by the CD14 Molecule.” The Journal of Immunology. Vol. 159, pp 3178-3188 (1997)
56. D. Lang et al., “Heme-induced heme oxygenase-1 (HO-1) in human monocytes inhibits apoptosis despite caspase-3 up-regulation.” International Immunology. Vol. 17 No. 2, pp 155-165 (2004)
57. MCNP – A General Monte Carlo N-Particle Transport Code, Version 5. edited by Thomas E. Booth et al., LA-UR-03-1987, Los Alamos National Laboratory, April 24 (2003)
58. Victor Kreft, “Phantom Validation and Beam Line Characterization for Boron Neutron Capture Synovectomy Studies at McMaster University” Master of Science Thesis, Department of Medical Physics and Applied Radiation Sciences, McMaster University (2005).

59. M.B. Chadwick, P. Obložinský, M. Herman, N.M. Greene, R.D. McKnight, D.L. Smith, P.G. Young, R.E. MacFarlane, G.M. Hale, S.C. Frankle, A.C. Kahler, T. Kawano, R.C. Little, D.G. Madland, P. Moller, R.D. Mosteller, P.R. Page, P. Talou, H. Trellue, M.C. White, *et al.*, "ENDF/B-VII.0: Next Generation Evaluated Nuclear Data Library for Nuclear Science and Technology", Nuclear Data Sheets. Vol. 107 Iss. 12, pp 2931-3118 (2006)
60. J. Capala et al., "Accumulation of Boron in Malignant and Normal Cells Incubated *In Vitro* with Boronophenylalanine, Mercaptoborane or Boric Acid." Radiation Research. Vol. 146, pp 554-560 (1996)
61. R.M. Wohlheuter et al., "A rapid mixing technique to measure transport in suspended animal cells: Application to nucleoside transport in Novikoff rat hepatoma cells." Methods in Cellular Biology. Vol. 20, pp 211-236 (1978).
62. M. Crittin et al., "The new prompt gamma-ray activation facility at the Paul Scherrer Institute, Switzerland." Nuclear Instruments and Methods in Physics Research A. Vol. 449, pp 221-236 (2000).
63. HH. Chen-Mayer et al., "Capillary neutron optics for prompt-gamma activation analysis." Journal of Radioanalytical and Nuclear Chemistry. Vol. 215, pp141-145 (1997).
64. Simon Day, Reactor Supervisor - Analysis, McMaster Nuclear Reactor, Private Communication, June 2006

Appendix: MCNP Input Files

A.1 LDPE Vial with Lyophilized RPMI

```
LDPE Vial with Lyophylized RPMI
c The following MCNP input deck is based on an original by Jovica Atanakovic
c using the original origin/co-ordinate system definition
c
c Cell cards
1       11 -11.35 9 -1 -13 (2 : -12) (3 : -11) 4 imp:n,p=1 $lead blocks
2       2 -0.00122 (10 (-4 : 11) (-3 : 12) -2 -13) (-14 : 6 : 17) imp:n,p=1 $air
3       3 -0.12 7 -3 (-9 : -4) -10 imp:n,p=1 $detector gas
4       4 -0.6 8 -1 -9 3 imp:n,p=1 $plywood
5       5 -1.64 7 -1 -8 3 imp:n,p=1 $boroflex shielding
6       2 -0.00122 16 -5 -17 imp:n,p=1 $air
7       10 -1.848 15 -5 -16 imp:n,p=1 $beryllium crystal
8       3 -0.12 14 -6 -17 (5 : -15) imp:n,p=1 $detector gas
9       6 -0.93 -18 (1 : 13 : -9) imp:n,p=1 $big wax shielding
10      7 -2.702 -19 imp:n,p=1 $Al table
11      6 -0.93 -20 imp:n,p=1 $small wax shielding
12      2 -0.00122 (-7 : 1 : 13) (-21 : 26 : 24) 18 19 20
                   27 28 29 30 31 32 33 34 -35
                   (36 : -37 : -38 : 39) imp:n,p=1 $outside air
13      8 -0.0473 22 -25 -23 -40 imp:n,p=1 $RPMI sample back
14      9 -0.92 21 -26 -24 (-22 : 25 : 23) -40 imp:n,p=1 $poly vial back
15      11 -11.35 -27 imp:n,p=1 $lead blocks
16      11 -11.35 -28 imp:n,p=1 $lead blocks
17      1 -2.3 -29 imp:n,p=1 $concrete wall
18      1 -2.3 -30 imp:n,p=1 $concrete wall
19      1 -2.3 -31 imp:n,p=1 $concrete wall
20      6 -0.93 -32 imp:n,p=1 $wax wall
21      1 -2.3 -33 imp:n,p=1 $concrete wall
22      1 -2.3 -34 imp:n,p=1 $concrete wall
23      0 35 imp:n,p=0 $irrelevant world
24      12 -2.2 -36 37 38 -39 -40 imp:n,p=1 $poly guide tube back
25      8 -0.0473 22 -25 -23  40 imp:n,p=1 $RPMI sample front
26      9 -0.92 21 -26 -24 (-22 : 25 : 23)  40 imp:n,p=1 $poly vial front
27      12 -2.2 -36 37 38 -39  40 imp:n,p=1 $poly guide tube front

c Surface cards
1       cy 15.2
2       cy 6.3
3       cy 3.2
4       cy 1.9
5       cy 2.95
6       cy 4.14
7       py -1.27
8       py -0.9525
9       py 0
10      py 1.5875
11      py 4.7625
12      py 9.8425
13      py 34.6075
14      py 9.9
15      py 11.09
16      py 11.14
17      py 17.04
18      rpp -56.69 26.67 0 77.47 -97.79 29.21 $big wax box
19      rpp -29.845 26.67 -39.37 0 -17.78 -16.51 $ Al table
20      rpp -29.845 26.67 -39.37 0 -69.85 -17.78 $ small wax box
21      pz -1.26111 $vial
22      pz -1.13919 $sample
23      pz  1.13919 $sample
24      pz  1.26111 $vial
25      c/z 0 -8.89 0.46228 $sample
```

```
26      c/z 0 -8.89 0.58420 $vial
27      rpp -19.05 26.67 -39.37 -31.75 -16.51 16.51 $big Pb block
28      rpp -11.43 19.05 -31.75 -24.13 -16.51 6.35 $small Pb block
29      rpp 27 32 -39.37 77.47 -97.79 82.21 $reactor wall concrete
30      rpp -140.56 -135.56 -39.37 77.47 -97.79 82.21 $opp rwall concrete
31      rpp -140.56 32 -39.37 77.47 -102.79 -97.79 $floor concrete
32      rpp -140.56 32 -39.37 77.47 82.21 87.21 $top wall wax
33      rpp -140.56 32 -44.37 -39.37 -102.79 87.21 $front  wall concrete
34      rpp -140.56 32 77.47 82.47 -102.79 87.21 $back wall concrete
35      so 200
36      pz  15.24000 $guide tube
37      pz -15.24000 $guide tube
38      c/z 0 -8.89 0.95250 $guide tube ID=3/4"
39      c/z 0 -8.89 1.11125 $guide tube thichness=1/16"
40      px 0

c Data cards
mode n
sdef par=1 pos=26.67 -8.89 0 x=26.67 y=d1 z=d2 erg=d3 vec=-1 0 0 dir=1
si1 h -10.16 -7.62
sp1 d 0 1
si2 h -2.54 2.54
sp2 d 0 1
#       si3               sp3
        6.25e-9           0
        0.000000008       0.015062417
        0.00000001        0.020191285
        0.000000012       0.022808583
        0.000000014       0.024911363
        0.000000016       0.026562721
        0.000000018       0.027819131
        0.00000002        0.02873109
        0.000000022       0.029343703
        0.000000024       0.029697205
        0.000000026       0.029827447
        0.000000028       0.029766325
        0.00000003        0.029542177
        0.000000032       0.029180139
        0.000000034       0.028702466
        0.000000036       0.028128828
        0.000000038       0.027476574
        0.00000004        0.026760968
        0.00000005        0.121702577
        0.00000006        0.100316501
        0.00000007        0.079922021
        0.00000008        0.062151344
        0.00000009        0.047465168
        0.0000001         0.03574367
        0.0000002         0.094218639
        0.0000003         0.003276555
        0.0000004         9.11025e-5
        0.8               0.0006
c ccccccccccccccccccccccccccccccccccccccc
c Tallies
f4:n 24
fc4 GT (back)
fs4 -21 -24
sd4 7.193883239 1.297996921 7.193883239
fm4 3.47e8
e4 0 24i 10e-6
f14:n 14
fc14 Vial (back)
fm14 3.47e8
e14 0 24i 10e-6
f24:n 13
fc24 RPMI Sample (front)
fm24 3.47e8
```

```
e24 0 24i 10e-6
f34:n 25
fc34 RPMI Sample (front)
fm34 3.47e8
e34 0 24i 10e-6
f44:n 26
fc44 Vial (front)
fm44 3.47e8
e44 0 24i 10e-6
f54:n 27
fc54 GT (front)
fs54 -21 -24
sd54 7.193883239 1.297996921 7.193883239
fm54 3.47e8
e54 0 24i 10e-6
f64:n (13 25)
fc64 RPMI Sample (total)
fm64 3.47e8
e64 0 24i 10e-6
f74:n 24
fc74 GT (back whole)
fm74 3.47e8
e74 0 24i 10e-6
f84:n 27
fc84 GT (front whole)
fm84 3.47e8
e84 0 24i 10e-6
c ccccccccccccccccccccccccccccccccccccccc
c Material cards
c
c      ANSI/ANS 6.6.1-1987 Concrete Composition @ 2.3 g/cm3
m1     1001.70c 7.86e+21 8016.70c 4.38e+22 11023.70c 1.05e+21
       12000.60c 1.40e+20 13027.70c 2.39e+21 14000.60c 1.58e+22
       19000.60c 6.90e+20 20000.60c 2.92e+21 26000.50c 3.10e+20
c
c      Air @ 0.00122 g/cm3
m2     7014.70c -0.755 8016.70c -0.232 18000 -0.013
c
c      Mixture @ 0.12 g/cm3
m3     3007.70c -0.035 6000.70c -0.725 8016.70c -0.12 1001.70c -0.12
c
c      Plywood @ 0.6 g/cm3
m4     6000.70c -0.481 1001.70c -0.062 8016.70c -0.457
c
c      Boroflex @ 1.64 g/cm3
m5     14000.60c -0.2675 5010.70c -0.0502 5011.70c -0.2033
       8016.70c -0.2415 6000.70c -0.2008 1001.70c -0.0276
       26000.50c -0.0041 29000.50c -0.0026 20000.60c -0.0004
       22000.60c -0.002
c
c      Wax @ 0.93 g/cm3
m6 6000.70c -0.851 1001.70c -0.149
c
c      Aluminum @ 2.702 g/cm3
m7 13027.70c 1
c
c      RPMI (Lyophylized) Composition @ 0.0473 g/cm3
m8     1001.70c -1.8114E-02 6000.70c -1.1595E-01 7014.70c -1.1506E-02
       8016.70c -2.3509E-01 11023.70c -2.6307E-01 12000.60c -8.1803E-04
       15031.70c -1.4479E-02 16000.60c -2.5101E-03 17000.60c -3.1965E-01
       19000.60c -1.7401E-02 20000.60c -1.4095E-03 27059.70c -1.8034E-08
c
c      Polyethylene @ 0.92 g/cm3
m9     1001.70c -0.14372 6000.70c -0.85628
mt9    poly.60t
c
c      Beryllium @ 1.848 g/cm3
```

```
m10    4009.70c 1
c
c      Lead @ 11.35 g/cm3
m11 82000.50c 1
c
c      Teflon @ 2.20000 g/cm3
m12    9019.70c -0.759817 6000.70c -0.240183
c ccccccccccccccccccccccccccccccccccccccccc
vol 12j 0.764814733 0.587338613 9j 15.6857634 0.764814733 0.587338613 15.6857634
print
rand seed=20091201
nps 100000000
```

A.2 Teflon Vial with Lyophilized RPMI

```
LDPE Vial with Lyophylized RPMI
c The following MCNP input deck is based on an original by Jovica Atanakovic
c using the original origin/co-ordinate system definition
c
c Cell cards
1       11 -11.35 9 -1 -13 (2 : -12) (3 : -11) 4 imp:n,p=1 $lead blocks
2       2 -0.00122 (10 (-4 : 11) (-3 : 12) -2 -13) (-14 : 6 : 17) imp:n,p=1 $air
3       3 -0.12 7 -3 (-9 : -4) -10 imp:n,p=1 $detector gas
4       4 -0.6 8 -1 -9 3 imp:n,p=1 $plywood
5       5 -1.64 7 -1 -8 3 imp:n,p=1 $boroflex shielding
6       2 -0.00122 16 -5 -17 imp:n,p=1 $air
7       10 -1.848 15 -5 -16 imp:n,p=1 $beryllium crystal
8       3 -0.12 14 -6 -17 (5 : -15) imp:n,p=1 $detector gas
9       6 -0.93 -18 (1 : 13 : -9) imp:n,p=1 $big wax shielding
10      7 -2.702 -19 imp:n,p=1 $Al table
11      6 -0.93 -20 imp:n,p=1 $small wax shielding
12      2 -0.00122 (-7 : 1 : 13) (-21 : 26 : 24) 18 19 20
                   27 28 29 30 31 32 33 34 -35
                   (36 : -37 : -38 : 39) imp:n,p=1 $outside air
13      8 -0.0473 22 -25 -23 -40 imp:n,p=1 $RPMI sample back
14      12 -2.2 21 -26 -24 (-22 : 25 : 23) -40 imp:n,p=1 $poly vial back
15      11 -11.35 -27 imp:n,p=1 $lead blocks
16      11 -11.35 -28 imp:n,p=1 $lead blocks
17      1 -2.3 -29 imp:n,p=1 $concrete wall
18      1 -2.3 -30 imp:n,p=1 $concrete wall
19      1 -2.3 -31 imp:n,p=1 $concrete wall
20      6 -0.93 -32 imp:n,p=1 $wax wall
21      1 -2.3 -33 imp:n,p=1 $concrete wall
22      1 -2.3 -34 imp:n,p=1 $concrete wall
23      0 35 imp:n,p=0 $irrelevant world
24      12 -2.2 -36 37 38 -39 -40 imp:n,p=1 $poly guide tube back
25      8 -0.0473 22 -25 -23  40 imp:n,p=1 $RPMI sample front
26      12 -2.2 21 -26 -24 (-22 : 25 : 23)  40 imp:n,p=1 $poly vial front
27      12 -2.2 -36 37 38 -39  40 imp:n,p=1 $poly guide tube front

c Surface cards
1       cy 15.2
2       cy 6.3
3       cy 3.2
4       cy 1.9
5       cy 2.95
6       cy 4.14
7       py -1.27
8       py -0.9525
9       py 0
10      py 1.5875
11      py 4.7625
12      py 9.8425
13      py 34.6075
14      py 9.9
15      py 11.09
16      py 11.14
17      py 17.04
18      rpp -56.69 26.67 0 77.47 -97.79 29.21 $big wax box
19      rpp -29.845 26.67 -39.37 0 -17.78 -16.51 $ Al table
20      rpp -29.845 26.67 -39.37 0 -69.85 -17.78 $ small wax box
21      pz -1.26111 $vial
22      pz -1.13919 $sample
23      pz  1.13919 $sample
24      pz  1.26111 $vial
25      c/z 0 -8.89 0.46228 $sample
26      c/z 0 -8.89 0.58420 $vial
27      rpp -19.05 26.67 -39.37 -31.75 -16.51 16.51 $big Pb block
28      rpp -11.43 19.05 -31.75 -24.13 -16.51 6.35 $small Pb block
```

```
29      rpp 27 32 -39.37 77.47 -97.79 82.21 $reactor wall concrete
30      rpp -140.56 -135.56 -39.37 77.47 -97.79 82.21 $opp rwall concrete
31      rpp -140.56 32 -39.37 77.47 -102.79 -97.79 $floor concrete
32      rpp -140.56 32 -39.37 77.47 82.21 87.21 $top wall wax
33      rpp -140.56 32 -44.37 -39.37 -102.79 87.21 $front  wall concrete
34      rpp -140.56 32 77.47 82.47 -102.79 87.21 $back wall concrete
35      so 200
36      pz  15.24000 $guide tube
37      pz -15.24000 $guide tube
38      c/z 0 -8.89 0.95250 $guide tube ID=3/4"
39      c/z 0 -8.89 1.11125 $guide tube thichness=1/16"
40      px 0

c Data cards
mode n
sdef par=1 pos=26.67 -8.89 0 x=26.67 y=d1 z=d2 erg=d3 vec=-1 0 0 dir=1
si1 h -10.16 -7.62
sp1 d 0 1
si2 h -2.54 2.54
sp2 d 0 1
#       si3               sp3
        6.25e-9           0
        0.000000008       0.015062417
        0.00000001        0.020191285
        0.000000012       0.022808583
        0.000000014       0.024911363
        0.000000016       0.026562721
        0.000000018       0.027819131
        0.00000002        0.02873109
        0.000000022       0.029343703
        0.000000024       0.029697205
        0.000000026       0.029827447
        0.000000028       0.029766325
        0.00000003        0.029542177
        0.000000032       0.029180139
        0.000000034       0.028702466
        0.000000036       0.028128828
        0.000000038       0.027476574
        0.00000004        0.026760968
        0.00000005        0.121702577
        0.00000006        0.100316501
        0.00000007        0.079922021
        0.00000008        0.062151344
        0.00000009        0.047465168
        0.0000001         0.03574367
        0.0000002         0.094218639
        0.0000003         0.003276555
        0.0000004         9.11025e-5
        0.8               0.0006
c ccccccccccccccccccccccccccccccccccccccc
c Tallies
f4:n 24
fc4 GT (back)
fs4 -21 -24
sd4 7.193883239 1.297996921 7.193883239
fm4 3.47e8
e4 0 24i 10e-6
f14:n 14
fc14 Vial (back)
fm14 3.47e8
e14 0 24i 10e-6
f24:n 13
fc24 RPMI Sample (front)
fm24 3.47e8
e24 0 24i 10e-6
f34:n 25
fc34 RPMI Sample (front)
```

```
fm34 3.47e8
e34 0 24i 10e-6
f44:n 26
fc44 Vial (front)
fm44 3.47e8
e44 0 24i 10e-6
f54:n 27
fc54 GT (front)
fs54 -21 -24
sd54 7.193883239 1.297996921 7.193883239
fm54 3.47e8
e54 0 24i 10e-6
f64:n (13 25)
fc64 RPMI Sample (total)
fm64 3.47e8
e64 0 24i 10e-6
f74:n 24
fc74 GT (back whole)
fm74 3.47e8
e74 0 24i 10e-6
f84:n 27
fc84 GT (front whole)
fm84 3.47e8
e84 0 24i 10e-6
c ccccccccccccccccccccccccccccccccccccc
c Material cards
c
c      ANSI/ANS 6.6.1-1987 Concrete Composition @ 2.3 g/cm3
m1     1001.70c 7.86e+21 8016.70c 4.38e+22 11023.70c 1.05e+21
       12000.60c 1.40e+20 13027.70c 2.39e+21 14000.60c 1.58e+22
       19000.60c 6.90e+20 20000.60c 2.92e+21 26000.50c 3.10e+20
c
c      Air @ 0.00122 g/cm3
m2     7014.70c -0.755 8016.70c -0.232 18000 -0.013
c
c      Mixture @ 0.12 g/cm3
m3     3007.70c -0.035 6000.70c -0.725 8016.70c -0.12 1001.70c -0.12
c
c      Plywood @ 0.6 g/cm3
m4     6000.70c -0.481 1001.70c -0.062 8016.70c -0.457
c
c      Boroflex @ 1.64 g/cm3
m5     14000.60c -0.2675 5010.70c -0.0502 5011.70c -0.2033
       8016.70c -0.2415 6000.70c -0.2008 1001.70c -0.0276
       26000.50c -0.0041 29000.50c -0.0026 20000.60c -0.0004
       22000.60c -0.002
c
c      Wax @ 0.93 g/cm3
m6 6000.70c -0.851 1001.70c -0.149
c
c      Aluminum @ 2.702 g/cm3
m7 13027.70c 1
c
c      RPMI (Lyophylized) Composition @ 0.0473 g/cm3
m8     1001.70c -1.8114E-02 6000.70c -1.1595E-01 7014.70c -1.1506E-02
       8016.70c -2.3509E-01 11023.70c -2.6307E-01 12000.60c -8.1803E-04
       15031.70c -1.4479E-02 16000.60c -2.5101E-03 17000.60c -3.1965E-01
       19000.60c -1.7401E-02 20000.60c -1.4095E-03 27059.70c -1.8034E-08
c
c      Polyethylene @ 0.92 g/cm3
m9     1001.70c -0.14372 6000.70c -0.85628
c mt9    poly.60t
c
c      Beryllium @ 1.848 g/cm3
m10    4009.70c 1
c
c      Lead @ 11.35 g/cm3
```

```
m11 82000.50c 1
c
c      Teflon @ 2.20000 g/cm3
m12    9019.70c -0.759817 6000.70c -0.240183
c ccccccccccccccccccccccccccccccccccccccc
vol 12j 0.764814733 0.587338613 9j 15.6857634 0.764814733 0.587338613 15.6857634
print
rand seed=20091201
nps 100000000
```